

Smart Eutectic Gallium–Indium: From Properties to Applications

Zhibin Zhao, Saurabh Soni, Takhee Lee, Christian A. Nijhuis,* and Dong Xiang*

Eutectic gallium–indium (EGaIn), a liquid metal with a melting point close to or below room temperature, has attracted extensive attention in recent years due to its excellent properties such as fluidity, high conductivity, thermal conductivity, stretchability, self-healing capability, biocompatibility, and recyclability. These features of EGaIn can be adjusted by changing the experimental condition, and various composite materials with extended properties can be further obtained by mixing EGaIn with other materials. In this review, not only the unique properties of EGaIn introduced, but also the working principles for the EGaIn-based devices are illustrated and the developments of EGaIn-related techniques are summarized. The applications of EGaIn in various fields, such as flexible electronics (sensors, antennas, electronic circuits), molecular electronics (molecular memory, opto-electronic switches, or reconfigurable junctions), energy catalysis (heat management, motors, generators, batteries), biomedical science (drug delivery, tumor therapy, bioimaging and neural interfaces) are reviewed. Finally, a critical discussion of the main challenges for the development of EGaIn-based techniques are discussed, and the potential applications in new fields are prospected.

wearable devices. While the metal traces may face limitations, such as poor device stability and limited service life due to their large modulus.^[1] Liquid metals not only have the properties of traditional metals, but also have certain fluidity, which makes them deformable, making it possible to improve the performance of such devices. Although mercury is one of the most commonly used liquid metals, its toxicity has limited a wide range of application scenarios.^[2] Due to its low toxicity,^[3] gallium-based liquid metals have gradually become one of the major focus points of liquid metal research.

Liquid metals can be treated as a kind of smart materials (a type of functional materials that can perceive external stimuli, judge and handle the stimuli appropriately, and can react to changes in their environment). So far, the most popular gallium-based liquid metals are the eutectic gallium–indium alloy (EGaIn)

and eutectic gallium indium tin alloy (Galinstan). Compared to Galinstan, EGaIn has a wider range of applications. EGaIn can form a mechanically stable structure due to the existence of a very thin layer (0.7–3 nm) of oxide layer on its surface,^[4,5] so that it can be cast into varied and intricate shapes. Since the Whitesides group used a conical EGaIn tip to measure the properties of molecular layers in 2008,^[6] the measurement of tunneling currents across large-area molecular junctions using an EGaIn tip as a soft-top electrode has become one of the most widely used techniques in the field of molecular electronics.^[7,8] Compared with pure gallium (melting point 29.8 °C),^[9] the melting point of Ga–In alloys can be fine-tuned by adjusting the ratio of gallium and indium which is liquid at room temperature at its eutectic point.^[10] While Galinstan has similar properties to EGaIn, the excess tin component may have an additional impact on the former's use in metrology techniques. These comprehensive factors make EGaIn the more preferred material.

Here, we review the properties of EGaIn, one of the important components of liquid metals, and its applications in multiple fields, including applications in the field of molecular electronics that are often overlooked. We aim to provide a comprehensive overview of essentially all the research areas of EGaIn applications, even though more detailed descriptions are lacking compared to recent reviews on liquid metals, which normally focus on one or a few applications. As shown in Figure 1, EGaIn has many excellent properties, such as good

1. Introduction

Metals can be seen everywhere from industrial production to our everyday life. Traditional coinage metals (such as gold and silver) have high conductivity, for several applications, such as

Z. Zhao, D. Xiang
Institute of Modern Optics and Center of Single Molecule Sciences
Tianjin Key Laboratory of Micro-scale Optical Information Science and Technology
Nankai University
300350 Tianjin, P. R. China
E-mail: 015008@nankai.edu.cn

S. Soni, C. A. Nijhuis
Department of Molecules and Materials
MESA+ Institute for Nanotechnology
Molecules Center and Center for Brain-Inspired Nano Systems
Faculty of Science and Technology
University of Twente
Enschede 7500 AE, The Netherlands
E-mail: c.a.nijhuis@utwente.nl

T. Lee
Department of Physics and Astronomy
Institute of Applied Physics
Seoul National University
Seoul 08826, Korea

 The ORCID identification number(s) for the author(s) of this article can be found under <https://doi.org/10.1002/adma.202203391>.

DOI: 10.1002/adma.202203391

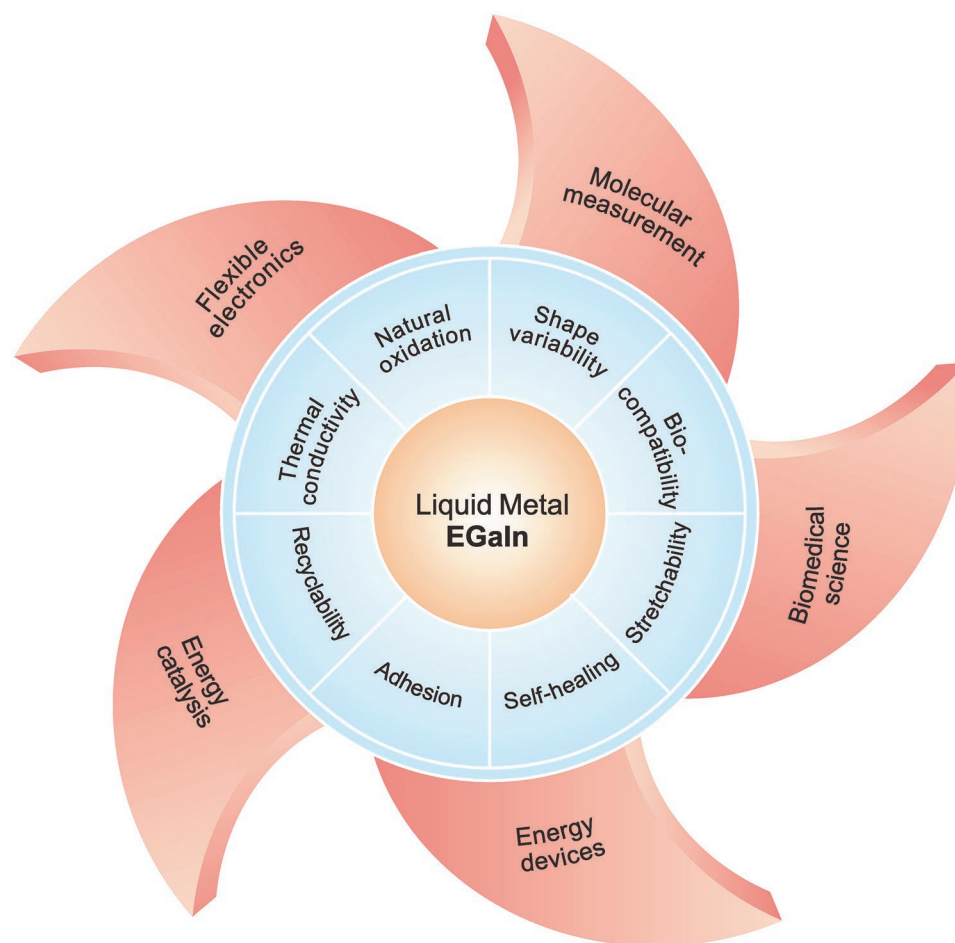


Figure 1. Summary of the properties and related applications of EGaln.

electrical and thermal conductivity, stretchability, recyclability, self-healing, and biocompatibility. These properties make it possible to measure molecular layer properties by preparing EGaln tips or using it in microfluidic channels,^[8,11] to prepare sensors, antennas, electronic circuits, and other flexible electronic devices.^[12–22] Furthermore, EGaln can be used for heat management devices, motors, generators, batteries, and other energy devices,^[23–31] or for catalysts to improve catalytic performance.^[32–35] In addition, EGaln can also be used in biomedical sciences^[36–42] for drug delivery, tumor therapy, bioimaging, and neural interfaces, and it also plays an important role in other fields.^[43–45] Thus, the wide applications of EGaln in such numerous fields further showcase that this liquid metal is crucial to the development of new multifunctional devices in the future.

2. Properties of EGaln

A eutectic alloy is a mixture of components with a single melting point lower than its individual components. In this case, Ga has a melting point (mp) of 29.8 °C and In of 156.6 °C, but Ga-In at its eutectic mixture (75.5% Ga and 24.5% In by weight) has an mp of 15.7 °C. As an important family

member of liquid metals, EGaln has most of the properties of traditional liquid metals, such as excellent electrical (and thermal) conductivity, low viscosity, and high fluidity. Beyond the common properties, EGaln has several unique properties, such as instantaneous oxidation, shape variability, stretchability, self-healing, and biocompatibility. We will introduce them one by one in this section.

2.1. Natural Oxidation

The EGaln surface can spontaneously react with oxygen in the air to form an oxide layer with a thickness of about 0.7–3 nm depending on the different environmental conditions.^[46–49] Moreover, it can be formed even at ppm level concentrations of oxygen,^[50] indicating that the oxide layer is always present under ordinary laboratory conditions. This oxide shell acts as a shield between the external environment and bulk EGaln, stabilizing and generating a self-limiting oxide shell.^[49,51] As shown in **Figure 2a**, through transmission electron microscopy (TEM) imaging and element mapping of the surface of EGaln nanoparticles (NPs), it can be seen that the surface oxide layer is mainly composed of gallium oxide.^[46] **Figure 2b** shows the relationship between metal surface oxides and Gibbs free energy,

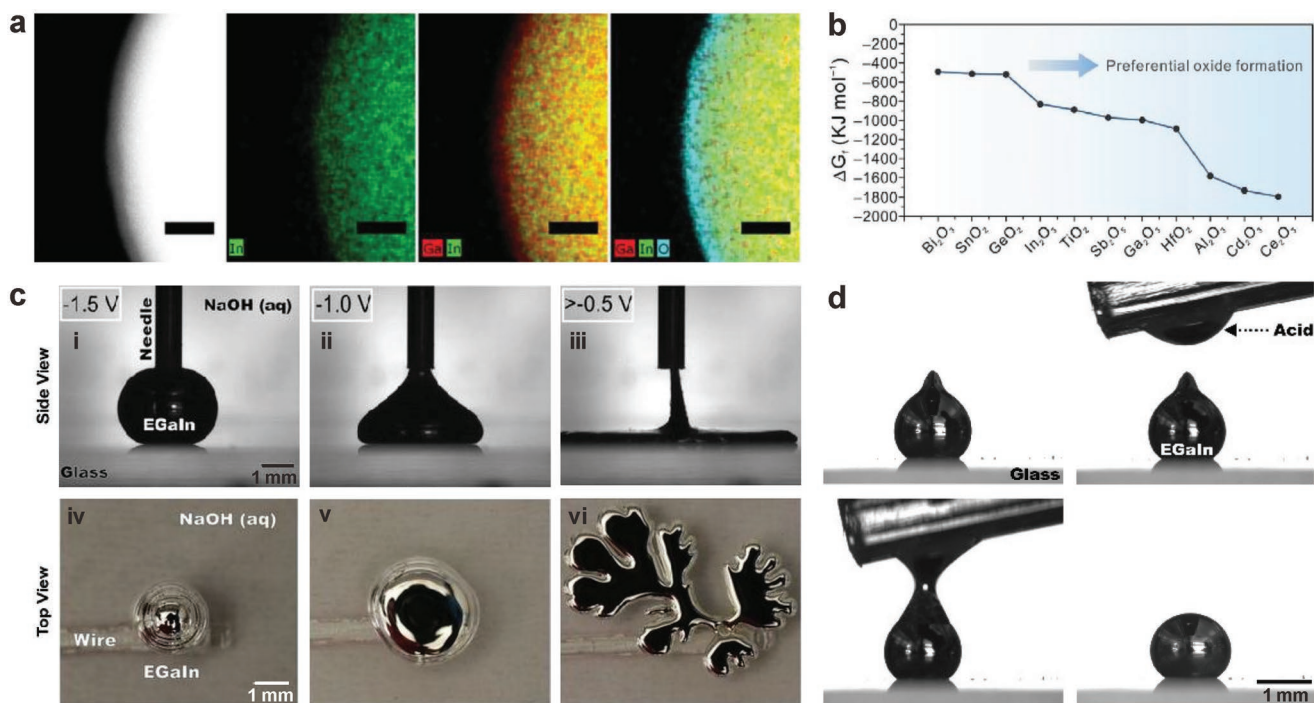


Figure 2. Characteristics of the natural oxide layer of EGaln. a) TEM imaging and element mapping of EGaln nanoparticles. The first column shows the TEM image and the other columns show the element mapping of EGaln nanoparticles. Scale bars: 10 nm. Adapted with permission.^[46] Copyright 2015, Wiley-VCH. b) Gibbs free energy distribution of oxides formed on the surface of different metals. Reproduced with permission.^[51] Copyright 2021, Wiley-VCH. c) The electrochemical formation/dissolution of the oxide layer on the surface of EGaln is controlled by applying a bias voltage in the NaOH solution. Note: The open bias voltage is -1.5 V, which is the potential relative to a saturated Ag-AgCl reference electrode, and means that there is zero external bias at this time. Reproduced with permission.^[56] Copyright 2014, National Academy of Sciences. d) The surface oxide layer can be removed by acid to change the shape of EGaln. Reproduced with permission.^[50] Copyright 2014, American Chemical Society.

which is a thermodynamical parameter that governs the direction of the reaction, where $\Delta G < 0$ indicates that the reaction can proceed spontaneously, so the metal oxide with the largest reduction in Gibbs free energy will cover the surface of the alloy most readily.^[51] It can be seen that the surface of EGaln is more inclined to grow gallium oxide. Although β -Ga₂O₃ is the most stable gallium oxide, it is reported to be amorphous or weakly crystalline due to the free random growth of oxides on the surface of EGaln.^[49,52] Moreover, due to the existence of multiple oxygen vacancies in the naturally grown surface oxide layer, combined with the ultraviolet photoelectron spectroscopy (UPS) and bulk naturally prepared Ga₂O₃ with n-type bandgap, the Ga₂O₃ on the surface of EGaln is reported to be n-type,^[53] and is highly conductive,^[54] because the Ga₂O₃ on EGaln is too thin to form depletion layers and hence it normally form ohmic contacts with most of the target surfaces.^[55]

The presence of the oxide layer on the surface of EGaln creates a solid shell,^[4,57,58] so that it can be formed into various shapes and retain those shapes. The oxide layer can be removed by aqueous acidic or basic solutions, or by electrochemical reduction, as shown in Figure 2c,d. Figure 2c shows that the surface oxide can be dissolved in NaOH aqueous. When the oxidation was increased (from panels i to iii), the deposited oxide gradually reduces the interfacial tension of the EGaln droplets, making the droplets flatten under the action of gravity, reaching a new equilibrium shape. When the potential was increased further, the EGaln continued to flatten and flow in several directions

(panels iv to vi). This indicates that the interfacial tension of EGaln can be modulated electrochemically to generate different shapes.^[56,59,60] In Figure 2d, the non-spherical shape formed under the action of the oxide layer dissolves and becomes a spherical shape after contact with acid. At the same time, the rapidly formed oxide layer keeps the shape stable.^[50] Recently, Amini et al. investigated the physical and mechanical interactions of EGaln with its native Ga₂O₃ layer by depth-sensing nanoindentation (DSN).^[61] They found that the oxide layer is repeatedly ruptured and reformed during the flow, and its existence and chemical properties are directly related to the environment (air or various water environments) and strongly influence the mechanical and interfacial adhesion responses of EGaln.

In addition to the methods described above, the oxide layer on the surface of EGaln can also be manipulated by mechanical deformation, where the surface oxide layer is fragmented under mechanical forces such as stirring or vibration. By modifying the surface of EGaln, its properties can be tuned, so that it can be used in sensors, actuators, biomedicine, and other fields. Common surface modification methods include marbles and ligand binding.^[62–64] Chi et al. constructed tungsten trioxide (WO₃)/EGaln liquid metal marbles by wrapping WO₃ nanoparticles on EGaln micro-nano droplets, which can be used as gas sensors by enhancing the response to gas sensing through efficient interfacial transport.^[65] Lu et al. combined EGaln nanoparticles with drug molecules and ligands, and the prepared nanomedicine could be used for tumor treatment.^[66]

It is worth noting that the interfacial force between the oxide layer shell and the EGaIn core is weak. When an oxygen-containing plate is used to contact the EGaIn surface, the oxide layer and the plate can adhere together due to the van der Waals (vdW) force, making it possible to exfoliate the native oxide layer from the EGaIn surface to be used as a natural 2D material.^[67] It is also possible to use EGaIn as a sacrificial agent to prepare and peel off other types of oxide structures through surface chemical reactions, which provides a method for preparing multiple types of 2D materials (see Section 3.3.2 for details).^[68,69]

2.2. Electrical and Thermal Conductivity

Table 1 summarizes the physical properties of EGaIn relevant for the context of this review. EGaIn has a high conductivity of about $3 \times 10^6 \text{ S m}^{-1}$,^[6] which is close to the conductivity of traditional metals such as silver ($6.3 \times 10^7 \text{ S m}^{-1}$), and much higher than the conductivity of other types of materials, such as poly(3,4-ethylenedioxythiophene)-poly(styrenesulfonate) (PEDOT:PSS), silicon, or insulators it is often encapsulated in such as polydimethylsiloxane (PDMS), as shown in **Figure 3a**.^[70] The high conductivity makes EGaIn widely used in antennas,^[71–73] electronic circuits,^[74,75] sensors,^[76–79] etc. Notably, the conductance of EGaIn can be manipulated using stimuli from the external environment,^[80] such as temperature,^[81] oxidation degree,^[82] and electric field.^[83] Therefore, just like constructing the basis of computing by controlling the voltage of transistors, scientists can control the state of liquid metal by changing the external environment, and take its conductivity difference in different states as a controllable computing logic unit.^[84]

Further, EGaIn is widely used in coolants and thermal interface materials due to its high thermal conductivity (ten times

larger than that of water).^[85–87] As shown in **Figure 3b**, when the EGaIn microdroplets are dispersed in a silicone elastomer to form a liquid metal embedded elastomer (LMEE) composite material, the function of rapid cooling was achieved. Furthermore, when the volume fraction of liquid metal in the composite is 50%, the thermal conductivity of the composite increases as the amount of stretching increases, and the thermal conductivity of the composite is 50 times different from that of the pure elastomer when it is stretched 400%.^[85] This allows the use of EGaIn as a flexible and stretchable soft medium material with high thermal conductivity in soft robots,^[88–90] wearable devices,^[91–94] and other applications.

2.3. Shape Variability

EGaIn can form a mechanically stable structure due to the presence of the surface oxide layer and, therefore, it can be made into various shapes by injection, additive manufacturing techniques, sintering, and other methods,^[12,103] which can be used to fabricate stretchable devices,^[104–106] sensors,^[107] or printed circuits.^[14,108,109]

Figure 4 shows various microstructures formed using EGaIn, including various 2D and 3D structures. A directly printed 3D structure is shown in **Figure 4a**. When multiple EGaIn droplets are in contact with each other, the presence of oxide layer makes it possible to form a free-standing microstructure that does not merge into one large droplet.^[58] **Figure 4b** shows that after EGaIn is injected into microfluidic channels, the mold could be chemically etched away forming a line array microstructure.^[58] Besides, embedding EGaIn into elastomers and polymers can also form free-standing microstructures. Lu et al. used CO₂ lasers to pattern EGaIn embedded in PDMS to prepare elastic microstructures with various sizes and shapes (**Figure 4c**),^[110] which provides a new technology to pattern

Table 1. Physical properties of EGaIn, Hg, Ag, In, Sn, and Bi.

| Physical properties | EGaIn | Hg | Ag | In | Sn | Bi |
|---|---------------------------------------|---------------------------------------|--|--|--|---------------------------------|
| Electrical conductivity [S m ⁻¹] | 3.4×10^6 ^[6] | 1.0×10^6 ^[95] | 6.3×10^7 ^[36] | 1.25×10^7 ^[32] | 8.7×10^6 ^[32] | 9×10^5 ^[32] |
| Thermal conductivity [W m ⁻¹ K ⁻¹] | 26.43 ^[52] | 8.4 ^[96] | 429 ^[52] | 81.6 ^[32] | 66.6 ^[32] | 7.87 ^[32] |
| Melting point [°C] | 15.7 ^[50] | -38.8 ^[95] | 961.8 ^[52] | 156.6 ^[97] | 231.9 ^[97] | 271.4 ^[32] |
| Boiling Point [°C] | 2000 ^[95] | 357 ^[95] | 2162 | 2060 ^[98] | 2260 ^[98] | 1560 ^[98] |
| Density [g cm ⁻³] | 6.25 ^[52] | 13.55 ^[37] | 10.49 ^[52] | 7.31 ^[32] | 7.29 ^[32] | 9.79 ^[32] |
| Specific heat [J Kg ⁻¹ K ⁻¹] | 404 ^[99] | 140 ^[100] | 235 | 233 ^[32] | 227 ^[32] | 122 ^[32] |
| Viscosity [Pa s] | 1.99×10^{-3} ^[57] | 1.53×10^{-3} ^[37] | $\approx 2.8 \times 10^{-3}$ ^[97] | NA | NA | NA |
| Stretchability | $\approx 700\%$ ^[101] | NA | NA | NA | NA | NA |
| Young's modulus [Pa] | 2.1×10^5 ^[91] | NA | $\approx 5 \times 10^9$ ^[97] | 1.1×10^{10} | 5×10^{10} | 3.2×10^{10} |
| Surface yield stress [N m ⁻¹] | 0.5 ^[57] | NA | NA | NA | NA | NA |
| Surface tension [N m ⁻¹] | 0.624 ^[57] | 0.487 ^[37] | NA | 556 (157 °C) ^[98] | 561.6 (232 °C) ^[98] | 270 (382 °C) ^[98] |
| Surface free energy [dynes cm ⁻¹] | 630 ^[6] | NA | NA | NA | NA | NA |
| Sound speed [m s ⁻¹] | 2740 ^[95] | 1450 ^[95] | 2680 | 1215 | 2730 | 1790 |
| Vapor pressure [Pa] | NA | 1 (42 °C) ^[37] | NA | ≈ 13 (1000 °C) ^[98] | $\approx 9.87 \times 10^{-4}$ (727 °C) ^[98] | NA |
| Prandtl number | 0.030 ^[99] | 0.0278 ^[102] | NA | NA | NA | NA |
| Water compatibility | Insoluble ^[89] | Soluble ^[95] | Insoluble | Insoluble | Insoluble | Insoluble |

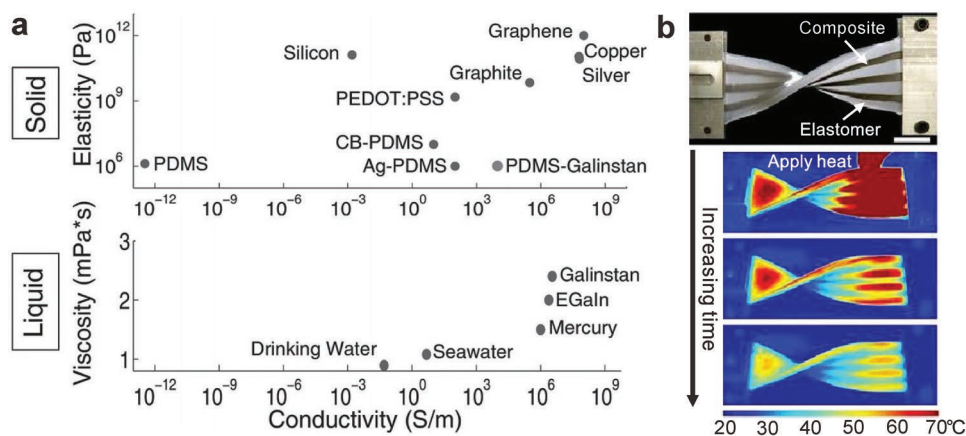


Figure 3. Excellent electrical and thermal conductivity of EGaIn. a) Electrical conductivity (x-axis) and mechanical rigidity and viscosity (y-axis) of different materials, where elasticity refers to modulus. Reproduced with permission.^[70] Copyright 2015, Wiley-VCH. b) Heating of alternating strips of liquid metal EGaIn microdroplet-dispersed elastomer (LMEE) and unfilled elastomer with a heat gun shows that the LMEE composite dissipates heat faster over time (scale bar: 25 mm). Adapted with permission.^[85] Copyright 2017, National Academy of Sciences.

EGaIn. Further, using EGaIn as the printing ink, various complex structures can be created (Figure 4d,e). Mohammed et al. sprayed EGaIn particle ink on a single printing platform, and then mechanically sintered it into conductive patterns, realizing fully automatic printing to prepare complex 2D conductive patterns, such as laboratory gears (Figure 4d).^[104] Park et al. used

EGaIn ink to prepare high-resolution, reconfigurable 2D and 3D hybrid microstructures with an impressive minimum line width for direct printing of 1.9 μm (Figure 4e).^[109] Such free-standing 3D microstructures can effectively reduce the number and space of interconnections, providing a promising avenue for the further integration of electronic circuits.

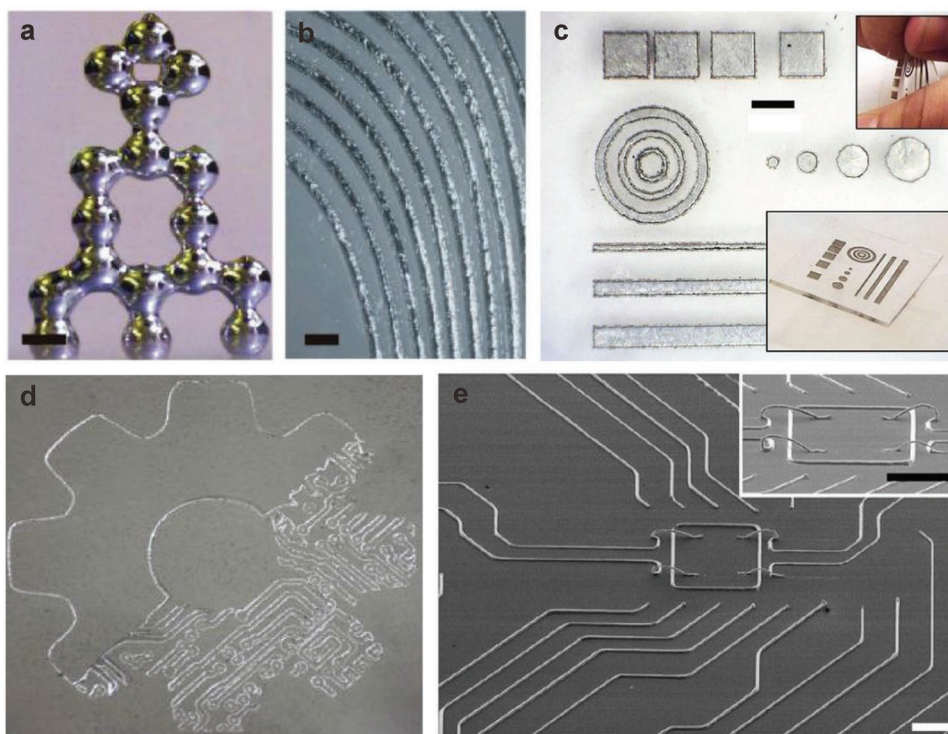


Figure 4. The shape variability of EGaIn. a) Free-standing EGaIn arch microstructure, scale bar: 500 μm . b) EGaIn injected into microchannels and dissolved in the mold to obtain a stable linear array microstructure. Scale bar: 500 μm . Reproduced with permission.^[58] Copyright 2013, Wiley-VCH. c) The elastic composites of various shapes and sizes with embedded EGaIn in PDMS. Scale bar: 2 mm. Reproduced with permission.^[110] Copyright 2014, Wiley-VCH. d) The complex pattern of laboratory gears fully printed by EGaIn. Reproduced with permission.^[104] Copyright 2017, Wiley-VCH. e) SEM image of high-resolution EGaIn 2D and 3D structure. Scale bars: 100 μm . Reproduced with permission.^[109] Copyright 2019, The American Association for the Advancement of Science.

2.4. Stretchability

Traditional rigid metals are usually relatively brittle and do not endure stretching compared to liquid metals, while liquid metals exhibit stretchability and can be used for flexible stretchable devices, improving the durability and service life of the device.^[12,111] As shown in **Figure 5a**,^[101] when EGaln ink is written on a 700% pre-stretched flexible substrate and then the stretch is released to 100%, EGaln lines are still adhered to the substrate and deformed with the deformation of the substrate. However, the resistance of each wire does not change significantly during the stretching process. This behavior indicates the potential of using EGaln wires in stretchable devices. **Figure 5b** shows that the stretchable fiber prepared by using the hollow shell made of elastomer and the core made of EGaln can be flexibly stretched without losing electrical conductivity,^[105] which can be used as stretchable wires for chargers, earphones, and other electrical appliances.

In addition to using EGaln as the conductive core to prepare uniform conductive stretchable wires, EGaln can also be randomly dispersed into a composite or individually adhered to the surface of the elastomer for a stretchable device. **Figure 5c** shows that the liquid metal microdroplets dispersed into an elastomer remain stable even after being stretched by 250–500%.^[112] **Figure 5d** shows that Ag-EGaln serpentine structures printed on an elastomer can deform without breaking under 400% stretching.^[113] Products based on the stretchability of EGaln have great potential in stretchable devices and wearable devices,^[12,91] and are expected to improve their performance.

2.5. Self-Healing

Devices are often unavoidably damaged by the outside world during operation, which makes how to extend the service life

of the devices become a focus of attention. Traditional soft materials are mechanically damaged after repeated stretching and deformation cycles, while liquid metals have become one of the important candidates for repairable devices due to their good self-healing ability. The self-healing of a device can be categorized as autonomous and non-autonomous. Autonomous self-healing means that when the device is damaged it can automatically restore its function without external stimulation. Non-autonomous self-healing means that when the device is damaged it needs external stimuli,^[114] such as high temperature, pH, or ultraviolet light, to realize the self-healing function.

Figure 6a shows an electronic circuit composed of a power supply, self-healing polymer wire and light-emitting diode (LED). The self-healing polymer wire is composed of EGaln injected into Reverlink polymer microfluidic channels. When the wire is disconnected, due to the presence of the oxide layer on the surface of EGaln, EGaln at the disconnect point remains stable and will not shrink or flow out, which enables the self-healing function to be realized when the wire is reconnected, so that the circuit works normally again and the LED lights up again.^[115] **Figure 6b** shows that when the EGaln line is cut by a knife, it can be reconnected by applying pressure.^[111] In a multilayer microelectronic device with EGaln capsules dispersed, even if the crack destroys the conductive path, the broken EGaln will automatically adhere to the damaged area, so that the electrical conductivity in the broken circuit can be automatically restored (**Figure 6c**).^[116] When the circuit is disconnected, you only need to lightly press the two sides of the cut part to realize the self-healing function, and the incision will be invisible under the optical microscope after 13 min, and stretching 60% after 48 hours can also work normally, which can be used for wearable electronic devices.^[117]

Most flexible devices composed of EGaln often require external stimuli or manual intervention to achieve the self-healing function. During the recovery of self-healing, the

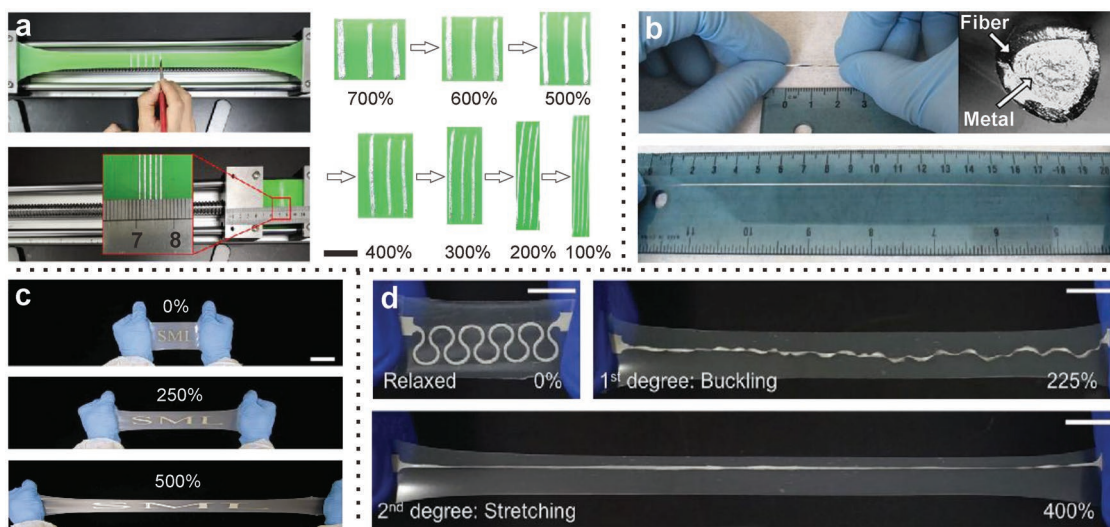


Figure 5. The Stretchability of EGaln. a) Diagram of a device with EGaln lines printed and released on a pre-stretched substrate (left) and its morphological evolution during release (right), scale bar: 1 cm. Reproduced with permission.^[101] Copyright 2019, American Chemical Society. b) A stretchable fiber composed of an elastomer shell and a core of EGaln. Reproduced with permission.^[105] Copyright 2013, Wiley-VCH. c) The change of the elastomer dispersed by EGaln microdroplets under different stretching ratios, scale bar: 5 cm. Adapted with permission.^[112] Copyright 2016, Wiley-VCH. d) Photographs of Ag-EGaln serpentine electrodes on elastic substrates under different stretching ratios, scale bars: 1 cm. Reproduced with permission.^[113] Copyright 2020, Wiley-VCH.

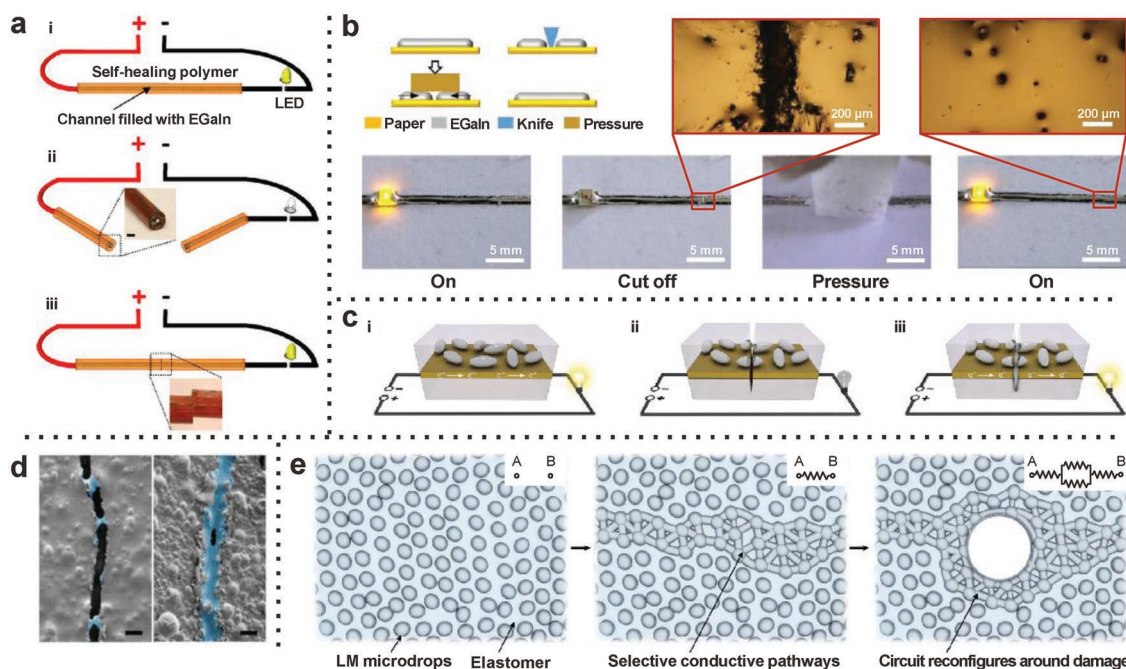


Figure 6. Self-healing ability of EGaIn. a) A schematic diagram of the disconnection and reconnection of self-healing wire of the Reverlink polymer microfluidic channel filled with EGaIn. Scale bar: 5 mm. Reproduced with permission.^[115] Copyright 2013, Wiley-VCH. b) A schematic diagram and pictures of EGaIn line self-healing under pressure. Adapted with permission.^[111] Copyright 2018, Wiley-VCH. c) Schematic diagram of the self-healing of the multilayer microelectronic device composed of EGaIn microcapsules, in which the EGaIn capsules automatically flow to the damaged area after rupture, so that the electrical conductivity recovers automatically. Reproduced with permission.^[116] Copyright 2012, Wiley-VCH. d) The color SEM image of the fractured area of the Ag-EGaIn composite. The EGaIn content on the left image is 30 wt%, and the EGaIn content on the right image is 70 wt%. The blue color represents EGaIn capsules which provide conductive paths in the crack area. Scale bars: 10 μm . Reproduced with permission.^[118] Copyright 2019, American Chemical Society. e) Schematic illustration of the principle of EGaIn-elastomer self-healing in electricity, as electrical stimulation induces reconfiguration around damaged areas. Reproduced with permission.^[88] Copyright 2018, Springer Nature.

device functionality may be temporarily lost. Various composite materials composed of EGaIn are expected to overcome these shortcomings and achieve instantaneous and fully automated self-healing functions. Park et al. used Ag-EGaIn composite materials, which can achieve controllable instantaneous and repeatable self-healing function under environmental conditions. Moreover, as the content of EGaIn capsules in the composite material increases, more conductive paths can be provided in the damaged area, and the self-healing ability can be improved (Figure 6d).^[118] As shown in Figure 6e, Markvicka et al. embedded EGaIn microdroplets into an insulating elastomer to form a composite material. When a conductive EGaIn path is formed, even if the composite material is severely damaged, the current will pass through other EGaIn microdroplets to form a conductive path.^[88]

2.6. Adhesion and Wetting

Liquid wettability refers to its ability to spread on the surface when it is in contact with a solid interface, and it also reflects the strength of adhesion at different interfaces. Generally, it is difficult for liquid metal to wet a non-reactive surface due to its high surface tension, but the presence of a native oxide layer on EGaIn surface has a great influence on its adhesion and wetting characteristics. Adjusting the wettability of EGaIn can have different effects for different applications. For example,

in reconfigurable devices,^[119,120] the adhesion of EGaIn should be minimized to avoid affecting the performance of the device. However, in flexible electronic devices,^[121] it is necessary to increase the adhesion of EGaIn to achieve device stability. Through selective wetting of the substrate, it can be used to prepare a variety of patterns to achieve diversification of device structures.^[120,122] Therefore, addressing how to tune the adhesion and wettability of EGaIn to various substrates is crucial for the fabrication of high-performance reconfigurable and flexible electronic devices.

It is worth noting that there are several promising methods that can change the adhesion and wettability of liquid metals. Contact angle measurements can often quantify the wetting behavior of liquids on surfaces.^[123–125] However, the presence of Ga_2O_3 layer on the gallium-based liquid metal surface complicates the interpretation of contact angle measurements and allows the conventionally measured static contact angle to be manipulated to almost any value, possibly due to the forces created by the syringe tip pulling away from the substrate.^[126] Therefore, traditional static contact angle measurements may not be suitable for characterizing the true contact angle of liquid metals. It is more convincing to use the advancing contact angle or the receding contact angle to characterize its wetting characteristics. Furthermore, due to the pinned oxide skin, it was shown that the receding contact angle does not reach an equilibrium value. Therefore, it is more appropriate to use a stable advancing angle to characterize its wetting characteristics.

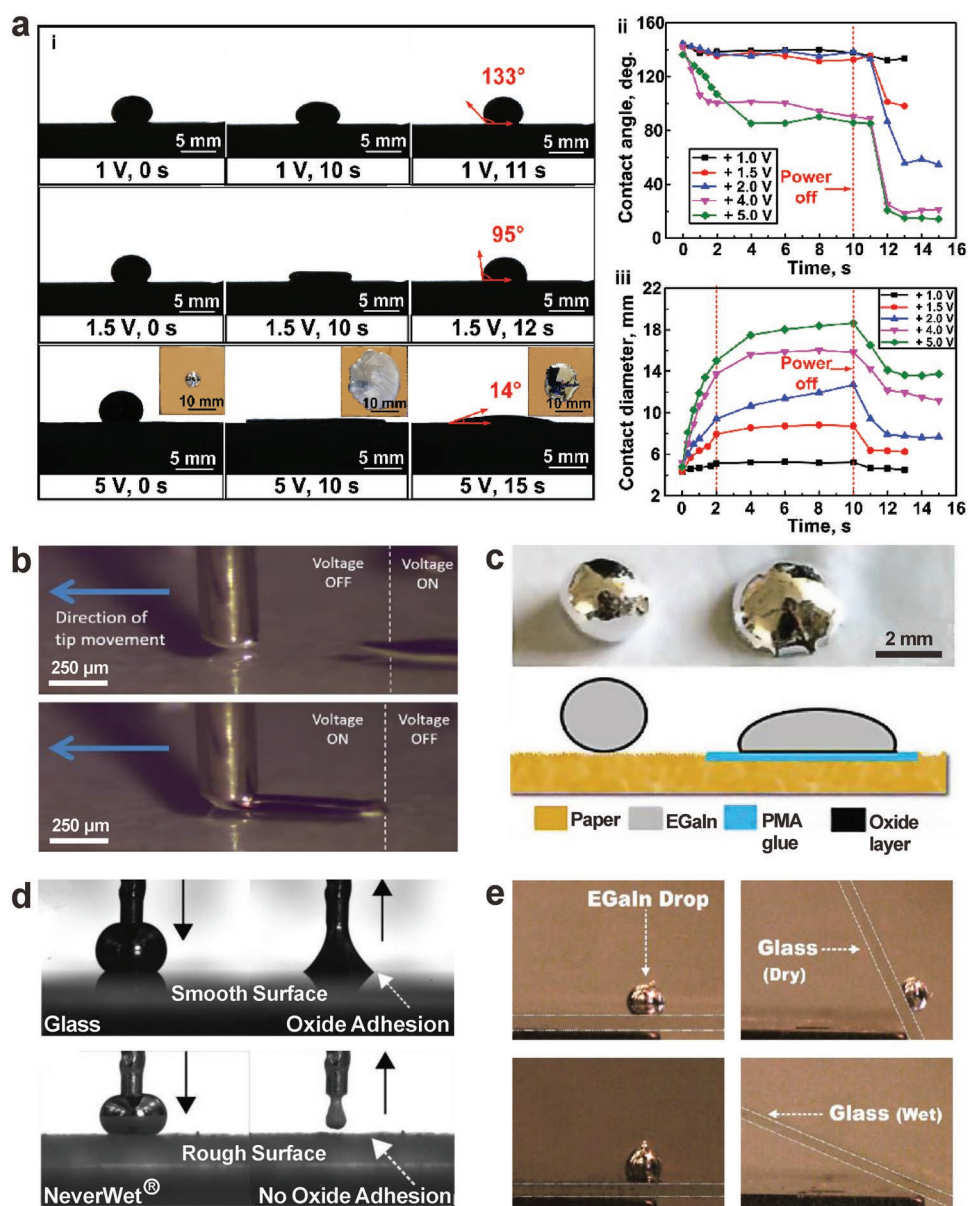


Figure 7. Adhesion and wettability of EGaIn. a) In a 0.5 mol L⁻¹ solution, the substrate is connected to the anode, and the changes in i) droplet profiles, ii) contact angle, and iii) contact diameter with time were reported under different bias voltages. The bias was applied for 10 s. Reproduced with permission.^[127] Copyright 2019, Elsevier B.V. b) An AC bias is applied between the substrate electrode and the EGaIn electrode, separated by a dielectric layer, to control the wetting process of EGaIn. Reproduced with permission.^[131] Copyright 2019, Wiley-VCH. KGaA, Weinheim. c) Photograph and schematic diagram of EGaIn droplets with and without PMA glue on paper. Reproduced with permission.^[111] Copyright 2018, Wiley-VCH. KGaA, Weinheim. d) Different adhesion abilities of EGaIn on smooth glass surfaces and rough surfaces sprayed with NeverWet. Adapted with permission.^[120] Copyright 2018, American Chemical Society. e) Different adhesion abilities of EGaIn droplets on dry and water-moistened glass slides. Reproduced with permission.^[132] Copyright 2014, American Chemical Society.

Figure 7a shows the changes in the morphology, contact angle and contact diameter of the EGaIn droplets under the application of different DC bias voltages in a 0.5 mol L⁻¹ alkaline (NaOH) solution with a Cu substrate connected to the anode, where the bias voltage was applied from 0 to 10 s, and powered off after 10 s.^[127] With the increase of the bias voltage, the contact angle was smaller, indicating that the wettability was enhanced. This is because the native oxide layer on the surface of EGaIn removed by NaOH solution is formed again

due to the anodic bias oxidation, reducing the interfacial tension. At the same time, the interfacial tension gradient formed due to the uneven distribution of OH⁻ ions on the surface of EGaIn promotes the spread of EGaIn to a larger area. When the bias was removed (after 10 s), the droplet tended to shrink back into a spherical shape, and the contact angle was also reduced. This shrinking of EGaIn occurs because the oxide layer on the surface of EGaIn gets redissolved, which increases the tension at the EGaIn-solution interface, and the adsorbed OH⁻ ions

on the surface of EGaIn also get dispersed into the solution. This indicates that in NaOH solution, the wetting properties of EGaIn droplets can be regulated by the bias voltage. The pinning behavior after the retraction of the stage is believed to be caused by the formation of CuCa_2 at the interface between the EGaIn droplet and the Cu substrate due to reactive wetting. Previous studies have shown that the liquid metal EGaIn can react with metals such as Cu and Al under electrochemical conditions,^[128–130] thereby increasing the wettability. This demonstrates that reactive wetting via EGaIn can also be a means of modifying material properties. The wettability of EGaIn can also be controlled by applying AC voltage. Watson et al. applied an AC voltage between the EGaIn electrode and the underlying substrate electrode, separated by a dielectric layer.^[131] The resulting electric field enhances the wettability of the liquid metal, effectively reducing the surface tension between the substrate and the liquid metal, and realizing the electrowetting-assisted selective printing of liquid metal (Figure 7b).

The adhesion properties of EGaIn can also be changed by adding an adhesive layer. The wettability between the EGaIn and paper is poor, while the adhesion to polymethacrylates (PMA) is good, and PMA does not easily adhere to the paper. Guo et al. took advantage of this feature to print the required PMA patterns on paper, and then transfer printed EGaIn to prepare paper electronics based on liquid metal transfer printing technology, as shown in Figure 7c.^[111] The roughness of the substrate surface also has a significant effect on the adhesion of EGaIn.^[123,133] Figure 7d shows that EGaIn droplets adhere to the smooth glass surface with residue oxide adhesion. In contrast, there will be no oxide residue after contact with the glass coated with NeverWet (a commercial superhydrophobic coating), which introduces surface roughness.^[120] When a slip layer such as water is added to the interface, the adhesion properties of EGaIn can also be significantly changed, as shown in Figure 7e.^[132] EGaIn droplets can adhere to the inclined dry glass substrate, but when the glass is immersed in deionized water for wetting treatment, the adhesion reduces significantly. This is because the water changes the chemical composition of the oxide, lowering the critical yield pressure, and weakening its mechanical strength. Adjusting the adhesion and wetting characteristics of EGaIn through electrochemistry, voltage, pressure, rough interface, and slip layer provides new possibilities for future reconfigurable electronic devices, sensors, printing devices, etc.

2.7. Biocompatibility

Traditional biomaterials such as rigid metals, polymers, and ceramics may not work well in the face of some complex medical scenarios, and it is important to avoid immune rejection reaction of the human body when they are applied. In this context, especially compared with the toxic Hg, EGaIn emerges as a non-toxic, biocompatible new generation of intelligent biomaterial potentially interesting for drug delivery applications,^[134] tumor treatment,^[135,136] bioimaging,^[137,138] and other fields.^[139–141]

Figure 8a shows the ion concentration of a Roswell Park Memorial Institute (RPMI) cell culture medium immersed by EGaIn at different periods of time, Figure 8b shows the relative

viabilities of 4T1 murine breast cancer cells in the cell culture medium treated with EGaIn over time, and Figure 8c shows the relative viability of 4T1 and McA-RA7777 rat liver cancer cells in different culture conditions. It was found that the ion release concentration of EGaIn in the cell culture medium has no obvious increasing trend over time, and the relative survival rate of 4T1 cells in the EGaIn-treated cell culture medium does not decrease over time, which shows that EGaIn has no effect on the normal survival rate of cells. In the control group, pure EGaIn with alternating magnetic field (AMF) conditions did not affect the relative viabilities of 4T1 and McA-RA7777 cells. However, when EGaIn and AMF exist at the same time, the relative viabilities of these two kinds of cancer cells are significantly reduced, which can be applied to AMF-induced tumor hyperthermia treatment.^[142]

Although EGaIn is basically non-toxic to mouse cells, its toxicity to human cells remains to be studied. Kim et al. used human HeLa cells and adipose-derived stem cells (ADSCs) to compare the live/dead staining images on the first day and the third day in the growth medium without EGaIn (control group) and with EGaIn (Figure 8d).^[143] The results show that EGaIn is also biocompatible with human cells. They also found that when there was no external agitation, only Ga ions were mainly released from EGaIn, while the concentration of In ions increased dramatically under the action of ultrasound, possibly affecting cell viability. Chechetka et al. also compared the effects of different nanomaterials on the viability of human HeLa cells in an in vitro toxicity test.^[137] As the concentration of nanomaterials such as representative carbon nanotubes and gold nanorods increases, it shows an increasingly adverse effect on cell viability. However, EGaIn nanocapsules with photopolymerization functionalized phospholipid shells have no effect on cell viability.

Furthermore, EGaIn can also form a mixture with other metals to improve the working performance of EGaIn in biological applications while ensuring biocompatibility. Wang et al. reported that Mg-EGaIn mixtures with different doping ratios of Mg particles can significantly increase the photothermal conversion rate (PTC) and thus be applied to the photothermal treatment of tumors in vivo.^[144] In the in vitro toxicity test experiment, this mixture showed biological compatibility (Figure 8e). Among the Mg-EGaIn with different doping ratios of Mg particles, the rare dead cells in the fluorescence image of human melanoma C8161 cells and the cell viability after 12, 24, 36, and 48 h of culture were nearly 100%, indicating its safety in biological applications.

2.8. Recyclability

In today's world, the rise of electronic waste and the resulting increase in environmental pollution has inspired research communities to seek functional devices that can assist green, sustainable, and environment-friendly development. When the liquid metal composite device dissolves, it can recover easily because the liquid metal can flow, realizing the recyclability of the device. The devices based on EGaIn are widely considered because of their recyclability and degradability,^[145–147] which can support green development and reduce costs.

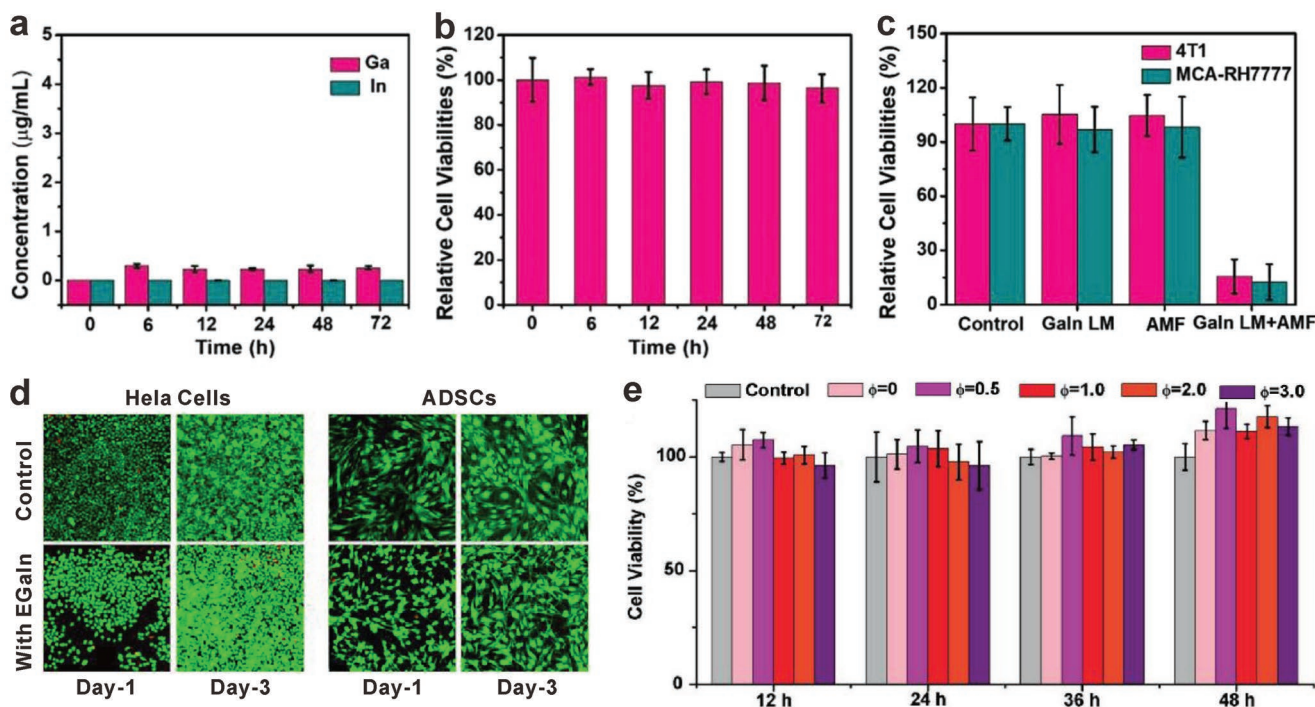


Figure 8. Biocompatibility of EGaIn. a) Ion concentration of RPMI cell culture medium immersed by EGaIn for different periods. b) The relative viabilities of 4T1 murine breast cancer cells in the cell culture medium treated with EGaIn over time. c) The relative viabilities of 4T1 (rat liver cancer cells) in natural control group, only EGaIn, only alternating magnetic field (AMF), and EGaIn with AMF. Reproduced with permission.^[142] Copyright 2020, Wiley-VCH. KGaA, Weinheim. d) Fluorescence images of human HeLa cells and adipose-derived stem cells (ADSCs) in growth media without EGaIn (control group) and with EGaIn at different periods. Adapted with permission.^[143] Copyright 2018, American Chemical Society. e) Cell viability of C8161 cell culture medium immersed in EGaIn with different Mg particle doping ratios (ϕ) at different periods. Reproduced with permission.^[144] Copyright 2018, Wiley-VCH. KGaA, Weinheim.

Figure 9a shows that in an electronic device composed of a LED connected with Fe particles doped EGaIn (Fe-EGaIn) in a polyvinyl alcohol (PVA)/fructose film,^[148] the PVA/fructose film can be completely dissolved in 205 s in an aqueous solution, causing the structure to be destroyed, turning the LEDs off. Notably, the oxide layer is less passivating in water.^[132] The Fe-EGaIn droplets and LED deposited on the bottom of the beaker can be recycled again for the preparation of another set of LED array devices. Moreover, this LED array circuit can also be rapidly degraded in the grass, as shown in Figure 9b. When water was sprinkled on the device to simulate a rainy scene, the device was dissolved in 85 s. Recently, Zhang et al. printed Fe-EGaIn on a laser-patterned silicone substrate to prepare electronic circuits.^[149] The fabricated device could be degraded within 30 min under the action of ultrasound in an ethanolic solution. This is because EGaIn can be dissolved in ethanol by ultrasonication and dispersed into particles. When the ethanol evaporates, the remaining EGaIn particles and LED lights can be recycled and reused (Figure 9c).

The mixture of EGaIn with biological nanofibers can also achieve this function of biodegradation. Figure 9d shows that EGaIn and cellulose nanofibers can be completely degraded in natural soil within 15 days, which provides a new way for biodegradable composite devices.^[150] For the EGaIn wire on the paper and polymethacrylates (PMA) glue, since the oxide on the EGaIn surface can be dissolved by the acid solution, the HCl solution destroys the adhesion between EGaIn and PMA glue,

thereby removing the EGaIn adhered to the PMA glue, recycling EGaIn and greatly reducing the cost of liquid metal paper electronic products.^[111] Furthermore, EGaIn-based devices can also be degraded via combustion. Guo et al. used Ni-EGaIn semi-liquid-metal to prepare flexible electronic devices on paper, which can also achieve device degradation through combustion (Figure 9e).^[151]

3. Applications of EGaIn

EGaIn has been shown to be a very useful in molecular electronics (ME) as a top electrode, for contacting soft organic materials and probing their intrinsic properties, as reported by our group^[152–154] and several other groups.^[155–157] As reviewed in Section 2, EGaIn has interesting properties which make it suitable for a large variety of applications which are discussed in this section. This section also introduces the working principles of EGaIn used in these applications briefly.

3.1. Top Electrode for Molecular Electronics

The rapid development of electronic communication and computation technologies has put forward higher requirements for the evolution of electronic devices. The need for power-efficient and further miniaturized electronic devices has become

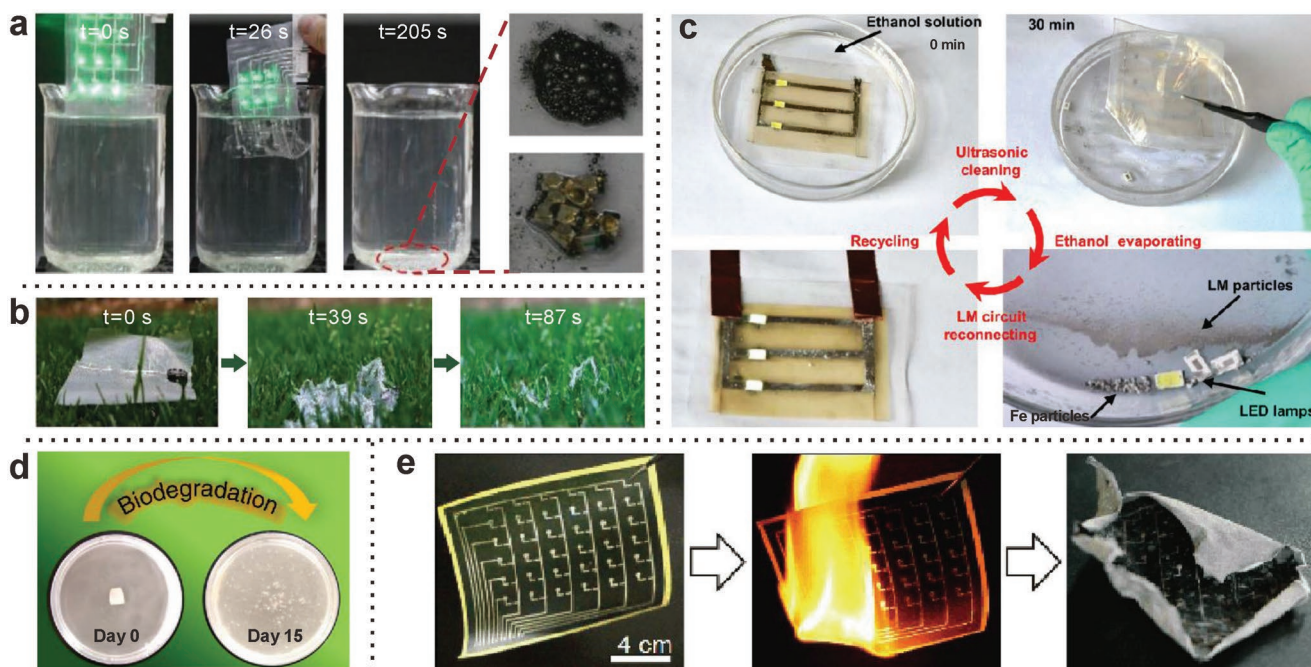


Figure 9. Recyclability of EGaIn. a) The process of dissolving and recycling the LED array composed of Fe particles doped EGaIn (Fe-EGaIn), PVA/fructose film in an aqueous solution. b) The degradation process of the Fe-EGaIn LED array in the grass. Adapted with permission.^[148] Copyright 2019, Wiley-VCH, KGaA, Weinheim. c) The biodegradation process of the mixed film of EGaIn and cellulose nanofibers (CNFs) in natural soil. Reproduced with permission.^[149] Copyright 2021, IOP Publishing. d) The cyclic process of Fe-EGaIn electronic circuit on a laser-printed silica gel substrate. Reproduced with permission.^[150] Copyright 2019, Springer Nature. e) Burning degradation process of Ni-EGaIn thread printed on paper. Reproduced with permission.^[151] Copyright 2019, Springer Nature.

inevitable. At present, traditional electronic devices based on semiconductor materials such as silicon and germanium face severe challenges. These challenges include both theoretical physical limitations and technical process limitations.^[158,159] In addition to the above limits, as the size of the chip decreases the cost of chip fabrication also increases.^[160] One of the ways to solve the above problems is to develop integrated circuit technology based on ME devices, and aim to realize high-tech products that are smaller in size, lower in power consumption, are environmentally friendly, but more importantly, provide unconventional molecule-based functionalities that are complementary to traditional (silicon-based) electrical devices.^[161]

In a narrow sense, ME devices use organic functional molecular materials to construct various components in electronic circuits, such as molecular wires,^[162,163] molecular switches,^[140,164–167] molecular diodes,^[168–171] molecular field-effect transistors,^[172,173] or molecular memory devices.^[174,175] Its ultimate goal is to replace or complement solid-state electronic components such as silicon-based semiconducting transistors with single molecules, supramolecular assemblies or molecular ensembles to assemble logic circuits, resulting in operational, multi-functional ME devices. At present, the research on a diverse range of ME materials and their device applications has attracted great attention from scientists from all over the world.

So far, the mature methods to measure the characteristics of molecular junctions include mechanically controllable break junctions (MCBJ),^[84,176,177] scanning tunneling microscope break junctions (STM-BJ),^[178,179] EGaIn-based molecular tunneling junctions (MTJs),^[180,181] to name a few.^[161,182] Currently,

the most common way of incorporating EGaIn in ME devices is to measure the current-voltage characteristics of a molecular layer by either constructing a cone-shaped EGaIn tip or by using microfluidic channels filled with EGaIn as a top electrode to complete the MTJ.^[140,183,184] Both of these techniques will be discussed in more detail below.

3.1.1. EGaIn Tip as Top Electrode

The use of EGaIn to study the tunneling properties of MTJs was first proposed by the Whitesides Group.^[6] In their work, Chiechi et al. obtained ultra-flat bottom electrode surface through the template-stripped method and used EGaIn as the top electrode to measure the tunneling characteristics of a self-assembled monolayer (SAM) of n-alkanethiolates (C_nSH). It was demonstrated that compared to the traditional use of mercury as a soft-contact top electrode for measuring molecular layers,^[185] the use of EGaIn has the following advantages: i) EGaIn is non-toxic and safer to handle, ii) EGaIn can easily be molded into a tapered tip (due to the presence of the native oxide layer as discussed in Section 2.3), forming a smaller contact area than the spherical mercury electrodes, and iii) EGaIn MTJs are more stable than the mercury junctions, providing higher yields of working devices.

Figure 10a shows the formation of a conical EGaIn tip.^[49] By extruding a droplet from a syringe containing EGaIn on a metal-plated substrate, when the substrate is moved away from the needle tip, the EGaIn droplet adheres well to the metal

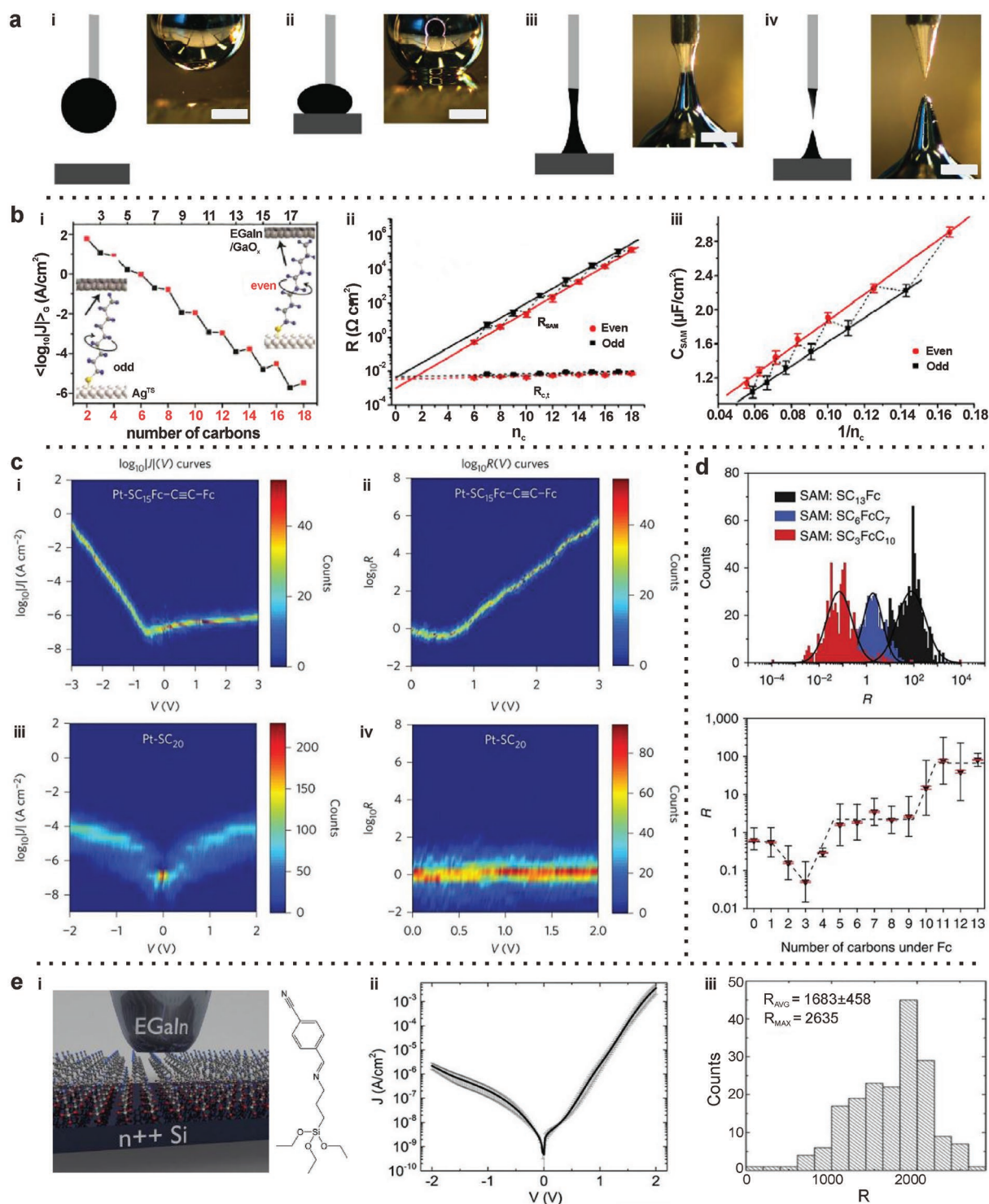


Figure 10. The top EGaIn tip electrode used to measure molecular layer properties. a) The preparation process of the EGaIn tip. Scale bars: 500 μm. Reproduced with permission.^[49] Copyright 2012, American Chemical Society. b) Measurement of the odd–even effect of alkanethiolates containing different carbon atoms on Ag^{TS} substrates: i) parity characteristics of charge transport; ii) parity characteristics of R_{SAM} and SAM-top EGaIn electrode resistance ($R_{C,t}$); iii) parity characteristics of C_{SAM} . Reproduced with permission.^[186] Copyright 2015, American Chemical Society. c) Comparison of rectification characteristics of CnSH SAMs with (i and ii) and without (iii and iv) ferrocene headgroups on Pt substrate. Reproduced with permission.^[153] Copyright 2017, Springer Nature. d) Manipulating the molecular rectification behavior by controlling the position of the ferrocene group along the length of the alkanethiol chain on Ag^{TS} substrate. Reproduced with permission.^[196] Copyright 2015, Springer Nature. e) Measuring the rectification characteristics of the CPh-TPI molecular layer on a doped-Si substrate: i) schematic diagram of CPh-TPI molecule and experimental structure; ii) the measured current density–voltage (J – V) characteristics of the CPh-TPI molecular layer; iii) histogram of SAM rectification. Reproduced with permission.^[197] Copyright 2019, American Chemical Society.

substrate, forming an hourglass-like shape, breaking into a conical EGaIn tip. By replacing the substrate with a target substrate containing a SAM followed by bringing the EGaIn tip in contact with the SAM, an MTJ of the form EGaIn/Ga₂O₃//SAM/Au^{TS} is formed (where, “/” and “//” represent covalent and van der Waals interactions, respectively and Au^{TS} is the template-stripped Au substrate). The current–voltage (*I*–*V*) characteristics of these MTJs can be measured by applying a voltage between the EGaIn and Au^{TS} substrates. Figure 10b shows the *I*–*V* measurements of junctions with monolayers derived from *n*-alkanethiols with the increasing number of carbon atoms on Ag^{TS} substrate, which was prepared using an annealing step before template-stripping.^[186] The C_{*n*}SH molecules form a covalent bond at the SAM–Au interface via a metal thiolate bond, while the C_{*n*}SH SAM interfaces with the EGaIn top electrode through van der Waals interactions. By applying a voltage between EGaIn and Ag^{TS}, and estimating the contact area by a microscope, the current density (log|*I*|) of the molecular layer was measured. It is interesting to find that the current density decreases in a zigzag shape with the increase of carbon atoms, with the contact resistance (*R*_{SAM}) and capacitance (*C*_{SAM}) also showing the same trends. Via impedance measurements and equivalent circuit analysis, it can be inferred that these odd–even effects are mainly driven by intrinsic odd–even effects in the SAM packing energies and contact resistance.^[11,186,187] Later, further experiments^[188–192] and simulations^[193–195] also proved the existence of similar parity effects in other types of junctions including molecular diodes.^[154,190]

EGaIn tip as a top electrode has also been used to develop molecular diodes with a thickness of just 2 nm that work as well as diodes based on semiconductors with associated thick depletion layers that can extend for hundreds of nanometers.^[169,198] Figure 10c shows a comparison of the rectifying properties of SAMs of ferrocenyl (Fc)-terminated C_{*n*}SH (FcC_{*n*}SH) with C_{*n*}SH SAMs on Pt substrates.^[153] By introducing positively charged Fc headgroups at the end of the molecular chain, the charge transport mechanism under positive and negative bias switches between coherent and incoherent tunneling, respectively, resulting in rectification ratios of five orders of magnitude. By adjusting the position of the Fc group along the length of the alkane chain, the magnitude of rectification can be varied and the direction of rectification can be reversed (Figure 10d).^[196] This high rectification ratio is close to that of conventional commercial diodes with a rectification ratio of 10⁵–10⁸ based on Schottky^[199] or P–N junctions.^[200] These works show that EGaIn provides an accessible platform for the study and design of molecular controllable rectifier devices.

In addition to using common sulfhydryl bonds to connect to metal electrodes, researchers have also investigated several other anchoring groups.^[201–203] Lampert et al. used (E)-1-(4-cyanophenyl)-*N*-(3-(triethoxysilyl) propyl) methanimine (CPh-TPI) molecules with triethoxysilane anchoring groups, which can form chemical bonds with Si substrates (Figure 10e).^[197] which can be well combined with current Si-based devices, making the fabrication of hybrid devices simple. However, its rectification rate is about 10³, and further research is needed to meet the requirements of commercial application.

Based on the cone-shaped EGaIn top electrode, apart from rectification behavior, many properties of the charge transport

of molecular layer devices have also been measured, such as the influence of anchoring groups,^[204,205] influence of head-group substituents,^[206–211] influence of environmental effects,^[156,212,213] influence of thermal gradients for thermoelectric effects,^[157,214] influence of bottom substrates,^[215–217] quantum interference effects,^[218–221] influence of dielectric properties of SAMs,^[54,222,223] etc. Recently, Li et al. introduce transition metal ions at one end of the molecule and used charge tunneling current density to study the non-covalent binding of ligands on the surface of the molecular layer, which provides a new tool for analyzing surface composition that undergoes reversible chemical reactions with species in solution.^[224]

3.1.2. EGaIn Microfluidic Channel Top Electrode Junction

EGaIn can be injected into a microfluidic channel under external force because of its fluidity. Meanwhile, the existence of the native oxide layer on the surface of EGaIn makes its structure stable in these channels, so that a variety of microfluidic channel-based devices can be prepared, such as antennas,^[71,72,225] optical elements,^[226] electrical elements,^[227,228] and heat transfer elements.^[87,99,229]

After employing the EGaIn tip to measure the properties of the molecular layer, the Whitesides group further develop this strategy by injecting EGaIn into microfluidic channels to use them as top electrodes and measure the rectification characteristics of SAM-based MTJs.^[230] Figure 11a shows a SAM-based array junction fabricated by lithography techniques, and an enlarged optical microscope image of the junction, where EGaIn is injected into the microfluidic channel as the top electrode, and the width of the channel and bottom electrode define the active junction area.^[230] When using the array junction to test the characteristics of the SC₁₁Fc molecular layer, the difference in transport mechanism for positive and negative bias makes the current density–voltage (*J*–*V*) curves of the molecular layer exhibit rectification behavior (Figure 11b), similar to our discussion in the previous Section 3.1.1.

In order to reduce the influence of junction defects on the measurement results and improve the repeatability of the electrical characteristics of the molecular junction, Wan et al. improved the microfluidic channel junction to achieve reversible electrical contact. They show that the top electrode of a single EGaIn microfluidic channel can be reversibly placed on and moved from the Ag^{TS} substrate to repeatedly make junctions, see Figure 11c.^[231] This method does not require the patterning of the bottom electrode, reduces the residual photoresist and the edge disorder of SAMs during the patterning of the bottom electrode, significantly improving the yields of working junctions (≈78%) to measure the *I*–*V* characteristics of the C_{*n*}SH MTJs. Later, they further built an array of microfluidic channel junctions on this basis, which can not only be placed and moved reversibly, but can also acquire a large number of data quickly and accurately at the same time (Figure 11d).^[232] Afterward, Karuppanan et al. introduced AlO_{*x*} micropores into the preparation process of the electrode junction on the top of the EGaIn microfluidic channel, which reduced the influence of leakage current and stray capacitance, broadening the temperature test range (8.5–300 K), and explored the influence

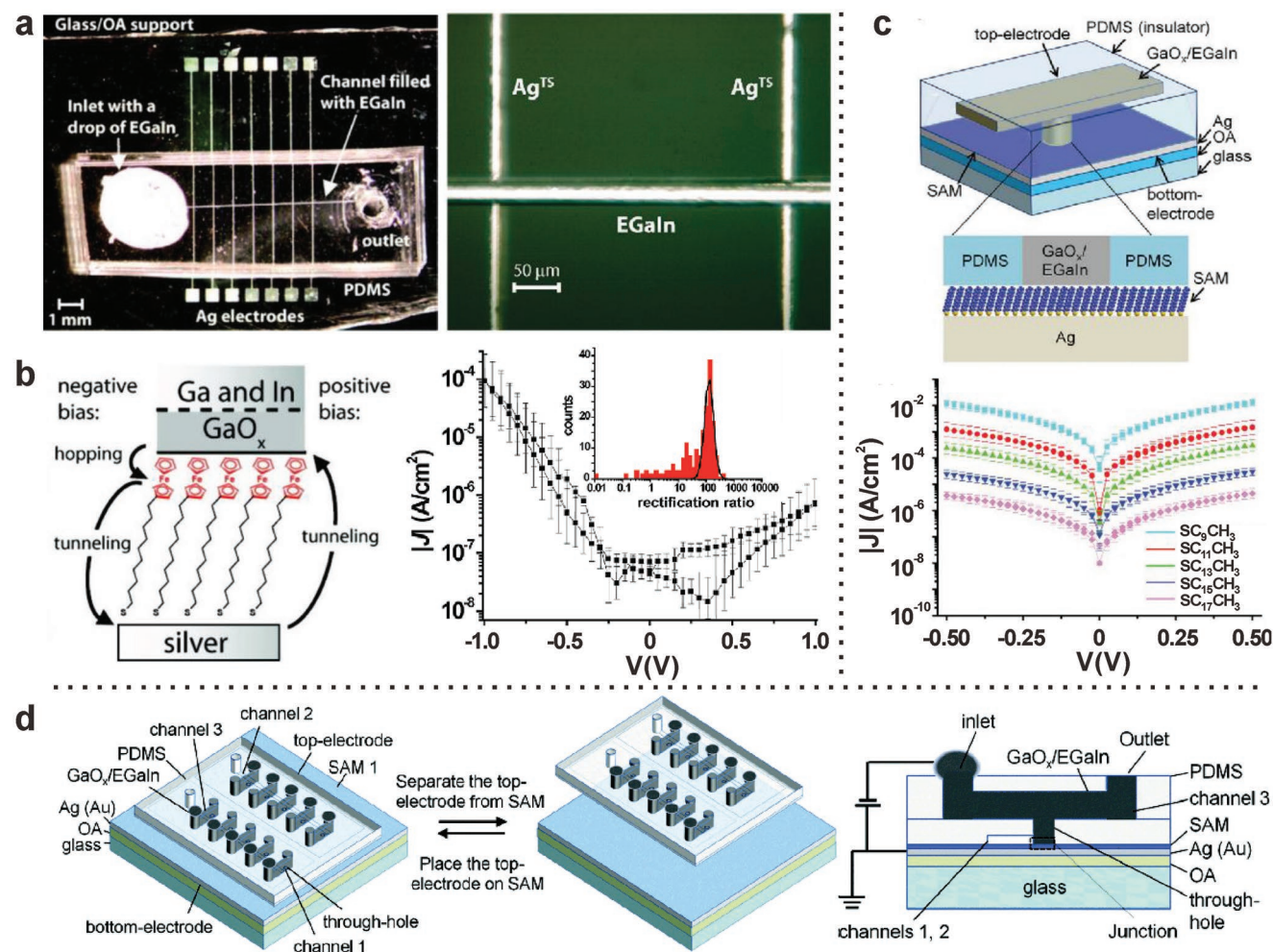


Figure 11. Microfluidic channels filled with EGaIn used as a top electrode to measure the I - V characteristics of molecular layers. a) The optical microscope image of the molecular junction array device (left) and the enlarged image of the EGaIn/Ga₂O₃/SAM/Ag MTJ (right). b) Schematic diagram of the structure of the SC₁₁Fc molecular layer measured by the array junction device (left) and the current density–voltage (J - V) curve and rectification rate distribution diagram (right). Reproduced with permission.^[230] Copyright 2010, American Chemical Society. c) Schematic diagram of the microfluidic top electrode junction (top) and the J - V curves of C_{*n*}SH SAM (bottom). Reproduced with permission.^[231] Copyright 2014, Wiley-VCH. KGaA, Weinheim. d) Schematic diagram of a reversibly placed microfluidic top electrode array junction, where channel 3 is used to fill EGaIn and a vacuum is applied to channels 1 and 2 such that the EGaIn in channel 3 completely fills the small-sized through-holes to serve as the top electrode. Reproduced with permission.^[232] Copyright 2015, The Royal Society of Chemistry.

of the fabrication process and surface roughness on electrical response characteristics.^[233]

Compared with the MTJs with EGaIn tips, although the fabrication process of EGaIn microfluidic channels is more complicated and requires cleanroom environment, its enhanced mechanical stability and well-defined contact area make it a useful technique also for other experiments, such as impedance and temperature-dependent I - V measurements,^[187] investigation of biomolecule-based MTJs,^[234,235] reconfigurable molecular ensembles,^[236] surface plasmon studies,^[237] etc. Although these two methods have similar performance in the measurement of molecular layer charge transport characteristics, the error in the measurement data of the microfluidic channel junctions can be relatively smaller.^[184] However, since the fabrication and measurements of MTJs with an EGaIn tip can be performed in an ordinary laboratory environment, this measurement method seems to rapidly increase in popularity.

3.1.3. Functional Molecular Devices with EGaIn

The advent to discover new functional MTJs has led to the development of next-generation devices where intrinsic molecular functionality can be utilized for newer circuit features. Further, recent advancements in our understanding of utilizing EGaIn as a top electrode in the device and elucidating molecule-EGaIn interaction have aided in functional molecular devices. For instance, a recent work from our group on MTJs comprising SAMs of methylviologen-terminated alkylthiols, with different counterions, showed dynamic one diode-one resistor (1D-1R) molecular memory behavior, as shown in Figure 12a.^[165] Large resistive on/off ratio and rectification ratios were reported, where these two-terminal MTJs were shown to exhibit dual functionality with conical EGaIn tips as well as with EGaIn stabilized in microfluidic channel devices, where 2.0×10^6 voltage sweeps could be performed, showing long term retention

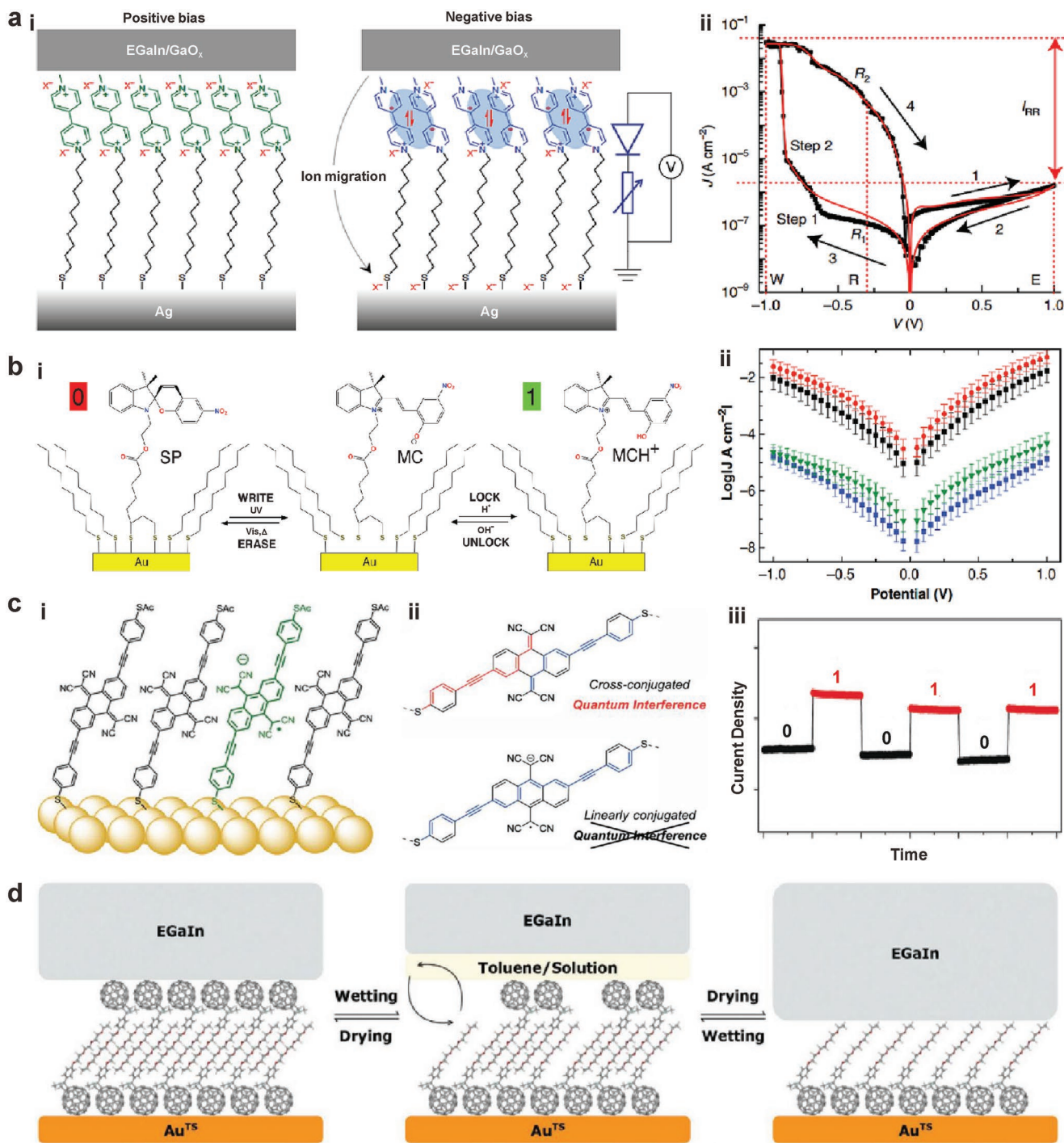


Figure 12. Functional MTJs with EGaIn top electrode. a) Demonstration of a dual functional 1D-1R molecular memory: i) methylviologen-terminated alkythiols in MTJs under positive and negative bias; ii) the J - V characteristic showing hysteresis and rectification. Reproduced with permission.^[165] Copyright 2020, Springer Nature. b) A 3-state molecular switch based on spirocyanine \leftrightarrow merocyanine photoisomerization, where (i) shows the two molecular conductance states, and (ii) J - V characteristics of differently reached ON-OFF states. Reproduced with permission.^[238] Copyright 2019, Wiley-VCH. KGaA, Weinheim. c) Two-terminal molecular memory based on destructive quantum interference showing i) the molecular structure in neutral and reduced states, ii) differences in quantum interference induced by cross-conjugated neutral and linearly conjugated reduced forms, iii) two-terminal molecular memory realized by reversible switch. Reproduced with permission.^[220] Copyright 2018, Wiley-VCH. KGaA, Weinheim. d) In operando switching of rectification in an EGaIn-based bilayer device by swapping the top layer. Reproduced with permission.^[236] Copyright 2020, Wiley-VCH.

characteristics with number of voltage sweep cycles as well as time. In addition to using electric field to manipulate molecular switches, light and pH can also be used to realize the switching function. Kumar et al. studied spiropyran (SP) \leftrightarrow merocyanine (MC) molecular switches that can switch between conductance states via photoisomerization,^[166,167,238] where the high conducting SP state converts to low conducting MC state upon illumination with UV light and back with white light (Figure 12b).^[238] The MC form converts back to SP form gradually at room temperature but can be locked in the MC form upon treatment with acid and unlocked by treatment with base. This process was utilized to encode ASCII data on a molecular punch card via the write-read-erase-read (WRER) operational cycle.

In another work, Carloti et al. demonstrated a two-terminal, non-volatile molecular memory in conical tip-based EGaIn MTJs (Figure 12c).^[220] utilizing destructive quantum interference, which is mostly used for fundamental ME investigations.^[218–221] The authors used conjugated molecular wires with symmetric thiol anchoring groups and the core based on a cross-conjugated tetracyano-anthraquinone moiety. It was demonstrated that the molecular core gets readily reduced by taking an electron from the Au^{TS} substrate, converting to linear conjugation, and losing quantum interference, increasing the molecular conductance. At negative bias the molecule converts back to its pristine cross-conjugated state with lower conductance because of destructive quantum interference, resulting in a hysteresis. Besides, the authors also constructed a vertical molecular transistor based on quantum interference.^[239] In another work, Qiu et al. used self-assembled bilayers^[201] and demonstrated in operando switching of rectification in microfluidic-stabilized EGaIn channels (Figure 12d).^[236] The authors demonstrated a working device where the top layer could be exchanged for different functional molecules, in operando switching the device behavior from a resistor to a rectifier. In our recent work on the detection of surface plasmons in SAM-based MTJs with EGaIn top electrode, we demonstrated that the direction of emitted plasmons could be entirely controlled by molecules in the junctions.^[237]

3.2. Flexible and Stretchable Electronics

Flexible and stretchable electronics play an important role in the development of sensors,^[240–244] antenna,^[245,246] electronic circuits,^[74,247] and area which is a natural fit for liquid metals. This section reviews the recent developments of flexible and stretchable electronics based on liquid metals, and we discuss the opportunities as well as challenges for this new generation of soft electronic devices.

3.2.1. Sensors

Typically, a sensor is a kind of device that can sense external physical quantity and convert it into an electrical signal or other signal output. Common flexible sensors based on EGaIn are strain sensors,^[248–251] pressure sensors,^[77,107,252,253] tactile sensors,^[254–256] or temperature sensor.^[257] Figure 13a shows that a

hydrogel composed of EGaIn and acrylic acid can be used as a wearable strain sensor,^[258] which can detect the bending of fingers and wrists via monitoring the changes in electrical resistance. Strain sensors can also detect human movement through changes in capacitance. As shown in Figure 13b,^[259] when EGaIn droplets are dispersed into the elastic body to form a soft material composite, they can be attached to the finger joints, the hand movement can be detected by the change of capacitance caused by the deformation of the sensor at the finger joint when grasping objects of different sizes.

Figure 13c shows a liquid metal elastic foam (LMEF) soft capacitance tactile sensor array composed of EGaIn droplets, sugar particles and uncured Ecoflex used to detect different touch positions by a human finger.^[260] Upon a finger touch, air with lower relative dielectric permittivity (ϵ_r) is squeezed out of the foam due to the applied pressure, increasing ϵ_r and concomitant change in the capacitance at the touch position, realizing the detection of its location. Besides, by incorporating EGaIn and a thermochromic material into a silicone elastomer, it can also be used for temperature and tactile sensing (Figure 13d).^[261] The local Joule heating caused by currents in EGaIn wires can change the temperature of thermochromic material in the outer layer and cause different discolorations. Furthermore, it can also be used as a tactile logic device. By providing different logic inputs in the form of pressing either region A or B or both, the current will be redirected to area C to cause a color change.

Further, Liu et al. showed that by embedding the 3D spiral channel filled with EGaIn into a PAA-alginate hydrogel, it can also be used as a pressure sensor (Figure 13e).^[262] The working principle proposed by the authors suggests that resistance varies differently under different pressures. This kind of hydrogel pressure sensor has the advantages of fast response speed (≈ 0.1 s) and high sensitivity (≈ 100 Pa), which provides the possibility for future applications in heartbeat and blood pressure monitoring. Cai et al. constructed a flexible composite sponge by incorporating gallium micro-nano droplets into a deformable polyurethane sponge and found that its resistance decreased with the increase of applied pressure, thus demonstrating its utility as pressure sensors.^[265] Compared to elastomers, this composite sponge exhibits good elastic recovery ($\approx 90\%$) and conductive durability without sacrificing structural integrity. Besides, the reversible change in the resistivity range is also significant.

Kim et al. showed that an all-soft microfluidic capacitive sensing platform composed of EGaIn and PDMS can be used for liquid and gas phase volatile organic compound (VOC) detection (Figure 13f).^[263] For liquid-phase VOC detection, solvents with different dielectric constants, such as isopropanol (i-PrOH), ethanol (EtOH), and methanol (MeOH), were used to directly contact EGaIn. Different solvents could be distinguished effectively by measuring the change in capacitance. For gas-phase VOC detection, the different diffusion coefficients of different gases in the sensing film made it possible to detect i-PrOH, EtOH and MeOH gases. By in situ growth of polyaniline nanofibrous on EGaIn nanoparticles, the prepared hybrid liquid metal-polymer nanocomposites can also be used for gas sensing and temperature sensing, in which the presence of EGaIn effectively enhances the temperature and gas sensitivity

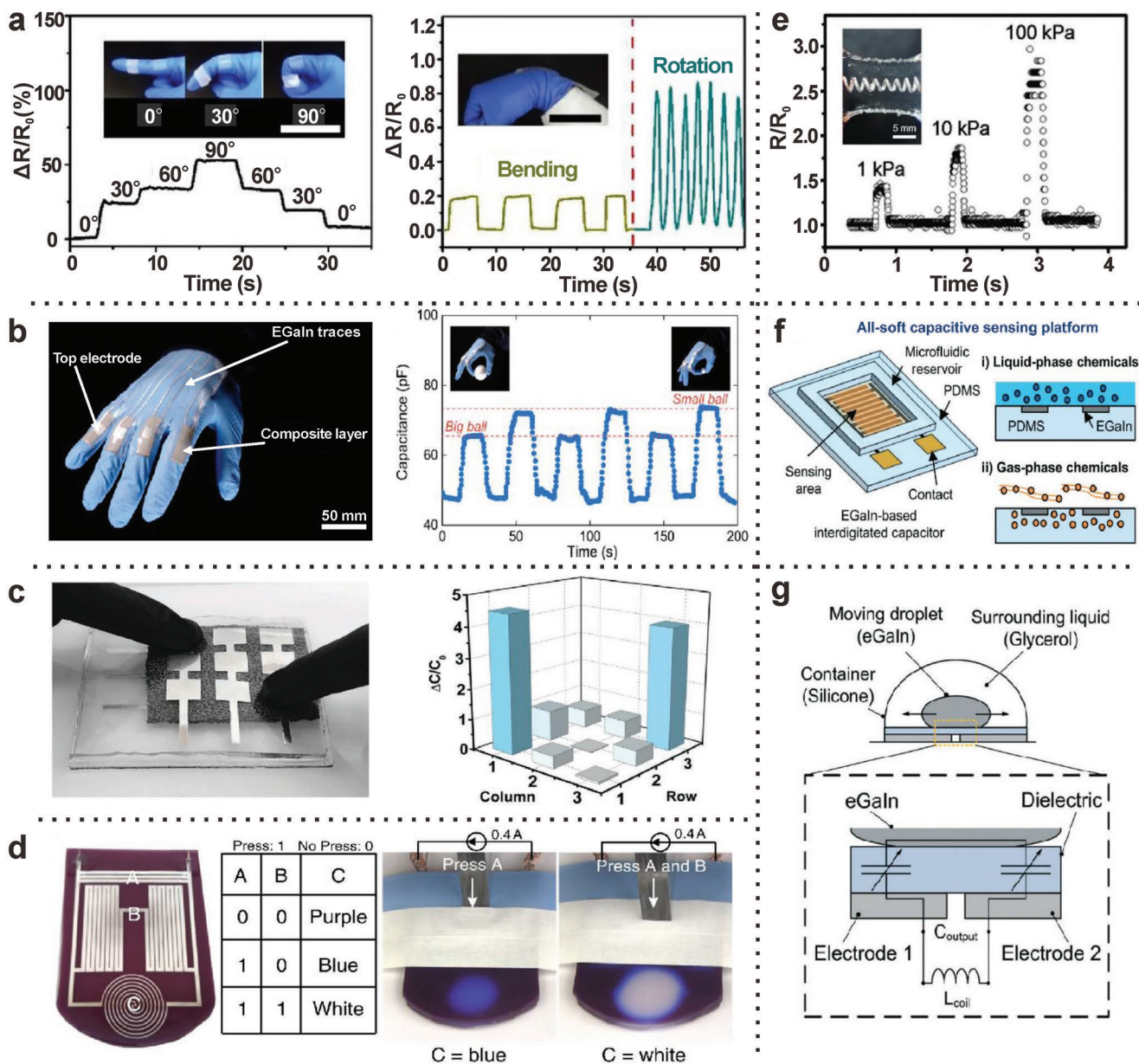


Figure 13. Application of strain sensor, touch sensor, pressure sensor, temperature sensor, gas sensor, and inertial sensor based on EGaln. a) The hydrogel resistive strain sensor composed of EGaln and acrylic is used to sense different bending angles of the fingers (left) and the bending of the wrist (right). R_0 : initial resistance product. ΔR : variation of resistance product. Scale bars: 5 cm. Reproduced with permission.^[258] Copyright 2019, Elsevier B.V. b) Wearable EGaln-elastomer soft composite capacitive strain sensor (left) can be used to detect the movement of the finger when grasping objects of different sizes (right). Reproduced with permission.^[259] Copyright 2019, American Chemical Society. c) Liquid metal elastic foam (LMEF) tactile sensor (left) is used to detect different touch positions of fingers (right). Reproduced with permission.^[260] Copyright 2020, Wiley-VCH. KGaA, Weinheim. d) Silicone composites doped with EGaln and thermochromic materials can be used for Joule heating color temperature sensing and touch logic gate circuits. Reproduced with permission.^[261] Copyright 2019, Springer Nature. e) EGaln 3D microfluidic channels embedded in hydrogels is used as a pressure sensor, inset shows its photograph. R_0 : initial resistance. R : resistance under external force. Adapted with permission.^[262] Copyright 2018, Wiley-VCH. KGaA, Weinheim. f) The EGaln-based interdigitated capacitor, used for detection of liquid and gas phase volatile organic compound. Reproduced with permission.^[263] Copyright 2017, The Royal Society of Chemistry. g) The inertial sensor based on EGaln, which senses the movement of an object through capacitance change. Reproduced with permission.^[264] Copyright 2017, The Royal Society of Chemistry.

of the nanocomposite.^[266] This work not only provides a reference for the direct synthesis of long organic molecular chains on liquid metal surfaces, but also provides a new method for liquid metal-embedded multifunctional nanocomposite sensing devices. Xie et al. used polydopamine (PDA) as the

surface coating of EGaln, which could effectively adsorb and precipitate Ga^{3+} ions, thereby inducing the phase separation of Ga and In in EGaln and realizing the transition from liquid phase to solid phase.^[267] This nanoalloy@PDA can be used as a gas sensor for efficient detection of NO_2 concentration. This is

done by physical adsorption of NO₂, and extraction of free electrons from the nanoalloy@PDA, reducing the electrical resistance. This way provides a novel means of smart gas sensing. Varga et al. demonstrated the fabrication of inertial sensors based on EGaIn droplets (Figure 13g).^[264] The movement of EGaIn droplets in the container caused changes in the capacitance and associated frequency characteristics of the sensors at different positions. The device was applied to detect the swing of the forearm of a human body.

3.2.2. Flexible Antennas

With the development of modern wireless communication technology, flexible and reconfigurable antennas based on liquid metals have gradually attracted people's attention. By taking advantage of the unique properties of liquid metals (Section 2), it is now possible to fabricate a variety of tunable and reconfigurable antennas, such as dipoles,^[72,268,269] patches antennas,^[270–272] coils,^[273] radio frequency, or antennas.^[73,245]

Figure 14a shows a multilayer microstrip patch antenna based on EGaIn,^[272] which is prepared by injecting EGaIn into the microfluidic channel of the elastomer, with certain flexibility which shows no significant change in device performance upon bending. **Figure 14b** shows a flexible and stretchable coil antenna composed of PDMS and EGaIn,^[273] which can be used for wireless energy transmission. When EGaIn, sugar particles and silicone elastomer are mixed to form a 3D liquid metal composite, the prepared dipole antenna can achieve 300% stretching, and as the stretching amount increases, the resonance frequency gradually decreases (**Figure 14c**).^[274] This strain-dependent wide-range tunable frequency characteristic provides new possibilities for wireless strain sensing.

A reconfigurable antenna based on EGaIn can also be used to achieve active control over resonance frequency. **Figure 14d** shows a potential-controlled reconfigurable monopole antenna,^[71] which controls the injection or withdrawal of EGaIn in the capillary by using the oxidation and reduction of the EGaIn surface oxide layer under the opposite bias polarity, in which NaOH alkaline solution was used to remove the surface oxide layer of EGaIn, so that it can be used as a slip layer. Since the length of the EGaIn-filled capillary is different, the antenna frequency can be adjusted. A reconfigurable antenna can also be realized by using the wetting characteristics of EGaIn (**Figure 14e**).^[275] The PVA film, which is often used to adhere liquid metals, becomes rough and uneven after femtosecond laser ablation, thereby reducing the wettability to EGaIn. The length of the reconfigurable area can be adjusted by brushing EGaIn on the ablated area, so as to achieve frequency control. Since the rough area has a weak adhesion to EGaIn, the EGaIn on the surface can be removed again by moving the roller in the reverse direction realizing the reversible reconstruction antenna. Qin et al. also reported a gravity-triggered frequency reconfigurable antenna,^[276] which fills EGaIn into a resin substrate as a radiation patch and uses NaOH to remove the surface oxide film. When the antenna rotates at different angles, the EGaIn inside the antenna deforms under the action of gravity, which causes the antenna frequency to be changed.

3.2.3. Electronic Circuit

At present, many electronic products are limited, such as their inability to bend, larger sizes, and poor portability. Liquid metals can be used as a stretched conductor^[277,278] or interconnecting wire,^[279,280] combined with commonly used circuit components, to prepare flexible and bendable electronic circuits,^[281–283] which provides a new way to solve this problem.

Figure 15a shows that an ink based on EGaIn doped with conductive nanoclay can be used for direct stamp printing of flexible electronics.^[284] When the stamp is pressed on the substrate and exceeds the yield stress, the oxide layer wrapped on the nanoclay will break up, thus forming hydrogen bonds with the hydrogel and other substrates, and strengthening adhesion force. Moreover, the doped conductive clay also has good electrical conductivity and significant electrical response to deformation, which can be printed directly and quickly on the skin to prepare multifunctional circuits.

EGaIn can also be used directly as a printing ink to print circuits. The printing technology uses a nozzle to directly print electronic circuits without photolithography and has good heat dissipation performance, which is especially required for electronic chips. **Figure 15b** shows an all-soft twistable and deformable LED array electronic circuit based on EGaIn dual-trans printing technology.^[75] Liquid metal dual-trans printing technology is based on liquid metal printing technology and introduces a solidification phase transition mechanism, thereby making the fabrication of circuits encapsulated by flexible substrates simpler and faster. First, the mirror circuit is printed on the PVC substrate by using the liquid metal printer and then covered with PDMS. After solidification of the PDMS, the multi-layer structure including the inner EGaIn is cooled, and the circuit on the soft substrate can be easily peeled off. According to the placement sequence of electronic components, it has two operation sequences, before peeling and after peeling. Through this liquid metal dual-trans printing technology, an integrated flexible temperature measurement circuit can also be prepared for wearable devices.

By changing the composition of the printing ink, EGaIn can also be used to improve the performance of printed circuit devices. Lopes et al. prepared digitally printed multilayer stretchable electronic devices using a composite ink “AgIn-GaSIS” prepared by mixing EGaIn, Ag flakes, and styrene-isoprene block copolymers (SIS) elastomer binder (**Figure 15c**).^[285] Compared with AgSIS ink without EGaIn, AgInGaSIS ink has higher conductivity and stretchability, and can improve the working stability of printed circuits. This means that the performance of printed circuit devices can be improved by changing the composition of the printing ink.

By changing the composition of substrates and wires, it can also be used to fabricate 2D electronic devices. Zhang et al. used EGaIn nanoparticles, PVA and cellulose nanocrystalline cotton (CNC) to prepare Janus films with asymmetric structure and conductivity on both sides, which can be used to prepare multilayer electronics (**Figure 15d**).^[286] Due to the difference in deposition density during the mixing process, EGaIn droplets were found to be mostly distributed in the lower layer, while CNC-PVA in the upper layers, and both layers were insulating before any treatment. However, when the lower layer was wiped

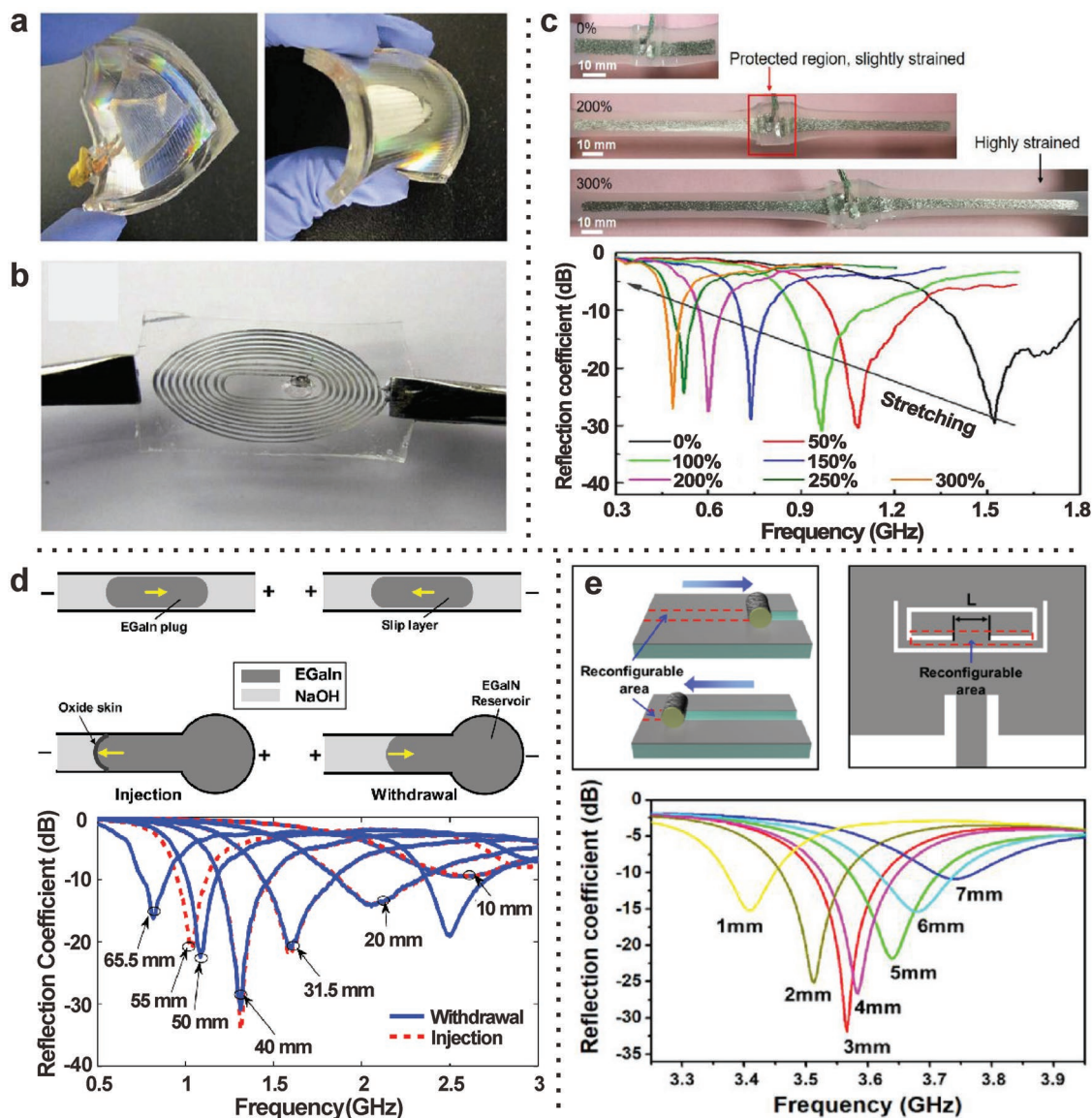


Figure 14. Stretchable and reconfigurable antennas based on EGaln. a) EGaln microfluidic channels embedded in elastomer to form a flexible microstrip patch antenna. Reproduced with permission.^[272] Copyright 2012, IEEE. b) A deformable coil antenna composed of EGaln microfluidic channels wrapped in PDMS. Reproduced with permission.^[273] Copyright 2014, IEEE. c) 3D liquid metal EGaln network is embedded in the elastomer to form a stretch adjustable frequency dipole antenna. Reproduced with permission.^[274] Copyright 2020, Elsevier B.V. d) Schematic illustration of the electrochemically controlled capillary action-driven reconfigurable liquid metal EGaln antenna (top). The working frequency of the antenna during withdrawal and injection, where the full length of the antenna is 75 mm (bottom). Reproduced with permission.^[71] Copyright 2015, AIP Publishing LLC. e) Schematic diagram of the reconfigurable patch antenna fabricated using the wetting properties of EGaln (top). The resonant frequencies of the antenna under different reconfigurable line lengths L (bottom), where the reconfigurable line length L can be adjusted by a soft brush, and the line width is 400 μm . Reproduced with permission.^[275] Copyright 2020, American Chemical Society.

with a rigid thin blade, the oxide layer of EGaln was broken under shear force and conductive channels were formed, while the unwiped areas remained insulating. Multilayer circuits, such as bilayer LED arrays with multiple intersections, can be easily fabricated using this liquid metal Janus film.

Recent studies have shown that anisotropic conductive adhesives prepared using gallium-based liquid metal nanodroplets as soft conductive filler micro/nanoparticles possess good anisotropic conductivity, which can be used in small-scale flexible integrated electronic circuits.^[287] The electrical connection

between two adjacent nanodroplets inside the conductive adhesive can be completed by mechanical breakthrough of the oxide skin, constructing anisotropic conductive paths in the glue matrix.

In addition to using EGaln to fabricate 2D electronic circuits, it can also be used to fabricate 3D electronic circuits.^[289] Figure 15e demonstrates the direct printing of high-resolution (minimum line width $\approx 1.9 \mu\text{m}$) microLED arrays with a mix of 2D and 3D structures by adjusting the printing path of the liquid metal printer nozzle.^[109] Moreover, when the micro-LED circuit

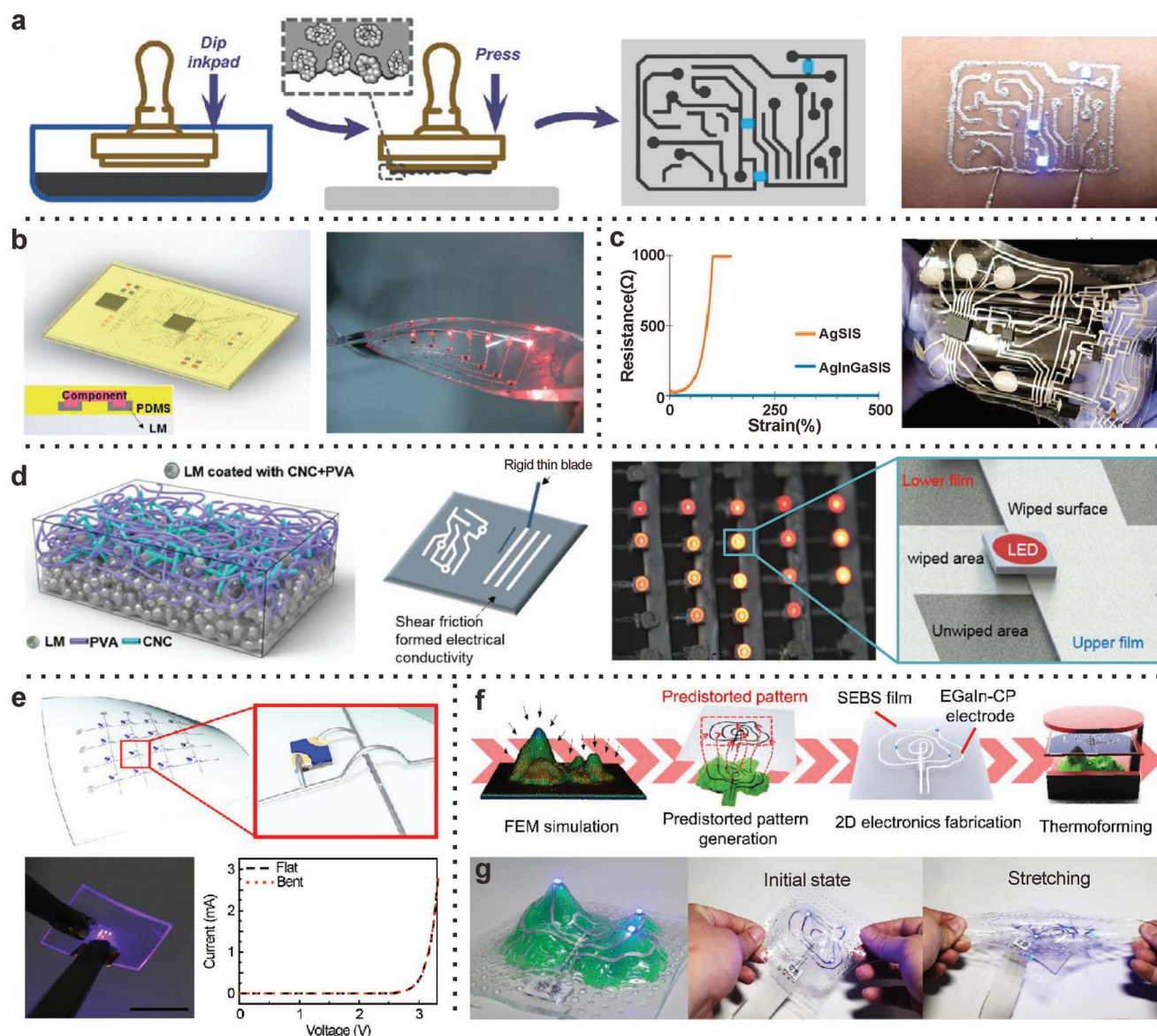


Figure 15. Electronic circuits based on EGaIn. a) Schematic diagram of the conductive nanoclay-based printed flexible electronics process (left), which can be applied to functional LED electronic circuits on the skin (right). Reproduced with permission.^[284] Copyright 2021, The Royal Society of Chemistry. b) PDMS-encapsulated liquid metal circuit (left) fabricated by the “before peeling” method, the inset is a cross-sectional view of the device. The flexible printed circuit fabricated by double-reverse printing technology (right). Reproduced with permission.^[75] Copyright 2015, Wiley-VCH. KGaA, Weinheim. c) The bi-phasic AgInGaSIS composite ink prepared by mixing Ag flakes and EGaIn in the SIS superelastic binder has good tensile properties and can be used to prepare printed multilayer stretchable circuits. d) Schematic diagram of the cross-section of Janus film composed of liquid metal micro-nano droplets, PVA, CNC (left), schematic diagram of wiping method (middle), and LED array circuit fabricated by single-sided conductive properties of Janus film under shear force (right). Reproduced with permission.^[286] Copyright 2019, The Royal Society of Chemistry. e) Schematic diagram (top) and physical image (bottom left) of the micro-LED array fabricated by 3D liquid metal interconnection, and the current-voltage characteristics of the micro-LED array under flat and bent conditions (bottom right). Scale bar: 1 cm. Adapted with permission.^[109] Copyright 2019, The American Association for the Advancement of Science. f) 3D electronic flow fabricated using thermoforming simulation and predistorted pattern generation method. g) Fabrication of 3D LED circuit with green mold (left), original state of 3D LED electronic circuit (middle) and stretchable deformation (right). Reproduced with permission.^[288] Copyright 2021, The American Association for the Advancement of Science.

printed on the flexible polyethylene terephthalate (PET) film is bent and deformed, the LEDs continue to work normally without a noticeable change in the respective current-voltage characteristics. Figure 15f shows a customized 3D electronic circuit fabrication flow based on a predistorted pattern and thermoforming process.^[288] On the basis of the 3D circuit model, a 3D electronic

device is fabricated by a combination of 3D modeling, finite element method simulation and predistortion pattern generation technology. It utilizes the thermoplastic elastomer substrate styrene-ethylene-butylene-styrene to form conformal contacts through the reverse texture of the mold, and EGaIn mixed with copper microparticles (EGaIn-CP) as electrodes. Compared with

other methods (such as 3D printing, spraying, etc.), this thermoforming method has high 3D consistency and gives access to 3D electronics with good stretchability (Figure 15g).

3.2.4. Other Flexible Devices

In addition to the above applications, EGaln can also be used to fabricate other kinds of flexible devices or devices components, such as supercapacitors, diodes, memristors, or photo-detectors. **Figure 16a** shows an all-soft supercapacitor based on EGaln, which uses photolithography and layer-by-layer (LbL) adsorption technology to prepare surface oxidized carbon nanotubes (O-CNT) functionalized EGaln electrodes.^[290] By controlling the number of steps of LbL, the areal capacitance can be controlled. For instance, the areal capacitance can be as high as 12.4 mF cm^{-2} for 30 steps. Besides, So et al. used the redox characteristics of the thin Ga_2O_3 layer on EGaln under different bias polarities to prepare an EGaln/polyethyleneimine (PEI) gel/polyacrylic acid(PAA) gel/EGaln structures that can be

used as an ion rectifier diode (Figure 16b).^[291] Without applied bias, the alkalinity of the PEI polyelectrolyte gel is sufficient to remove the Ga_2O_3 layer, thus this Ga_2O_3 layer is only present at the interface between the PAA polyelectrolyte gel and the EGaln electrode. When a positive bias is applied to the EGaln terminal, the surface is oxidized to form a thick Ga_xO_y layer, which suppresses the current in the circuit. When a negative bias is applied to the EGaln terminal, the Ga_xO_y layer shrink leading to an increase of the current. Based on a similar structure and principle, this group further prepared an array of memristors (Figure 16c) with an operating voltage of 1 V where each node works independently.^[82]

3.3. Energy Devices and Energy Catalysis

3.3.1. Energy Devices

With the advent of the low-carbon era, a new generation of LM-based energy harvesting devices has gradually been developing.

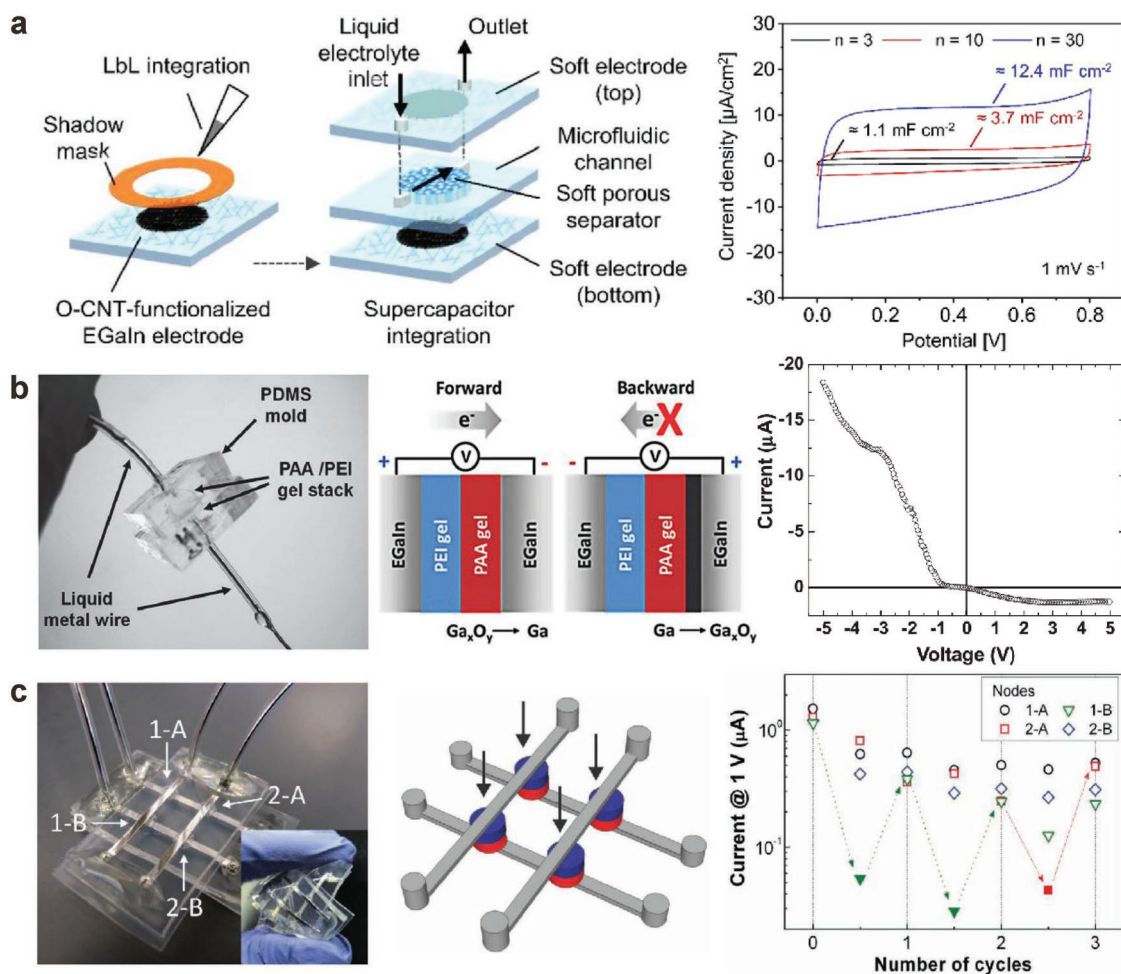


Figure 16. Application of other flexible devices based on EGaln. a) The established process and cyclic voltammogram characterization of an all-soft supercapacitor based on integrated functionalized carbon nanotube EGaln electrode. Reproduced with permission.^[290] Copyright 2020, American Chemical Society. b) The photograph, working principal diagram and I - V curve of a soft-matter rectifier diode with EGaln electrode. Reproduced with permission.^[291] Copyright 2012, Wiley-VCH. KGaA, Weinheim. c) The photograph, schematic diagram and switching performance of a memristor crossbar array based on EGaln. Reproduced with permission.^[82] Copyright 2011, Wiley-VCH. KGaA, Weinheim.

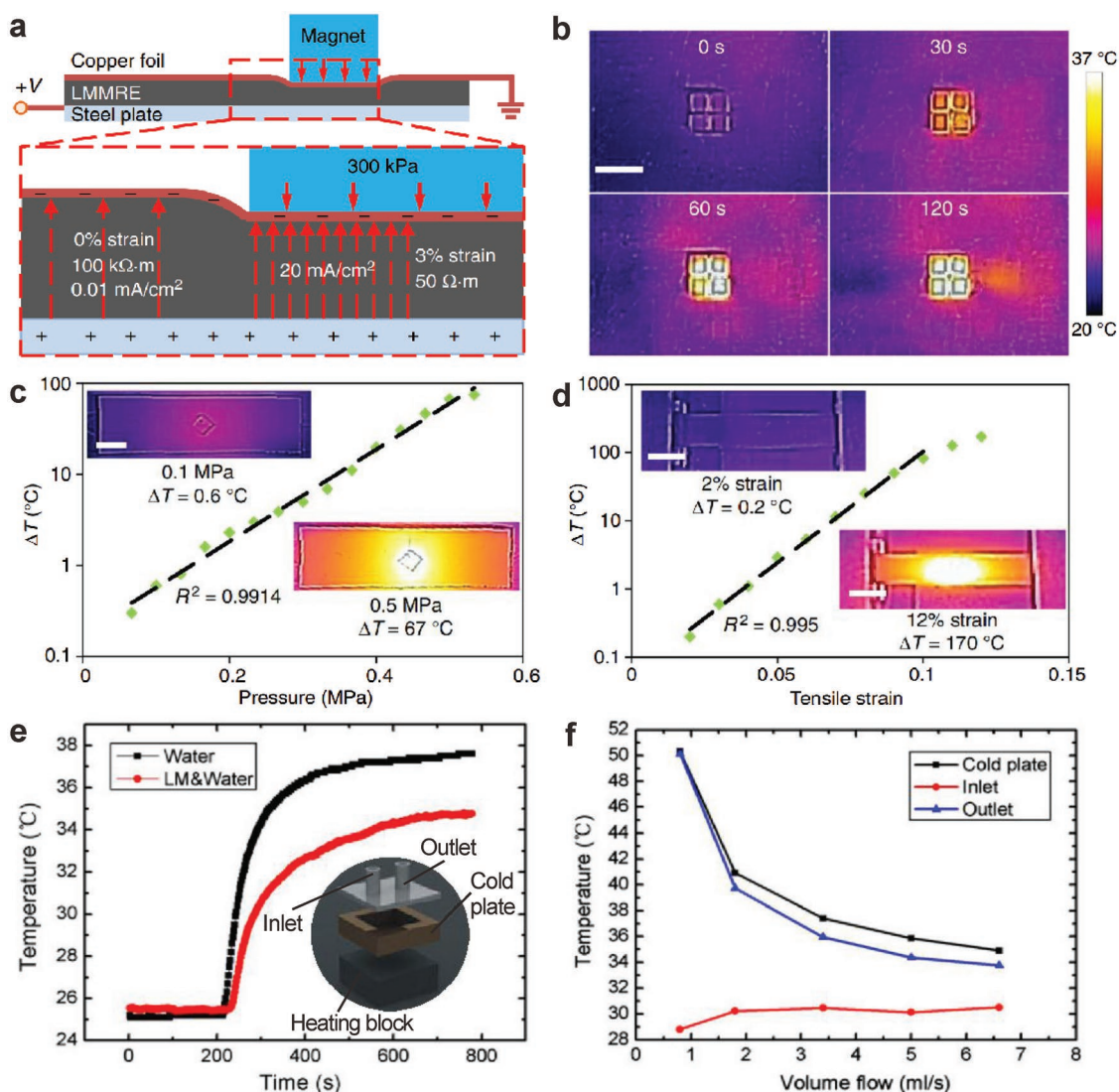


Figure 17. Thermal management device based on EGaIn. a) The working principle of the pressure-sensitive LMREE heating device. b) The temperature change of the film at different times after the heater applies magnetic field. c) Temperature change versus applied pressure. d) Temperature change versus applied strain. Scale bars are 1 cm. Reproduced with permission.^[250] Copyright 2019, Springer Nature. e) The temperature change during the heating process of a cold plate when using hybrid liquid metal-water cooling system (red) and pure water system (black), the inset is a schematic diagram of the system structure. f) The temperature change of the cold plate and the liquid metal inlet and outlet under different volume flow rates. Adapted with permission.^[87] Copyright 2010, Springer-Verlag.

These LM-based heat management devices,^[24,25,93,292] motors,^[43,293–296] generators,^[28,297,298] batteries,^[29,30,299–301] and other energy devices have opened up a new direction for the development of next generation of high-performance, multifunctional, and flexible devices.

Thermal Management: The high thermal conductivity of liquid metals can be used for heat management. It can be used both as heating devices based on Joule heating or as a coolant to cool devices. **Figure 17a–c** shows the application of liquid metal-filled magnetorheological elastomer (LMREE) composed of EGaIn microdroplets and metallic magnetic Ni microparticles in heating devices.^[250] The working principle of the heater is shown in Figure 17a. LMREE has a positive piezoconductive effect, that is, the conductivity increases when strain is applied. The local deformation of LMREE occurs in the magnet region

due to the pressure, which lowers the resistance of the magnet area significantly, thus inducing the local heating effect when a bias voltage is applied between top copper electrode and bottom steel electrode. Moreover, the magnet area can quickly heat up and stabilize within two min (Figure 17b). When a square PMMA sheet (side length 10 mm) is placed on the LMREE film and the pressure is applied by loading different weights, the local heating of the PMMA sheet causes the temperature to rise when the bias voltage is applied. Here, the increase of temperature is exponentially related to the pressure (Figure 17c). During the tensile strain process of LMREE film, the temperature also increases due to the local heating effect under applied voltage. When the stretching amount increases, the temperature change is more obvious due to the larger strain in the middle part of the LMREE film. Furthermore, the high temperature induced

by high tension begins to slow down the exponential growth of temperature change (Figure 17d).

As opposed to the use of EGaIn to prepare heating devices, it can also be used as a coolant (Figure 17e,f).^[87] When the heating block is used to heat a cold plate and the cooling agent is used to observe the temperature changes during this process, it can be found that using a hybrid LM-water cooling system composed of a water cooling module and an LM “heat spreader” has a better cooling effect than a pure water cooling module (Figure 17e). This is because the thermal conductivity of EGaIn ($26.43 \text{ W m}^{-1} \text{ K}^{-1}$)^[52] is much greater than that of water ($0.6 \text{ W m}^{-1} \text{ K}^{-1}$).^[96] The higher convective heat transfer coefficient makes the hybrid liquid metal–water cooling system have a better cooling effect. In addition, the larger the volume flow rate of the input liquid metal coolant, the better the cooling effect of the system (Figure 17f), which shows that the cooling effect of the coolant can be controlled by controlling the volume flow rate of the coolant. Recently, Wang et al. also mixed EGaIn with 3-chloropropyltriethoxysilane (CPTES) modified copper particles, which can improve the thermal conductivity ($65.9 \text{ W m}^{-1} \text{ K}^{-1}$) as the CPTES in the complex effectively acts as the thermal connection and diffusion barrier at the copper-gallium oxide interface.^[302] This makes it more advantageous than the traditional device heat dissipation methods, and can be effectively applied to the heat dissipation of, for example, a central processing unit (CPU) in a computer and other devices.

Motors: Self-propelled motors can move autonomously without aid from any form of external energy. Due to the flexibility of liquid metal, the direction of motor motion can be precisely controlled via the application of external fields, such as electric field or magnetic field, and has been applied in the fields of cargo transportation,^[303] and micro robots.^[26,27,304–306]

Figure 18a–c shows a Ni/Al/EGaIn motor controlled in different ways,^[307] in which part of the surface Ni layer is obtained by electroplating, and part of the Al layer is covered by Al foil and penetrated by EGaIn. Without any external force control, the chemical energy is converted into kinetic energy because of hydrogen evolution formed by the dissolution of Al surface layer,^[308] so that the motor can move spontaneously in a NaOH solution (Figure 18a). However, the direction of this type of motor that only relies on chemical fuel for propulsion is random,^[296] so it is necessary to precisely control the direction of movement by additional means. Figure 18b shows that the Ni/Al/EGaIn motor can adjust the direction of movement by applying an electric field. The electric field gradient forces the motor to respond to the direction of the external electric field and accelerates the movement of the motor. In the NaOH solution, Ni is more stable than Al, and the Ni cap can react to the external magnetic field, which means that the movement of the motor can also be controlled by a magnetic field (Figure 18c). The magnetic field can control the directional and rotational motion of the motor, and can even bring it to halt.

In addition to using a magnetic field to control the movement of a chemical fuel motor in a NaOH solution, it can also respond to an external magnetic field by incorporating magnetic particles into the liquid metal, which allows the motor to be applied in different working environments. Figure 18d shows by incorporating micro-sized steel beads in EGaIn, the motor can be controllably moved in water and on paper through

an external magnetic field.^[303] It can also be used to transport goods and release them at specific locations (Figure 18e). By using a motor with EGaIn as the core and the cargo-loaded gelatin hydrogel solution as the shell, a cargo carrier was obtained. It can reach the target position driven by a magnetic field, and then through a heating step ($37 \text{ }^\circ\text{C}$, 10 min), the cargo located in the hydrogel shell is released, and the release rate can further be controlled by the concentration and volume of the hydrogel shell. The remainder of the EGaIn motor can be moved back in the opposite direction through the magnetic field and recovered, waiting for the next loading task, highlighting its application potential in drug delivery.

Furthermore, the movement of such motors can also be controlled by sound waves. As shown in Figure 18f,^[309] an EGaIn colloidal motor can convert the energy of external sound waves into kinetic energy, and the moving speed of the motor can be controlled by different sound wave frequencies, thereby making the reconfigurable assembly of the colloidal motor possible. Figure 18g shows the process of using acoustic frequencies to control the EGaIn colloidal motor from random distribution to dandelion-like shape, and then to disperse, which provides a new method for the design of reconfigurable soft materials and systems.

Generators: As a form of energy harvesting devices, generators can convert mechanical energy, thermal energy, and other forms of energy into electrical energy, which can be used to supply power to the equipment or devices. Due to the high electrical and thermal conductivity, low Young’s modulus, and fluidity of liquid metal, liquid metal-based generators have the advantages of good power generation, high elasticity, stretchability, and high durability, and are often used in wearable electronic devices. Common liquid metal-based generators include thermoelectric generators (TEGs),^[310–313] triboelectric nanogenerators (TENGs),^[297,314] and magnetohydrodynamic generators (MHDGs).^[315–317] TEG devices can convert thermal energy into electrical energy, the temperature gradient between the hot and cold termini converts the heat flux into electrical energy to generate electricity. On the other hand, TENG devices can convert the triboelectric and electrostatic energy of the interface into electrical energy by relying on the potential difference generated when two objects are rubbed together. Finally, MHD devices can convert the mechanical energy of a flowing fluid into electrical energy, which is generated by the interaction between a moving conductive fluid and a rotating magnetic field.

Figure 19a shows a TEG device with a thermal interface of EGaIn embedded in an elastomer (LMEE) and liquid metal unfilled PDMS thermal shield. The strong combination of LMEE and unfilled PDMS can act as an insulating layer on both sides of the TEG, which can reduce unnecessary heat transfer and energy dissipation, thereby enhancing the thermal management of wearable thermoelectric devices. The TEG device utilizes the Seebeck effect where the temperature gradient across the device is converted to electrical energy. Moreover, the greater the temperature difference, the greater the open-circuit voltage (Figure 19b). EGaIn-based TEGs can also supply power to wearable electronic sleeves to achieve self-powered function. When the cold side temperature drops to $0 \text{ }^\circ\text{C}$, the power generated by the TEG sleeve is enough to light

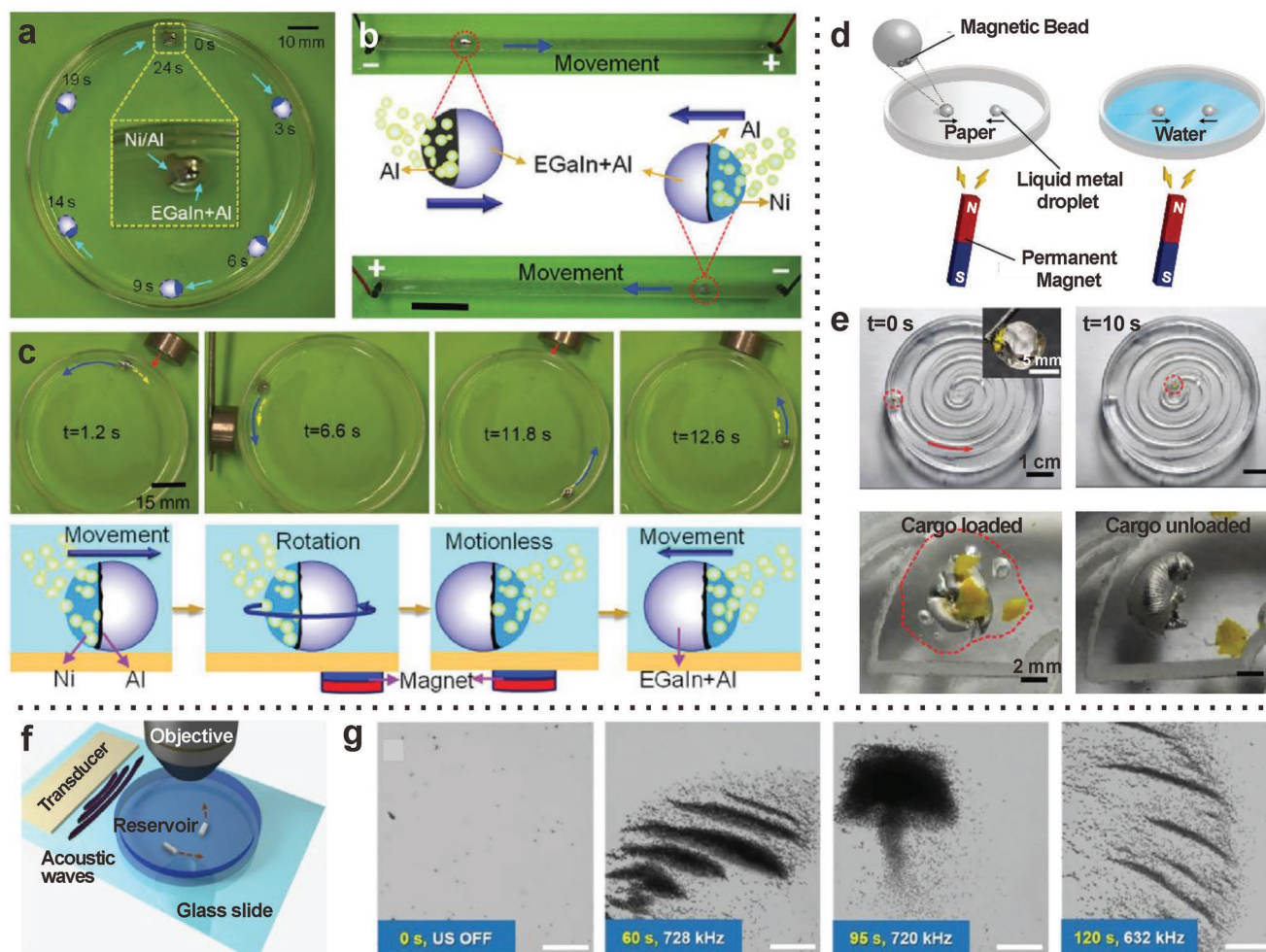


Figure 18. Various types of motors based on EGaln. a) The process of autonomous movement of Ni/Al/EGaIn motor in a petri dish containing 0.1 mol L^{-1} NaOH solution. Scale bar: 3 mm. b) The movement process of a Ni/Al/EGaIn motor under the action of an electric field. Scale bar: 2 cm. c) Snapshots of magnetic field controllability direction movement of Ni/Al/EGaIn motor in 0.15 mol L^{-1} NaOH solution (top) and a schematic diagram of its working principle (bottom). Reproduced with permission.^[307] Copyright 2016, The Royal Society of Chemistry. d) A Schematic diagram of the movement of EGaln doped with micro-magnetic steel beads on paper or in water under the action of an external magnetic field. e) Magnetically controlled liquid metal motors can be used to transport cargo. Adapted with permission.^[303] Copyright 2018, The Royal Society of Chemistry. f) A schematic diagram of the movement of liquid metal colloidal nanorods controlled by sound waves. g) The reconfigurable assembly of the acoustically controlled EGaln colloidal motor clusters. Scale bars: 60 μm . Adapted with permission.^[309] Copyright 2020, WILEY-VCH GmbH.

up two blue LEDs (Figure 19c). The preparation process of a sedimented liquid metal (SLM)-elastomer composite, which can be used as a TENG, is shown in Figure 19d. The composite is obtained by dispersing EGaln droplets into PDMS (wherein EGaln deposits at the bottom of the elastomer due to the difference in density) and curing. The upper layer of the composite is silicone-rich layer, which can be used as a dielectric and friction layer, and the lower layer is EGaln-rich layer, which can be used as the electrode for the TENG. A wearable device based on SLM-TENG is shown in Figure 19e, in which the skin acts as a second electrode, which can generate and separate charges repeatedly as follows. When the TENG is attached to a knee and separated from the moving body skin, it can generate energy through the triboelectric effect and electrostatic induction. It was demonstrated that the energy produced was enough to charge and discharge a capacitor power bank in a wearable computing device circuit consisting of a

digital hygrometer and an electronic display, and fully power the device (Figure 19f).

Recently Vallem et al. reported a variable-area electric double-layer capacitor fabricated from a liquid metal-hydrogel composite for converting mechanical energy from deformation into electrical energy.^[318] This composite is soft, deformable, and works well in both air and water, allowing it to harvest energy from human motion, wind, waves, and other applications.

Batteries: Rigid alkali metals are commonly used as electrode materials in batteries, and the growth of anode dendrites during use may cause a decrease in battery efficiency and safety issues.^[319,320] However, good deformability and self-healing properties of EGaln can slow down the growth of such dendrites and the appearance of cracks, and achieve better charge and discharge efficiency at high current densities, which provides a development path for a new generation of high-energy-density rechargeable batteries.

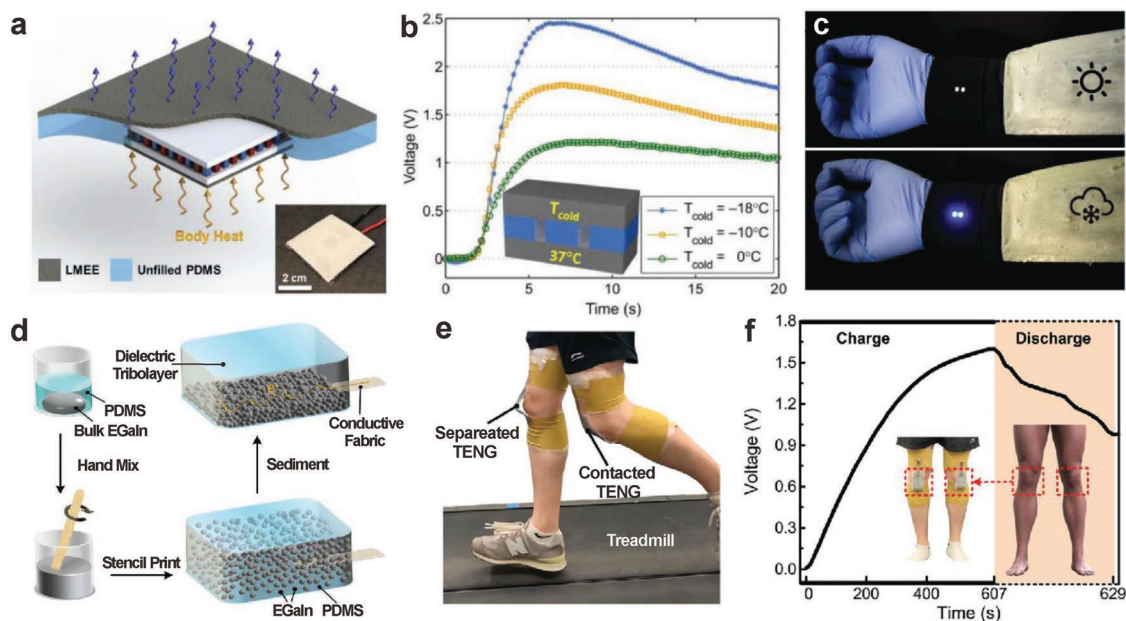


Figure 19. Generator application based on EGaln. a) Schematic and photograph of a TEG composed of LMEE and unfilled PDMS. b) The open-circuit voltage of TEG devices at different temperatures of the cold terminal. c) Wearable self-powered electronic sleeve based on TEG devices. Reproduced with permission.^[321] Copyright 2019, Wiley-VCH. KGaA, Weinheim. d) The preparation process of the SLM-elastomer composite used to prepare the TENG. e) Photograph of the contact and separation of TENGs on the knees when running on treadmill. f) The voltage change of the capacitor power bank during running. The TENG patch on the knee is used to harvest energy from the movement of the human body, where TENG is in contact with the knee. Reproduced with permission.^[314] Copyright 2020, WILEY-VCH GmbH.

Figure 20a shows an EGaln-air stretchable battery composed of liquid metal anode and flexible carbon fiber cathode.^[321]

During the discharge operation, the effective reaction involves the anode gallium losing electrons, the cathode oxygen gaining

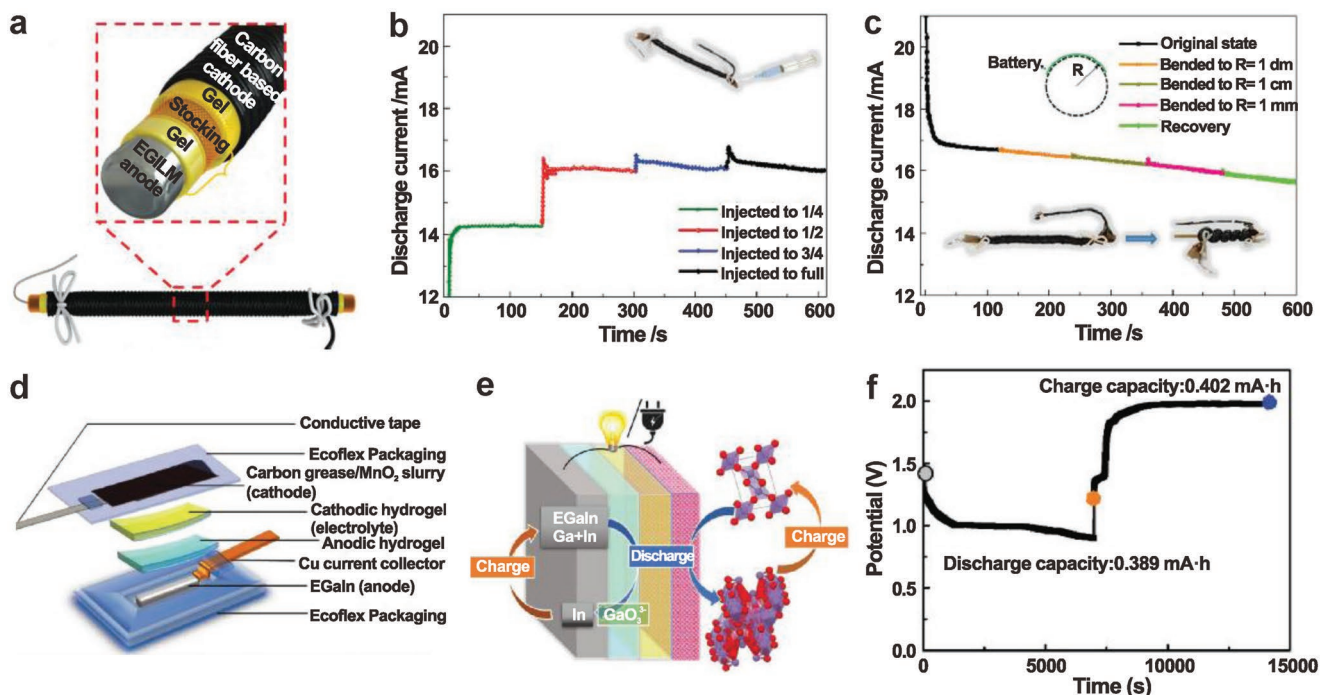


Figure 20. Application of EGaln as battery electrode. a–c) Schematic diagram of a) the structure of EGaln-air battery operating at room temperature, and b) the influence of length of injected EGaln, c) battery bent on battery discharge performance. Reproduced with permission.^[321] Copyright 2018, Wiley-VCH. KGaA, Weinheim. d) Rechargeable soft-matter EGaln-MnO₂ battery structure diagram) and e) its working principle, f) battery charge and discharge performance. Reproduced with permission.^[322] Copyright 2019, Wiley-VCH. KGaA, Weinheim.

electrons, and the indium of the anode is used to suppress the side reaction of gallium in alkaline electrolyte and keep the anode liquid at room temperature. This cable-type battery can also control the discharge performance by adjusting the amount of EGaIn injected into the anode, as shown in Figure 20b. Moreover, when the battery is bent and stretched, it does not affect the discharge performance of the battery (Figure 20c), achieving the function of flexibility and stretchability. Although the charging performance of the battery needs to be further improved, this use of EGaIn as a battery anode provides a new method to access deformable batteries for wearable electronics.

More recently, researchers began to use EGaIn as the battery anode to study rechargeable batteries. Guo et al. proved that EGaIn can be used as a self-healing anode for alkaline ion batteries with excellent cycle performance and capacity.^[323] Park et al. also used composite materials prepared by EGaIn particles as the two poles of the battery.^[324] Recently, Liu et al. prepared an EGaIn-MnO₂ battery and realized a rechargeable and stable stretchable battery, as shown in Figure 20d.^[322] The anode of the battery is EGaIn, the cathode is MnO₂ slurry, and the electrolyte is alkaline hydrogel. The reversible chemical reaction was realized at the two poles of the battery (Figure 20e). The charge and discharge performance are shown in Figure 20f. The discharge capacity and charge capacity are similar, indicating that it has a high coulombic efficiency, and its area-specific capacity can reach 3.8 mAh cm⁻². This kind of soft silicone-wrapped all-soft material battery also has good tensile and bending properties and can be applied to wearable electronic devices.

3.3.2. Energy for Catalysis Systems

Catalytic reactions refer to chemical reactions that take place under the action of catalysts. Unlike conventional chemical reactions, catalytic reactions require the presence of catalysts to selectively accelerate specific chemical reactions. Catalysis is very important to the development of new energy in the future. Liquid metal-based catalysts have received extensive attention in recent years, due to their flexibility, fluidity, recyclability, higher surface energy, and so on.^[32–34,325] Compared with traditional catalysts, liquid metal catalysts have the advantages of selectivity and stability,^[33] and can improve catalytic performance, becoming an important part of advanced energy and catalytic systems.

Liquid metals can be used as energy catalysts for the preparation of 2D materials. Traditional 2D material synthesis methods often cannot avoid defects, the introduction of residual impurities, cumbersome operation, long fabrication times, high cost, and other challenges,^[326,327] while liquid metal has good solubility, fluidity and weak interfacial force, which can realize the self-limited growth and orderly arrangement of 2D materials on the surface of liquid metal, enrich the organizational structure of the material, and obtain new properties. In addition, this technique enables the synthesis of a range of materials, including naturally layered, non-layered, and amorphous compounds, by mechanical exfoliation, reactive exfoliation, etc.,

thereby significantly expanding the available 2D material compound types.^[69]

As an important component of liquid metals, EGaIn can be used as a sacrificial agent to prepare a variety of 2D materials, such as Bi₂Te₃,^[328] MoO₂,^[329] reduced graphene oxide (rGO),^[330] 2D graphitic. Figure 21a shows the process of preparing self-limiting hydrated 2D MnO₂ on the surface of EGaIn through the Galvanic replacement reaction.^[68] The resulting core-shell structure can be used for photocatalysis, which can decompose Congo Red (CR) organic dyes (Figure 21b). With the increase of illumination time, the relative absorbance (A_t/A_0) of CR dye gradually decreases, indicating that the dye is gradually degrading. The photocatalytic effect is optimal when the concentration of KMnO₄ solution is 2.5 or 5 mM. When the core-shell structure (EGaIn/Mn-2.5) prepared in 2.5 mM KMnO₄ solution exists, the change from the UV-vis spectrum of CR dyes also reflects that EGaIn/Mn-2.5 has a good photocatalytic effect on the decomposition of organic dyes.

Recently, Mayyas et al. reported that 2D graphite can also be prepared electrochemically from gallium-based liquid metals,^[331] which can be doped with organic precursors and electrochemical devices at room temperature and low voltage, and can prepare graphene-like flakes to highly porous 2D graphite flakes, carbon-containing flakes of various sizes ranging from monolayer to multilayer, provide a novel method for the preparation of 2D materials. They also reported that nanomaterials can be extracted from gallium-based binary alloys in an electrolytic system.^[332] The nature of liquid-liquid interface between the gallium–bismuth liquid alloy and the aqueous electrolyte results in the precipitation of bismuth from the surface of the alloy into the electrolyte. By adjusting the chemical properties and temperature of the electrolyte, bismuth or bismuth oxide in various shapes and crystal phases can be prepared. Han et al. reported a proof-of-concept gallium-based liquid metal reactor.^[333] Gallium-based liquid metal is used as the reaction core, which can convert external electrical energy into mechanical motion, assist the formation and release of reaction products, and further can be used to synthesize Mn₃O₄, MoS₂, rGO, and other materials.

EGaIn droplets can be used to initiate and promote the self-polymerization of monomers. Ma et al. reported that sonication of EGaIn in aqueous solutions of vinyl monomers resulted in fast radical polymerization (FRP) without the use of conventional molecular initiators.^[336] The EGaIn nanoparticles produced by sonication can effectively increase the surface area of the metal, and the exposed metal initiates the polymerization reaction, which proceeds through the FRP mechanism and produces high molecular weight polymers that can form physical gels. The prepared hydrogel polymers exhibit good stretchability and thermal response properties, providing a facile method to synthesize functional polymers and gels.

EGaIn droplets can not only play a role in accelerating oxidation of the catalytic substrate, but also can be used as a reducing agent to promote the progress of a catalytic reaction. Figure 21c shows the use of EGaIn droplets as a heterogeneous catalyst to promote the oxidative self-polymerization of natural plant polyphenols under acidic or alkaline conditions.^[334] As

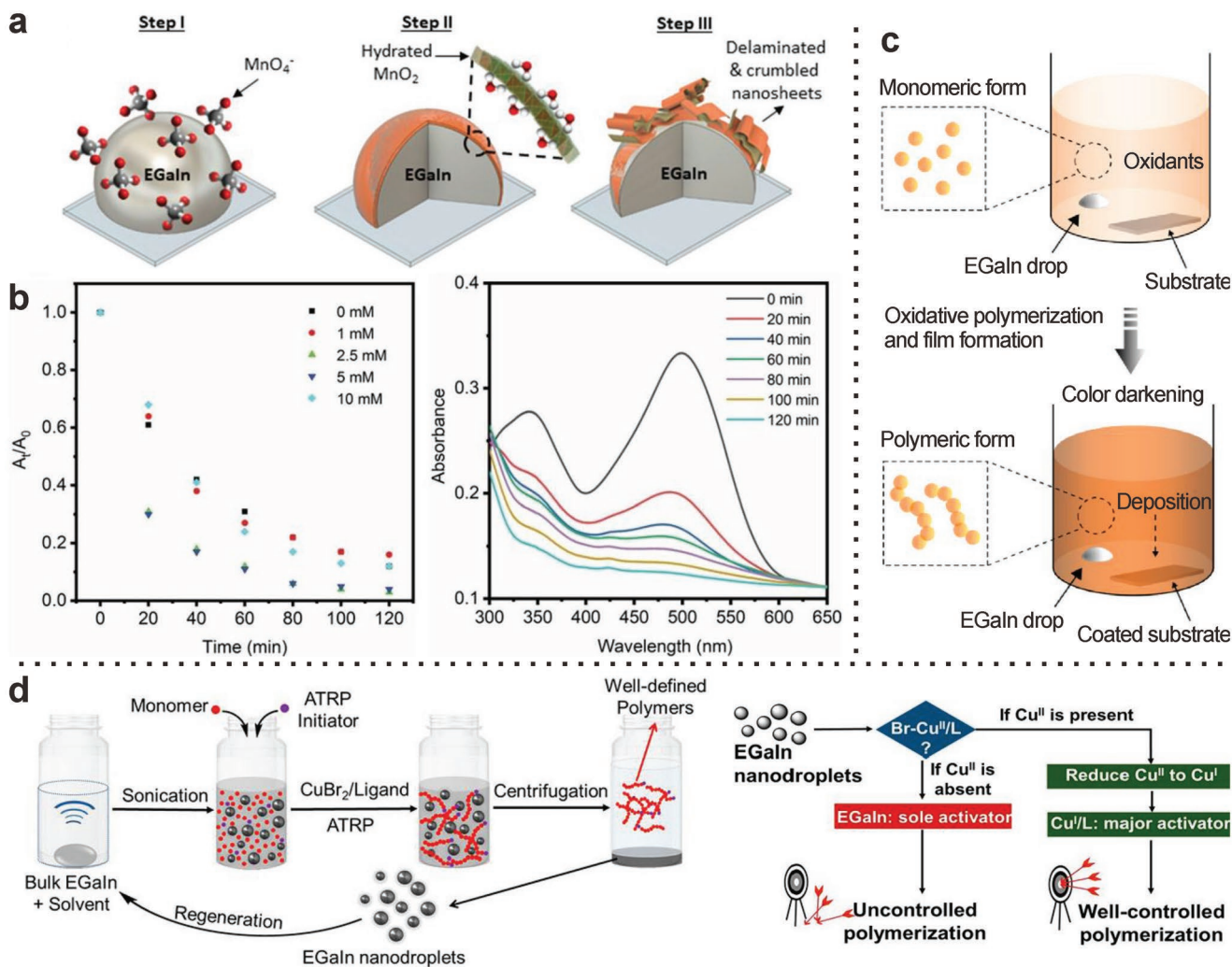


Figure 21. Role of EGaIn in catalysis. a) A schematic diagram of the preparation process of using EGaIn as a substrate to build a hydrated MnO_2 layer on the surface. b) The degradation process of Congo Red (CR) organic dye in different concentrations of KMnO_4 solution under visible light (left), the UV-vis spectra of CR under different illumination times in the presence of EGaIn/Mn-2.5 nm droplets (right). Reproduced with permission.^[68] Copyright 2019, Wiley-VCH, KGaA, Weinheim. c) A schematic diagram of the oxidation of polyphenol using EGaIn as a catalyst. Reproduced with permission.^[334] Copyright 2021, American Chemical Society. d) The process of preparing well-defined polymers by atom free radical polymerization (ATRP) assisted by EGaIn (left), and the role of EGaIn nanodroplets in catalytic reaction (right). Reproduced with permission.^[335] Copyright 2021, American Chemical Society.

the storage time increases, the color of the phenolic solution gradually becomes darker, and the color depth is much deeper than the natural placement without EGaIn droplets. The thin phenolic nanocoating prepared by oxidative self-polymerization can be prepared on a variety of substrates, and through further processing, it can also be used as an antioxidant and for sterilization, important for potential applications in biomedicine and food-related technologies. Figure 20d shows that in an atom free radical polymerization (ATRP) process, where EGaIn droplets can be used as reducing agent (RA) and supplementary activator (SA) to assist in the preparation of main ATRP activator Cu^I , so as to produce well-defined polymers in organic solvents with low ppm (parts per million) loading of Cu catalyst.^[335] Among them, Cu^I/L (L = ligand) activator will irreversibly transform into $\text{Br-Cu}^{II}/\text{L}$ deactivator under natural conditions, while EGaIn nanodrops can reduce Cu^{II} back to Cu^I ,

thereby recycling the activator and promoting the progress of ATRP for the synthesis of well-defined polymers.

3.4. Biomedical Science

Compared with traditional drug carriers, EGaIn-based drug carriers can form stable, safe and effective core-shell structures along with drug molecules owing to their biocompatibility and adhesion properties. Its movement can also be controlled using light and magnetic field,^[337] and its deformability reduces the possibility of vascular blockage during movement and realizes the rapid release of drugs at specific positions. In this section, we provide a brief overview of the prospects of EGaIn in biomedical applications,^[37-41,338,339] including drug delivery, tumor therapy, biological imaging, and neural interfacing.

3.4.1. Drug Delivery

Utilizing the properties of EGaIn, the accelerated and effective release of a drug at the respective target location can be realized. As shown in **Figure 22a**,^[66] EGaIn nanoparticles were used as the core in combination with thiolated (2-hydroxypropyl)- β -cyclodextrin (MUA-CD) ligands (L) that can be loaded with drugs and targeting ligands thiolated hyaluronic acid (m-HA), for the delivery of doxorubicin (DOX) drug molecules composed of EGaIn-NPs/DOX-L (≈ 107 nm in average diameter). After intravenous injection into the blood vessel, the drug molecules were shown to accumulate at the target tumor cells through active and passive effects, bounded to the CD44 receptor on the cell surface and entered the endosome through endocytosis. In the endosome, which has a weakly acidic environment, the oxide layer on the surface of EGaIn is gradually dissolved, thereby promoting EGaIn-NPs/DOX-L fusion, degradation and the release of DOX drugs. The released DOX drugs gradually accumulate and act on the nucleus, thereby affecting the normal gene expression of the target tumor cells. This targeted therapy and accelerated release of drugs can effectively improve the efficacy of drugs. Moreover, *in vivo* metabolism studies have shown that EGaIn-NPs/L composed of EGaIn and ligands may be excreted through feces and kidneys, and there is no obvious toxicity to organisms.

EGaIn nanoparticles wrapped in graphene quantum dots (GQDs) can effectively absorb and convert photoenergy to generate thermal effects and reactive oxygen species (ROS), which promote the transformation of internal Ga to (GaO)OH chemical reaction in a humid environment, resulting in a shape change from nanospheres to nanorods.^[340] Taking advantage of this feature, EGaIn NPs loaded with drug molecules entering the cell through endocytosis can release, the drug molecules under light illumination (**Figure 22b**). This remote-controlled

photodynamic therapy provides a new strategy that can effectively improve the efficacy of drugs.

Recently, Zhang et al. reported a new view of the anti-inflammatory mechanism associated with traditional Fe ions.^[341] By delivering liquid metal gallium nanodroplets into lipopolysaccharide-induced macrophages, Ga^{3+} ions can selectively inhibit nitric oxide production without affecting the accumulation of pro-inflammatory mediators, which provides a new avenue for gallium-based liquid metals to be used in future anti-inflammatory drugs.

3.4.2. Tumor Therapy

So far, common tumor treatment methods include hyperthermia, chemotherapy, electrochemical treatment, etc., among which photothermal therapy (PTT) is one of the most popular therapies that can induce thermal ablation of tumor cells by using photothermal conversion (PTC) materials to absorb photoenergy.^[342] Here we review the use of EGaIn in tumor treatment.

By using an EGaIn electrode, heat can be generated at the skin tumor through laser illumination or alternating magnetic field (AMF) to induce thermal ablation of tumor cells. Under laser irradiation, an Mg-EGaIn mixture prepared by doping Mg particles with EGaIn can improve the treatment of tumors.^[144] Compared with pure EGaIn, the temperature increase is improved under laser illumination (**Figure 23a**). This is because the intermetallic compound Mg_2Ga_5 is produced by the reaction and the increased surface roughness increases the light absorption efficiency. *In vivo* experiments with mice showed that the growth of tumors in mice treated with Mg-EGaIn was inhibited compared to other groups, further indicating that this Mg-EGaIn mixture can be used as a promising candidate for tumor photothermal therapy.

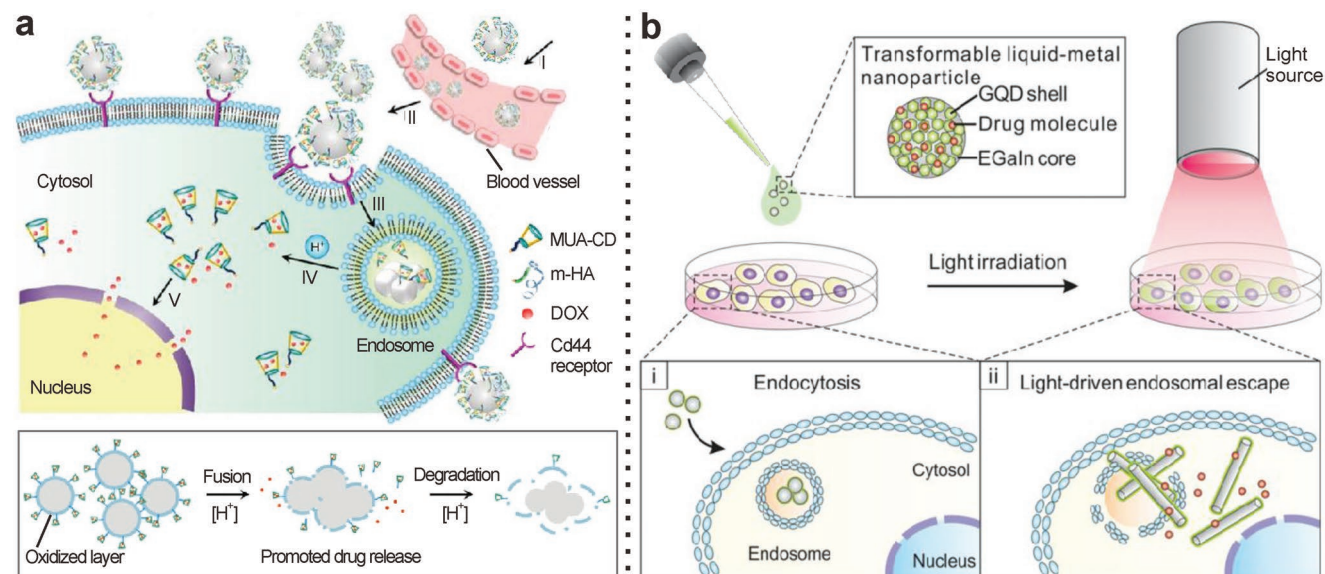


Figure 22. EGaIn nanoparticles for drug delivery. a) Schematic diagram of the accelerated drug release process at low pH after EGaIn loaded nano-medicine enters the cell. Adapted with permission.^[66] Copyright 2015, Springer Nature. b) Schematic diagram of the process of drug release from transformable EGaIn nanoparticles loaded with drug molecules in cells under illumination. Reproduced with permission.^[340] Copyright 2017, American Chemical Society.

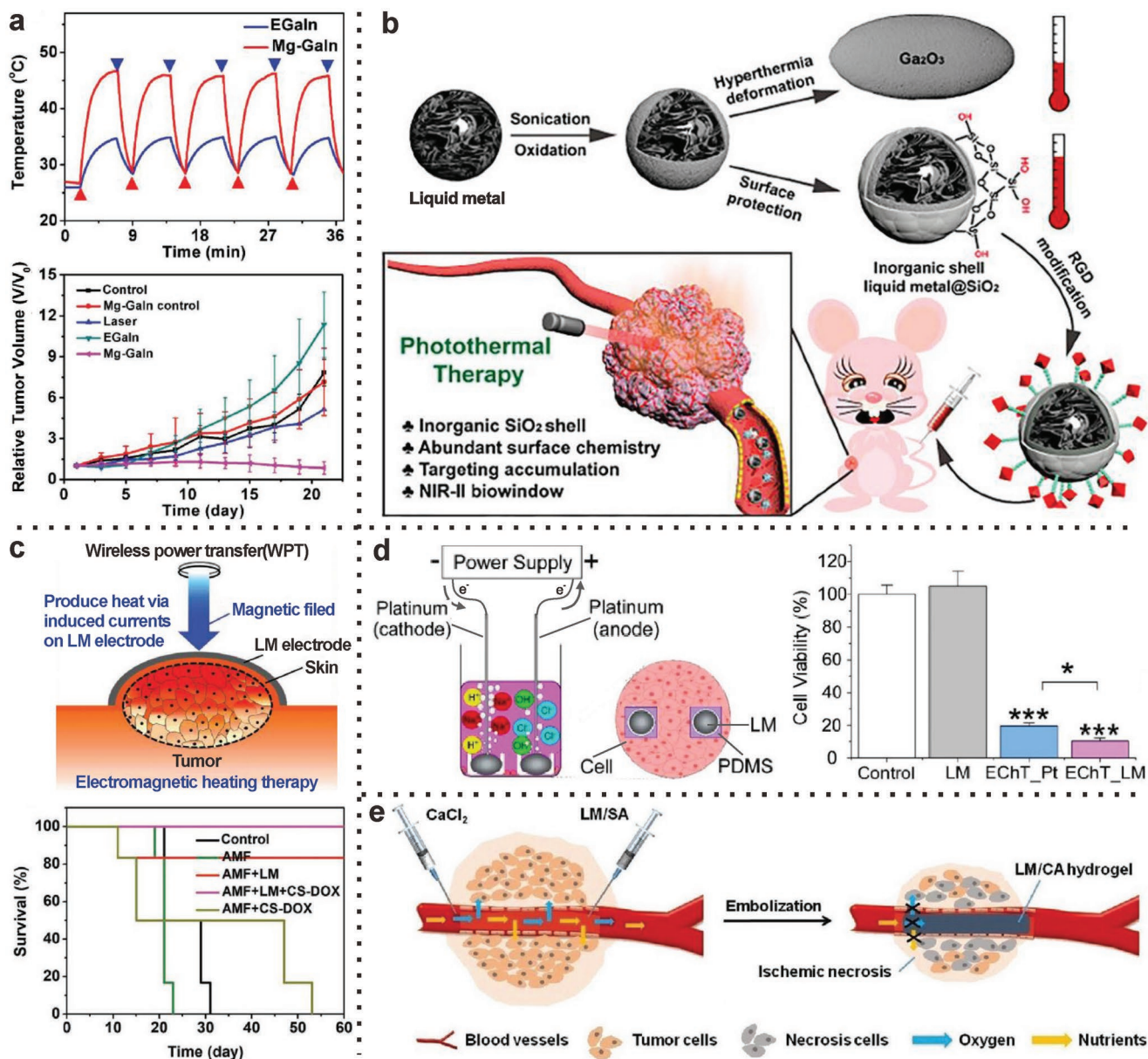


Figure 23. EGaln for tumor treatment. a) The temperature changes of EGaln and Mg-Galn doped with Mg particles for photothermal therapy (PTT) of skin tumors under repeated laser switching (top), and tumor growth curves of mice under different conditions (bottom). Reproduced with permission.^[144] Copyright 2018, Wiley-VCH. KGaA, Weinheim. b) The EGaln nanoparticles wrapped in an inorganic SiO₂ shell improve thermal stability, and realize the targeted accumulation of tumors and PTT under NIR illumination through the surface functionalization of RGD peptides. Reproduced with permission.^[343] Copyright 2019, American Chemical Society. c) The O-EGaln bioelectrode on the skin tumor can realize the treatment of the tumor (top) due to the thermal effect of the eddy current under the action of the AMF. The survival rate curve of mice under different conditions (bottom). Reproduced with permission.^[344] Copyright 2019, Wiley-VCH. KGaA, Weinheim. d) The schematic diagram of electrochemical treatment (EChT) using liquid metal electrodes in C8161 tumor cell culture dish (left). C8161 tumor cell viability under different treatments (right). Reproduced with permission.^[338] Copyright 2017, Elsevier Ltd. e) Schematic diagram of the prepared liquid metal/calcium alginate (LM/CA) hydrogel used to embolize the blood vessels around the tumor to realize the treatment of the tumor. Reproduced with permission.^[346] Copyright 2019, Wiley-VCH. KGaA, Weinheim.

By using EGaln as the core after surface functionalization, photothermal therapy can also be performed on tumor-targeted accumulation.^[135,138] Zhu et al. proved that before surface functionalization, the soft EGaln core can be wrapped with an inorganic silica nanoshell to form an EGaln@SiO₂ structure to improve thermal stability (Figure 23b).^[343] Then, the (Arg-Gly-Asp) RGD polypeptide is used to functionalize the EGaln

surface to achieve the targeted accumulation of tumors. Under irradiation with near-infrared (NIR) light, the absorption of light is enhanced due to local surface plasmon resonance (LSPR) with EGaln@SiO₂ particles and the success rate of photothermal induced cell ablation is improved compared to the bare EGaln particles, thereby effectively achieving the purpose of tumor treatment.

To use electromagnetic heating to achieve tumor hyperthermia, Wang et al. built an oxidized EGaIn (O-EGaIn) electronic skin (e-skin) (Figure 23c).^[344] The eddy currents generated on the EGaIn electrode by the AMF can generate sufficient heat and control the amount of temperature. By injecting the chitosan (CS) hydrogel loaded with DOX drug molecules (CS-DOX), the drug can be released quickly under the thermal effect induced by AMF. Wireless tumor treatment *in vivo* can be realized simultaneously with magnetothermal and chemotherapy, thereby improving the treatment effect. *In vivo* experiments in mice show that tumor-bearing mice treated with AMF+LM+CS-DOX can have a high probability of survival. Pure hyperthermia increases the temperature near the tumor to thermally ablate tumor cells, however, cooling can also kill tumor cells. Hou et al. used a combination of cryoablation and photothermal therapy.^[345] The high thermal conductivity of the EGaIn paste doped with Cu particles effectively reduced the temperature near the tumor tissue to achieve cryoablation, and then used Pluronic F127-modulated LM-NPs for photothermal therapy. This synergistic effect of cold and heat can further improve the therapeutic effect of tumor.

In addition to the above methods of tumor treatment, electrochemical treatment (EChT) can also be used. Sun et al. used EGaIn electrodes to achieve effective EChT (Figure 23d).^[338] In Hank's solution, EChT will cause the pH around the electrode to change. By applying a 5 V bias voltage for 5 min and continuing to incubate for 4 h, the cell viability of C8161 tumor cells in the metal platinum electrode EChT group (EChT_Pt; empty in PDMS container) and the liquid metal electrode EChT group (EChT_LM; liquid metal in PDMS container) was obtained. Through the comparison of different treatments, it can be found that the cell viability of the EChT_LM group is the lowest, indicating that it can effectively kill tumor cells.

Fan et al. also proposed a new method, which is to cut off the source of nutrition of tumor cells through embolization of blood vessels around the tumor, thereby causing ischemic necrosis of the tumor and realizing the treatment of the tumor (Figure 23e).^[346] Through rapid cross-linking of liquid metal/sodium alginate (LM/SA) mixed solution and calcium chloride solution injected by two separate syringes, the prepared liquid metal/calcium alginate (LM/CA) hydrogel can effectively block the blood vessels around tumor cells, blocking the source of oxygen and nutrients needed for sustenance, resulting in the death of tumor cells. Furthermore, *in vivo* experimental studies in rabbits showed that the tumor volume of rabbits treated with LM/CA hydrogel embolization gradually decreased with time, and the body weight was basically unchanged, indicating that the LM/CA hydrogel embolization treatment of tumors is effective and low toxicity. Recently, Wang et al. combined chemoembolization and photothermal therapy by encapsulating magnetic LM-NPs (Fe@EGaIn NPs) into calcium alginate (CA) microspheres (denoted as Fe@EGaIn/CA microspheres) loaded with the anticancer drug doxorubicin hydrochloride (DOX·HCl). By combining the photothermal/photodynamic sensitivity of Fe@EGaIn NPs and the embolization of CA microspheres, tumor growth can be further inhibited and tumor cells can be effectively killed.^[347]

It is worth noting that the above treatment methods may have a better therapeutic effect on skin tumors, because for

example, PTT has limited light transmission ability and cannot penetrate deep into the skin, and may have a poorer therapeutic effect on internal tumors. The electrode of EChT and the syringe needle of embolization therapy are difficult to reach the deep inside of the body, so they also have certain treatment limitations.

3.4.3. Biological Imaging

EGaIn can also be used in computed tomography (CT) imaging, X-ray imaging, photoacoustic (PA) imaging and other biomedical imaging fields, assisting the development of new nanomedical imaging applications. Figure 24a shows that EGaIn doped with Cu particles (Cu-EGaIn) can be used for stretchable e-skin and CT assistant localization marker.^[348] Guo et al. marked the surface of brain, chest and abdomen of rabbits and found that the CT value of Cu-EGaIn was significantly higher than that of other biological tissue parts. This was due to the high density of Cu-EGaIn relative to biological tissue, which improves the radiographic imaging capabilities, thereby improving the contrast and making the display clearer.

EGaIn was also shown to be useful for X-ray imaging by Larsson et al. who used an EGaIn jet source as the source of X-ray imaging, which can achieve high-resolution imaging of thicker samples and small animal tissues.^[349,350] Figure 24b shows the structural diagram of the liquid-metal-jet X-ray source imaging system and high-resolution X-ray imaging of mice, breaking through the limitations of traditional micro-focus X-ray sources.^[350]

In addition to being used as an X-ray jet source to obtain high-resolution X-ray images, EGaIn can also be used for targeted X-ray enhanced imaging. Chechetka et al. used LM nanocapsules (composed of EGaIn wrapped in phospholipid shell) to significantly increase the X-ray intensity under light, while the X-ray intensity of LM nanocapsule solutions at different concentrations in the absence of light did not show an obvious enhancement.^[137] Compared with traditional contrast agents that passively restore contrast to obtain clear structure images, light-induced LM nanocapsules are transformed into agglomerates to achieve adjustable contrast enhancement. This light-controlled X-ray enhancement method provides a new type of application scenario. By injecting such LM nanocapsules into rabbit heart, brain, or eyeball, light-controlled targeted enhanced X-ray imaging can be achieved (Figure 24c).

Such liquid metal nanocapsules can also exhibit stronger PA intensity by increasing the concentration or modifying the antibody, so that they can be used for PA imaging. When the light irradiates the tissue, while generating heat, it also sends out an ultrasound signal with the light absorption characteristic information of the tissue, so that the imaging information of the tissue in the body can be restored through the collected PA signal. The PA signal intensity distribution after injection of the epidermal growth factor receptor (EGFR) antibody (Anti-EGFR) functionalized liquid metal nanocapsules is subtracted from the pre-injected PA signal intensity distribution to obtain the variation of distribution map of PA intensity (Figure 24d). Then after three-dimensional imaging, a 3D

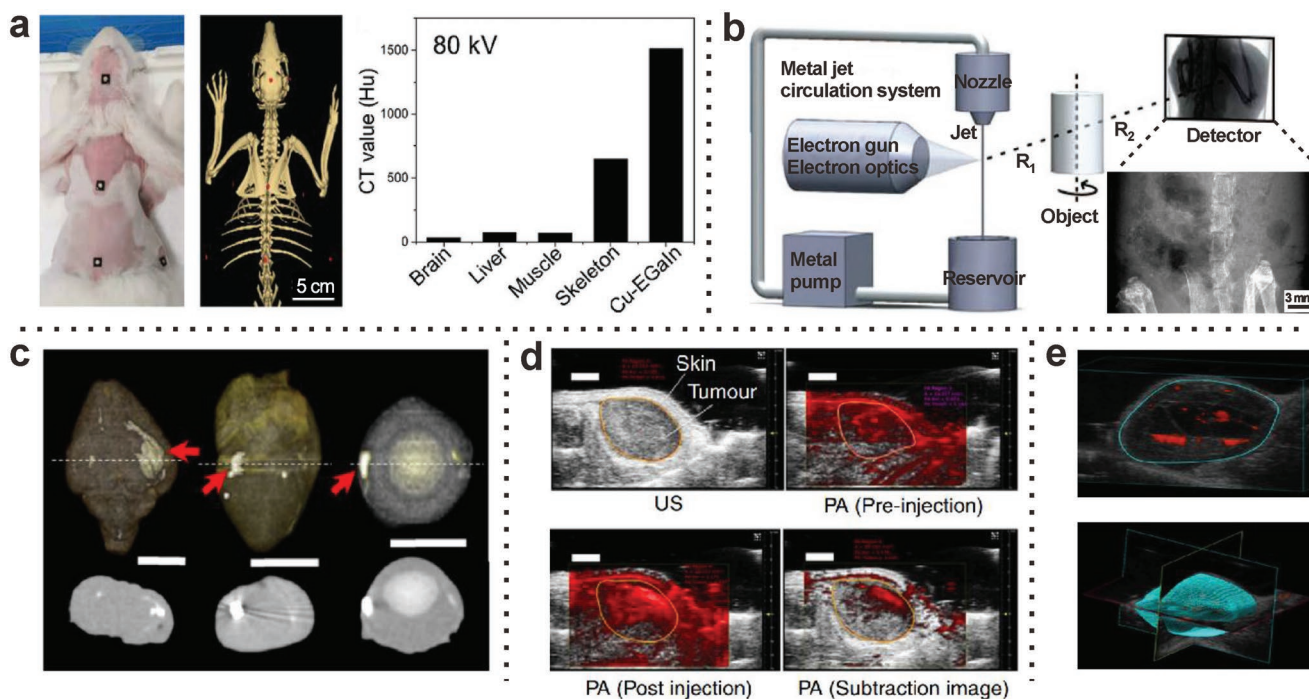


Figure 24. Application of EGaIn to biological imaging. a) Optical images and VR images of the musculoskeletal structures and bones in the brain, thorax and abdomen of rabbits with markers prepared from a liquid metal mixture (Cu-EGaIn) containing Cu particles (left), and the CT values of different parts of the rabbit and Cu-EGaIn at 80 kV (right). Reproduced with permission.^[348] Copyright 2020, The Royal Society of Chemistry. b) Schematic diagram of an imaging device based on a liquid metal EGaIn jet source, and the inset is the high-resolution X-ray imaging of mice. Adapted with permission.^[350] Copyright 2013, American Association of Physicists in Medicine. c) 3D X-ray images and cross-sections of rabbit heart, brain, and eyeball injected with LM nanocapsules. Scale bars: 1 cm. The red arrows indicate the laser irradiation position. d) Targeted tumor imaging of antibody-modified LM nanocapsules ($100 \mu\text{g mL}^{-1}$) in living mice, ultrasound (US) (grey) and PA (red) images obtained by 750 nm laser excitation of the tumor, orange circles indicate the part to be analyzed. Scale bars: 2 mm. e) 3D tumor imaging after treatment with antibody-modified LM nanocapsules. The blue circle shows the part for construction of 3D structure. Reproduced with permission.^[137] Copyright 2017, Springer Nature.

imaging map of the tumor is obtained (Figure 24e), indicating that it can be used to effectively target tumor detection and imaging.

3.4.4. Neural Interfaces

Cheng et al. reported that EGaIn can be used to prepare electronic blood vessels and can be used for neural interfaces without the limitation of traditional autologous transplantation that requires donor size matching.^[139] By combining EGaIn and poly(L-lactide-co-ε-caprolactone) (PLC) into a metal polymer conductor (MPC), a PLC-based MPC (MPC-PLC) membrane was prepared. Then, in combination with the use of multi-channel microfluidic chips, human umbilical vein endothelial cells (HUVECs, blue), human aortic smooth muscle cells (SMCs, green), and human aortic fibroblasts (HAFs, red) were successively placed on the MPC-PLC membrane, to mimic natural blood vessels, in which three different cells are distributed in different layers in the 3D multilayer tubular structure (Figure 25a). When this electronic blood vessel was implanted into the carotid artery of a rabbit, after three months the real-time blood flow of the surgical site and the synchronized ultrasound pulse were monitored by Doppler ultrasound, which showed that the blood can flow well in the electronic blood vessel (Figure 25b).

Recovery of motor function by electrical stimulation of nerve tissue can treat movement disorders caused by nerve damage. The use of LM electrodes can be adapted to body tissues and endure the effects of long-term electrical stimulation to achieve rapid recovery of nerve tissue functions. Guo et al. used EGaIn electrodes wrapped in PDMS to fix the EGaIn electrodes and nerves through a silicone tube, which can be used as nerve electrodes for stimulation and conduction electrical excitation (Figure 25c).^[351] When this EGaIn electrode was implanted into the sciatic nerve of a dead adult bullfrog, it had a higher monophasic action potential under electrode stimulation than the traditional metal platinum electrode. This experiment indicates that this liquid metal electrode has better conductivity in the nerve tissue than the platinum electrode. By stimulating the sural nerve and tibial nerve with liquid metal electrodes, the gastrocnemius and soleus muscle can be controlled to realize the movement of the hind limbs of the dead bullfrog.

A biological electrode prepared with liquid metal ink can also be used for nerve signal sensing.^[352] The biological electrode composed of filter paper base, EGaIn conductive layer, and Ecoflex wrapping layer can be used to stimulate and monitor the biological electromyographic signals in mice (Figure 25d).

A cardiac ablation catheter based on liquid metal electrodes can also be used to assist in the treatment of atrial fibrillation (AF).^[353] Its composition and schematic diagram are shown in Figure 25e. By combining the soft fiber-reinforced thick-walled

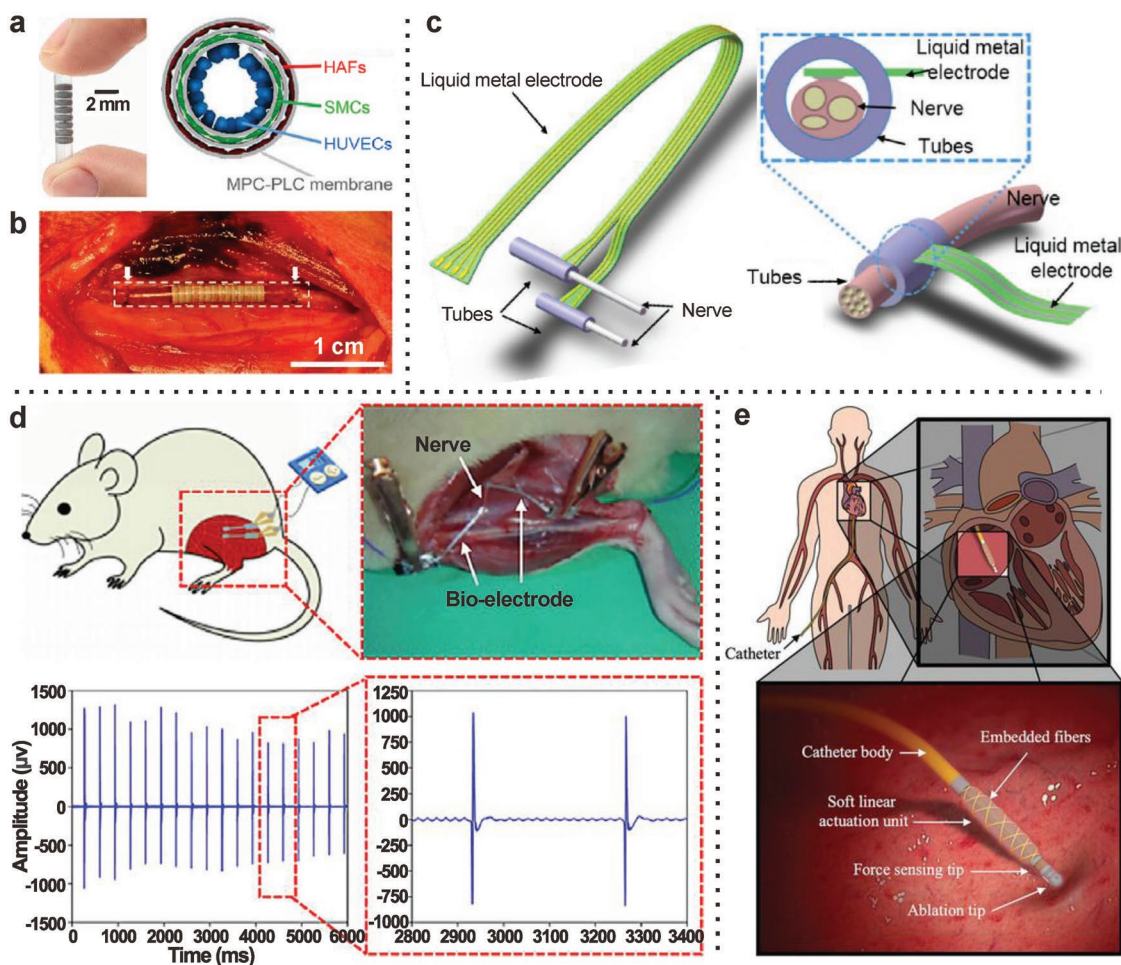


Figure 25. Neural interface application based on EGaln. a) Photo (left) and cross-sectional view (right) of electronic blood vessels composed of EGaln-based flexible electrode scaffold protective membrane and three vascular cells. b) Pictures of electronic blood vessel implantation into rabbit carotid artery. The dotted box indicates the range of electronic blood vessel implantation, and the arrow indicates the edge of electronic blood vessel. Reproduced with permission.^[139] Copyright 2020, Elsevier Inc. c) Schematic diagram of the connection of liquid metal biological electrode in vivo, in which silicone tube is used to fix the electrode and nerve. Reproduced with permission.^[351] Copyright 2017, IOP Publishing. d) Liquid metal nanoink-based bio-electrodes are used to stimulate and monitor electromyographic signals in mice (top), and the collected reflection signals (bottom). Reproduced with permission.^[352] Copyright 2020, Elsevier Ltd. e) Design of a cardiac ablation catheter with integrated soft drive and sensing unit for dynamic force control. Reproduced with permission.^[353] Copyright 2021, Mary Ann Liebert, Inc.

cylindrical hydraulic actuator and the soft sensor embedded in EGaln, the contact force can be controlled and tracked, making AF safer. This system can be used for ablation of the heart that is often used in minimally invasive surgery to locally destroy abnormal heart tissue. Both the soft actuator and the soft sensor can achieve stable system response within a sinusoidal input signal of 0.2–1.5 Hz, and can achieve good mechanical control.

3.5. Other Fields

In addition to the above-mentioned applications, EGaln can also be used in other fields. **Figure 26a** shows that the electrochemical physical reconstruction of a pair of EGaln droplets immersed in an alkaline electrolyte at low bias can be used as a transistor.^[83] By controlling the coalescence and separation

of LM droplets contact by bias voltage, the conductivity can be changed by three orders of magnitude. The fluid instability of the field-controlled gradient is considered to be the mechanism of EGaln physical reconstruction. EGaln droplets can also be used as the electrode of an interface field-effect transistor (IFET) (Figure 26b).^[354] the IFET composed of EGaln droplets, superhydrophobic $F_{16}CuPc$ semiconductor nanowires and graphene gates can achieve a high switching ratio of 3×10^4 . When the drain voltage V_D is fixed, the wettability between nanowires and liquid metal droplet through mechanical force, thereby controlling the performance of the IFET. Besides, EGaln droplets can be used to prepare bipolar resistive switching (Figure 26c).^[355] by constructing an EGaln/ $GaO_x/SiO_x/p^+-Si$ junction, conductive filaments are formed between EGaln and Si due to the movement of Ga ions under a positive bias, thereby entering the low resistance state, while under negative bias, the disconnection of the conductive filaments makes it enter the

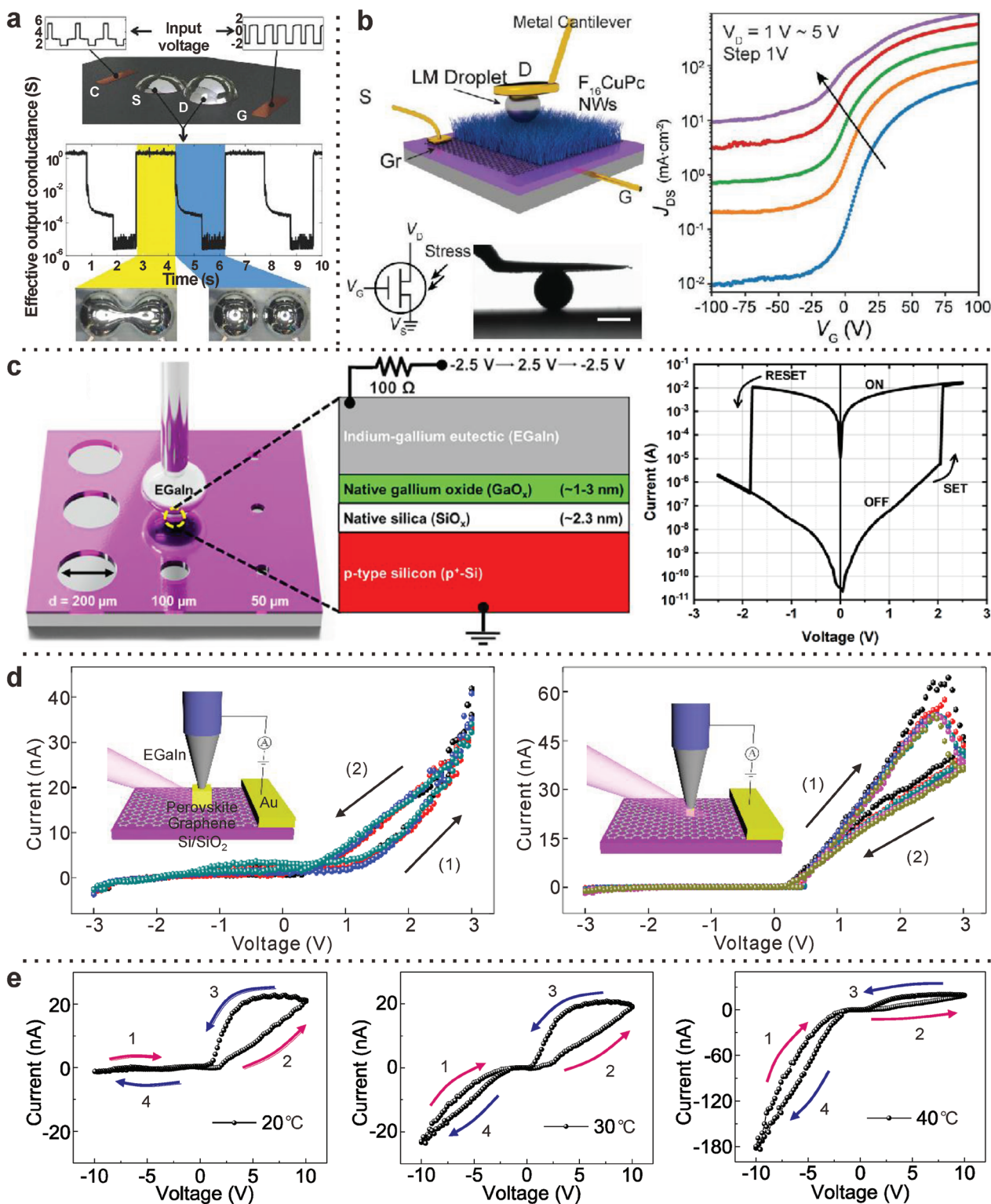


Figure 26. Other applications based on EGaIn. a) A EGaIn-based transistor controlled by an electric field, in which the source and drain are fixed on a copper pad by alloying, the counter and the gate are also composed of copper contact pads, and the working environment is an alkaline electrolyte aqueous solution. Reproduced with permission.^[83] Copyright 2017, Wiley-VCH, KGaA, Weinheim. b) IFET based on EGaIn drop electrode. Reproduced with permission.^[354] Copyright 2018, Wiley-VCH, KGaA, Weinheim. c) EGaIn resistance switch based on Ga ion conductive filament mechanism. Reproduced with permission.^[355] Copyright 2021, American Chemical Society. d) The EGaIn tip measures the size effect of perovskite microcrystals of different sizes. NDR behavior is solely observed for small size microscale perovskite crystal. Adapted with permission.^[357] Copyright 2020, American Chemical Society. e) The EGaIn tip measures the temperature-controlled rectification effect of KTN ferroelectric microcrystals. Reproduced with permission.^[358] Copyright 2021, American Chemical Society.

high resistance state, and its switching ratio can be as high as 10^8 .

Due to the existence of the oxide layer on the surface of the EGaIn, EGaIn can be prepared into a conical tip shape with a small radius of curvature (as discussed in Section 3.1.1), which can be used in some other fields.^[356] Figure 26d shows that a soft-contact EGaIn/ $\text{CH}_3\text{NH}_3\text{PbBr}_3$ microcrystal/graphene junction can be constructed using an EGaIn tip.^[357] It can be found that for different sizes of perovskite microcrystals, there are obvious differences in the carrier transport characteristics. The negative differential resistance (NDR) behavior solely observed with small-size microcrystals is likely caused by the compensation electric field formed by ion migration in the perovskite which screens the external electric field. By replacing perovskite microcrystals with ferroelectric microcrystals, EGaIn tip electrodes can also be used to study the properties of microscale ferroelectric crystal junctions. The results show that the rectification direction can be reversed by controlling the ambient temperature and thus the temperature-controlled rectification can be realized (Figure 26e).^[358] The underlying proposed mechanism for these observations involves carrier trapping/detrapping by surface defects.

4. Conclusions and Prospects

Liquid metals are recognized to be at the center of the second revolution in the use of metals.^[36] At present, many major transformative applications based on liquid metals are still imaginary, but it has already broadened the boundaries of human cognition of the world. As a special functional material, EGaIn has shown the characteristics of leading and developing major technological frontiers, and is expected to bring disruptive changes in the fields of electronic information, advanced manufacturing, flexible robots, biomedical health, and spawn a series of strategic emerging industries. Although the EGaIn has received extensive attention, so far, there are still some unsolved problems or challenges which may hinder its further wide applications.

- 1) Resolution limit: although the liquid metal EGaIn can be prepared into various small shapes and can be used as interconnection lines, or antennas,^[103] it is difficult to reduce the size of the liquid metal pattern to the nanometer level due to the liquid-liquid interaction between liquid metals.^[359] In the long run, this limits the preparation and application of miniaturized devices based on liquid metal patterns.
- 2) Toxicity: liquid metal EGaIn has long been considered a substitute for toxic mercury due to its low toxicity: EGaIn nanoparticles have been proven to be harmless to the body and can be used in biological applications. However, most of these experiments were carried out in a short period of time (less than three months).^[135,140] Although EGaIn nanoparticles may be excreted through kidneys and feces,^[66] the absorption of liquid metal by body organs is not yet known. Under long-term use, the accumulation of liquid metals by organs may cause potential safety hazards to organisms, which needs to be investigated.
- 3) Interface reaction: although EGaIn has been relatively mature in its application in measuring the properties of molecular layers, for the measurement of material properties, the effect of the interface between EGaIn and the surface of the material, especially the effect of GaO_x on the measurement results remains to be further studied.
- 4) Oxide layer regulation strategies: By precisely regulating the oxide layer by various means (e.g., solvent, temperature, electrochemistry, or ultrasound),^[98] and controlling the balance between the oxide layer shell and EGaIn core, more novel physicochemical properties may be discovered, which can be applied to more kinds of multifunctional devices.
- 5) Long-term life and cycle stability: some flexible devices prepared with EGaIn may lead to the rupture and oxidation of the surface oxide layer under the action of voltage or external force, thereby affecting the service life of the device, although this also brings us opportunities, for example, it can be used for diodes,^[291] or memristors.^[82] In addition, energy devices using internal effects or external stimuli may also face the problems of device fatigue and slow response during long-term use.

Although EGaIn still faces several challenges, its wide range of applications in many fields confirms that it has obvious advantages. Here, we would like to briefly highlight several potential applications based on liquid metals which are not summarized in the aforementioned sections independently.

- 1) Computer based on liquid metal: researchers have found that devices such as logic gates can be prepared with EGaIn as aforementioned.^[84] Besides, when the liquid metal is placed in a liquid, it will naturally form a sandwich structure of “liquid metal electrode–liquid film–liquid metal electrode”, in which the liquid film gap can be regulated through various physical fields such as force field, electric field and magnetic field, and the size can reach extremely small scales or even disappear. It is expected to realize the all-liquid quantum tunneling effect, which may lay the foundation for future liquid metal quantum computers.^[360] Compared to traditional solid-state devices, the thickness of the interlayer is more flexible, and the device can be deformed and segmented for multiple applications. These indicate that liquid metal computers with high flexibility, intelligence, and controllability may become the prototype of the next generation of new computers.
- 2) Liquid metal soft robots: soft robots with deformable shapes possess many advantages compared to traditional robots, and thus it is a hot research topic. Liu Jing’s group developed a deformable liquid metal machine that moves autonomously,^[308] taking an important step towards the development of a deformable robot. After that, they also studied more complex motions to manipulate the motion of liquid metal. But there is still a long way to go to realize a practical liquid metal robot.
- 3) Liquid metal catalyzes energy reactions: recent studies have reported that the use of mechanical energy-induced methods to convert CO_2 to carbon in Ga liquid metal suspensions near room temperature,^[361] and the low melting point of EGaIn can be used to convert CO_2 to carbon at room

temperature without supplementary reductant,^[36] which shows that EGaIn has a great potential for energy recovery and utilization. Moreover, it is also expected to reduce the greenhouse effect and play an important role in environmental protection.

In summary, new applications based on liquid metals are emerging, and it is believed that further technology based on EGaIn will be expected to further change the world and create a brighter future due to its unique properties in the near future.

Acknowledgements

This work was supported by National Key R&D Program of China (2021YFA1200103), National Natural Science Foundation of China (91950116, 11804170), Natural Science Foundation of Tianjin (19JCZDJC31000, 19JCQJC60900, 19JCYBJC16500). The authors acknowledge the National Research Foundation (NRF) for supporting this research under the Prime Minister's Office, Singapore, under its Medium-Sized Centre Programme and the Competitive Research Programme (NRF-CRP17-2017-08), National Research Foundation of Korea (NRF) grants (No. 2021R1A2C3004783).

Conflict of Interest

The authors declare no conflict of interest.

Keywords

3D electronic circuits, energy catalysis, eutectic gallium–indium, flexible electronics, molecular electronics

Received: April 14, 2022

Revised: July 30, 2022

Published online: November 20, 2022

- [1] H. Zhao, X. Hu, M. B. Bush, B. R. Lawn, *J. Mater. Res.* **2001**, *16*, 1471.
- [2] T. W. Clarkson, L. Magos, *Crit. Rev. Toxicol.* **2006**, *36*, 609.
- [3] J. E. Chandler, H. H. Messer, G. Ellender, *J. Dent. Res.* **1994**, *73*, 1554.
- [4] Q. Xu, N. Oudalov, Q. Guo, H. M. Jaeger, E. Brown, *Phys. Fluids* **2012**, *24*, 063101.
- [5] J. Cutinho, B. S. Chang, S. Oyola-Reynoso, J. Chen, S. S. Akhter, I. D. Tevis, N. J. Bello, A. Martin, M. C. Foster, M. M. Thuo, *ACS Nano* **2018**, *12*, 4744.
- [6] R. C. Chiechi, E. A. Weiss, M. D. Dickey, G. M. Whitesides, *Angew. Chem., Int. Ed.* **2008**, *47*, 142.
- [7] A. Vilan, D. Aswal, D. Cahen, *Chem. Rev.* **2017**, *117*, 4248.
- [8] Y. Liu, X. Qiu, S. Soni, R. C. Chiechi, *Chem. Phys. Rev.* **2021**, *2*, 021303.
- [9] Y. Gao, J. Liu, *Appl. Phys. A* **2012**, *107*, 701.
- [10] T. J. Anderson, I. Ansara, *J. Phase Equilib.* **1991**, *12*, 64.
- [11] D. Thompson, C. A. Nijhuis, *Acc. Chem. Res.* **2016**, *49*, 2061.
- [12] M. D. Dickey, *Adv. Mater.* **2017**, *29*, 1606425.
- [13] X. Wang, J. Liu, *Micromachines* **2016**, *7*, 206.
- [14] Y. G. Park, I. Yun, W. G. Chung, W. Park, D. H. Lee, J. U. Park, *Adv. Sci.* **2022**, *9*, 2104623.
- [15] Q. Wang, Y. Yu, J. Liu, *Adv. Eng. Mater.* **2018**, *20*, 1700781.
- [16] K. N. Paracha, A. D. Butt, A. S. Alghamdi, S. A. Babale, P. J. Soh, *Sensors* **2019**, *20*, 177.
- [17] E. Bury, S. Chun, A. S. Koh, *Adv. Electron. Mater.* **2021**, *7*, 2001006.
- [18] L. Zhu, B. Wang, S. Handschuh-Wang, X. Zhou, *Small* **2020**, *16*, 1903841.
- [19] F. M. Allieux, M. B. Ghasemian, W. Xie, A. P. O'Mullane, T. Daeneke, M. D. Dickey, K. Kalantar-Zadeh, *Nanoscale Horiz.* **2022**, *7*, 141.
- [20] Y. Hu, Z. Yang, G. Chen, X. Hao, J. Bian, F. Peng, *ACS Appl. Polym. Mater.* **2022**, *4*, 3647.
- [21] J. Cheng, J. Shang, S. Yang, J. Dou, X. Shi, X. Jiang, *Adv. Funct. Mater.* **2022**, *32*, 2200444.
- [22] J. Cao, F. Liang, H. Li, X. Li, Y. Fan, C. Hu, J. Yu, J. Xu, Y. Yin, F. Li, D. Xu, H. Feng, H. Yang, Y. Liu, X. Chen, G. Zhu, R. W. Li, *InfoMat* **2022**, *4*, e12302.
- [23] X.-H. Yang, J. Liu, *Front. Energy* **2018**, *12*, 259.
- [24] Q. Zhang, J. Liu, *Nano Energy* **2013**, *2*, 863.
- [25] S. Chen, J. Liu, *ES Energy Environ.* **2019**, *5*, 8.
- [26] Z. Li, J. Xu, Z. Wu, B. Guo, Q. He, *Acc. Mater. Res.* **2021**, *3*, 122.
- [27] H. Wang, S. Chen, B. Yuan, J. Liu, X. Sun, *Acc. Mater. Res.* **2021**, *2*, 1227.
- [28] C. Pan, E. J. Markvicka, M. H. Malakooti, J. Yan, L. Hu, K. Matyjaszewski, C. Majidi, *Adv. Mater.* **2019**, *31*, 1900663.
- [29] Y. Ding, X. Guo, G. Yu, *ACS Cent. Sci.* **2020**, *6*, 1355.
- [30] S. Zhang, Y. Liu, Q. Fan, C. Zhang, T. Zhou, K. Kalantar-Zadeh, Z. Guo, *Energy Environ. Sci.* **2021**, *14*, 4177.
- [31] V. Vallem, Y. Sargolzaeiaval, M. Ozturk, Y. C. Lai, M. D. Dickey, *Adv. Mater.* **2021**, *33*, 2004832.
- [32] K. Zuraiqi, A. Zavabeti, F.-M. Allieux, J. Tang, C. K. Nguyen, P. Tafazolymotie, M. Mayyas, A. V. Ramarao, M. Spencer, K. Shah, C. F. McConville, K. Kalantar-Zadeh, K. Chiang, T. Daeneke, *Joule* **2020**, *4*, 2290.
- [33] S. T. Liang, H. Z. Wang, J. Liu, *Chem. - Eur. J.* **2018**, *24*, 17616.
- [34] T. Daeneke, K. Khoshmanesh, N. Mahmood, I. A. de Castro, D. Esrafilzadeh, S. J. Barrow, M. D. Dickey, K. Kalantar-Zadeh, *Chem. Soc. Rev.* **2018**, *47*, 4073.
- [35] H. Kawasaki, T. Otsuki, F. Sugino, K. Yamamoto, T. Tokunaga, R. Tokura, T. Yonezawa, *Chem. Commun.* **2022**, *58*, 7741.
- [36] L. Yi, J. Liu, *Int. Mater. Rev.* **2017**, *62*, 415.
- [37] J. Yan, Y. Lu, G. Chen, M. Yang, Z. Gu, *Chem. Soc. Rev.* **2018**, *47*, 2518.
- [38] T. Cole, K. Khoshmanesh, S.-Y. Tang, *Adv. Intell. Syst.* **2021**, *3*, 2000275.
- [39] X. Sun, B. Yuan, H. Wang, L. Fan, M. Duan, X. Wang, R. Guo, J. Liu, *Adv. NanoBiomed Res.* **2021**, *1*, 2000086.
- [40] S. Kulkarni, A. Pandey, S. Mutalik, *Nanomedicine* **2020**, *26*, 102175.
- [41] H. Li, R. Qiao, T. P. Davis, S. Y. Tang, *Biosensors* **2020**, *10*, 196.
- [42] K. Kalantar-Zadeh, J. Tang, T. Daeneke, A. P. O'Mullane, L. A. Stewart, J. Liu, C. Majidi, R. S. Ruoff, P. S. Weiss, M. D. Dickey, *ACS Nano* **2019**, *13*, 7388.
- [43] T. Cole, S.-Y. Tang, *Mater. Adv.* **2022**, *3*, 173.
- [44] K. Nakakubo, H. Yoshioka, K. Morita, R. Ishimatsu, A. Kiani, H. Hallen, M. D. Dickey, Y. Oki, *Opt. Mater. Express* **2021**, *11*, 2099.
- [45] J. Shu, D. A. Ge, E. Wang, H. Ren, T. Cole, S. Y. Tang, X. Li, X. Zhou, R. Li, H. Jin, W. Li, M. D. Dickey, S. Zhang, *Adv. Mater.* **2021**, *33*, 2103062.
- [46] Y. Lin, C. Cooper, M. Wang, J. J. Adams, J. Genzer, M. D. Dickey, *Small* **2015**, *11*, 6397.
- [47] R. N. S. Sodhi, P. Brodersen, L. Cademartiri, M. M. Thuo, C. A. Nijhuis, *Surf. Interface Anal.* **2017**, *49*, 1309.
- [48] Z. J. Farrell, C. Tabor, *Langmuir* **2018**, *34*, 234.
- [49] L. Cademartiri, M. M. Thuo, C. A. Nijhuis, W. F. Reus, S. Tricard, J. R. Barber, R. N. S. Sodhi, P. Brodersen, C. Kim, R. C. Chiechi, G. M. Whitesides, *J. Phys. Chem. C* **2012**, *116*, 10848.
- [50] M. D. Dickey, *ACS Appl. Mater. Interfaces* **2014**, *6*, 18369.

- [51] S. Zhao, J. Zhang, L. Fu, *Adv. Mater.* **2021**, *33*, 2005544.
- [52] Y. Lin, J. Genzer, M. D. Dickey, *Adv. Sci.* **2020**, *7*, 2000192.
- [53] K. S. Wimbush, R. M. Fratila, D. Wang, D. Qi, C. Liang, L. Yuan, N. Yakovlev, K. P. Loh, D. N. Reinhoudt, A. H. Velders, C. A. Nijhuis, *Nanoscale* **2014**, *6*, 11246.
- [54] C. S. Sangeeth, A. Wan, C. A. Nijhuis, *J. Am. Chem. Soc.* **2014**, *136*, 11134.
- [55] C. S. Sangeeth, A. Wan, C. A. Nijhuis, *Nanoscale* **2015**, *7*, 12061.
- [56] M. R. Khan, C. B. Eaker, E. F. Bowden, M. D. Dickey, *Proc. Natl. Acad. Sci. U. S. A.* **2014**, *111*, 14047.
- [57] M. D. Dickey, R. C. Chiechi, R. J. Larsen, E. A. Weiss, D. A. Weitz, G. M. Whitesides, *Adv. Funct. Mater.* **2008**, *18*, 1097.
- [58] C. Ladd, J. H. So, J. Muth, M. D. Dickey, *Adv. Mater.* **2013**, *25*, 5081.
- [59] C. B. Eaker, D. C. Hight, J. D. O'Regan, M. D. Dickey, K. E. Daniels, *Phys. Rev. Lett.* **2017**, *119*, 174502.
- [60] M. Song, K. E. Daniels, A. Kiani, S. Rashid-Nadimi, M. D. Dickey, *Adv. Intell. Syst.* **2021**, *3*, 2100024.
- [61] S. Amini, X. Chen, J. Q. I. Chua, J. S. Tee, C. A. Nijhuis, A. Miserez, *ACS Appl. Mater. Interfaces* **2022**, *14*, 28074.
- [62] K. Y. Kwon, V. K. Truong, F. Krisnadi, S. Im, J. Ma, N. Mehrabian, T.-i. Kim, M. D. Dickey, *Adv. Intell. Syst.* **2020**, *3*, 2000159.
- [63] V. Sivan, S.-Y. Tang, A. P. O'Mullane, P. Petersen, N. Eshtiaghi, K. Kalantar-zadeh, A. Mitchell, *Adv. Funct. Mater.* **2013**, *23*, 144.
- [64] Y. Lin, J. Genzer, W. Li, R. Qiao, M. D. Dickey, S. Y. Tang, *Nanoscale* **2018**, *10*, 19871.
- [65] Y. Chi, J. Han, J. Zheng, J. Yang, Z. Cao, M. B. Ghasemian, M. A. Rahim, K. Kalantar-Zadeh, P. Kumar, J. Tang, *ACS Appl. Mater. Interfaces* **2022**, *14*, 30112.
- [66] Y. Lu, Q. Hu, Y. Lin, D. B. Pacardo, C. Wang, W. Sun, F. S. Ligler, M. D. Dickey, Z. Gu, *Nat. Commun.* **2015**, *6*, 10066.
- [67] A. Zavabeti, J. Z. Ou, B. J. Carey, N. Syed, R. Orrell-Trigg, E. L. H. Mayes, C. Xu, O. Kavehei, A. P. O'Mullane, R. B. Kaner, K. Kalantar-zadeh, T. Daeneke, *Science* **2017**, *358*, 332.
- [68] M. B. Ghasemian, M. Mayyas, S. A. Idrus-Saidi, M. A. Jamal, J. Yang, S. S. Mofarah, E. Adabifiroozjaei, J. Tang, N. Syed, A. P. O'Mullane, T. Daeneke, K. Kalantar-Zadeh, *Adv. Funct. Mater.* **2019**, *29*, 1901649.
- [69] P. Aukarasereenont, A. Goff, C. K. Nguyen, C. F. McConville, A. Elbourne, A. Zavabeti, T. Daeneke, *Chem. Soc. Rev.* **2022**, *51*, 1253.
- [70] A. Fassler, C. Majidi, *Adv. Mater.* **2015**, *27*, 1928.
- [71] M. Wang, C. Trlica, M. R. Khan, M. D. Dickey, J. J. Adams, *J. Appl. Phys.* **2015**, *117*, 194901.
- [72] J.-H. So, J. Thelen, A. Qusba, G. J. Hayes, G. Lazzi, M. D. Dickey, *Adv. Funct. Mater.* **2009**, *19*, 3632.
- [73] M. Kubo, X. Li, C. Kim, M. Hashimoto, B. J. Wiley, D. Ham, G. M. Whitesides, *Adv. Mater.* **2010**, *22*, 2749.
- [74] M. g. Kim, H. Alrowais, S. Pavlidis, O. Brand, *Adv. Funct. Mater.* **2016**, *27*, 1604466.
- [75] Q. Wang, Y. Yu, J. Yang, J. Liu, *Adv. Mater.* **2015**, *27*, 7109.
- [76] W. Park, K. Ro, S. Kim, J. Bae, *Sensors* **2017**, *17*, 420.
- [77] M. g. Kim, H. Alrowais, O. Brand, *Adv. Electron. Mater.* **2018**, *4*, 1700434.
- [78] Z. Zhou, C. Qian, W. Yuan, *Compos. Sci. Technol.* **2021**, *203*, 108608.
- [79] S. Kim, J. Oh, D. Jeong, J. Bae, *ACS Appl. Mater. Interfaces* **2019**, *11*, 20557.
- [80] L. Ren, X. Xu, Y. Du, K. Kalantar-Zadeh, S. X. Dou, *Mater. Today* **2020**, *34*, 92.
- [81] H. Wang, Y. Yao, Z. He, W. Rao, L. Hu, S. Chen, J. Lin, J. Gao, P. Zhang, X. Sun, X. Wang, Y. Cui, Q. Wang, S. Dong, G. Chen, J. Liu, *Adv. Mater.* **2019**, *31*, 1901337.
- [82] H. J. Koo, J. H. So, M. D. Dickey, O. D. Velev, *Adv. Mater.* **2011**, *23*, 3559.
- [83] J. Wissman, M. D. Dickey, C. Majidi, *Adv. Sci.* **2017**, *4*, 1700169.
- [84] S. Zhang, C. Guo, L. Ni, K. M. Hans, W. Zhang, S. Peng, Z. Zhao, D. C. Guhr, Z. Qi, H. Liu, M. Song, Q. Wang, J. Boneberg, X. Guo, T. Lee, E. Scheer, D. Xiang, *Nano Today* **2021**, *39*, 101226.
- [85] M. D. Bartlett, N. Kazem, M. J. Powell-Palm, X. Huang, W. Sun, J. A. Malen, C. Majidi, *Proc. Natl. Acad. Sci. U. S. A.* **2017**, *114*, 2143.
- [86] X. Sun, X. Wang, B. Yuan, J. Liu, *Mater. Today Phys.* **2020**, *14*, 100245.
- [87] Y. Deng, J. Liu, *Heat Mass Transfer.* **2010**, *46*, 1327.
- [88] E. J. Markvicka, M. D. Bartlett, X. Huang, C. Majidi, *Nat. Mater.* **2018**, *17*, 618.
- [89] X. Wang, R. Guo, J. Liu, *Adv. Mater. Technol.* **2018**, *4*, 1800549.
- [90] P. Lv, X. Yang, H. K. Bisoyi, H. Zeng, X. Zhang, Y. Chen, P. Xue, S. Shi, A. Priimagi, L. Wang, W. Feng, Q. Li, *Mater. Horiz.* **2021**, *8*, 2475.
- [91] Y. G. Park, G. Y. Lee, J. Jang, S. M. Yun, E. Kim, J. U. Park, *Adv. Healthcare Mater.* **2021**, *10*, 2002280.
- [92] M. H. Malakooti, N. Kazem, J. Yan, C. Pan, E. J. Markvicka, K. Matyjaszewski, C. Majidi, *Adv. Funct. Mater.* **2019**, *29*, 1906098.
- [93] R. Guo, H. Wang, X. Sun, S. Yao, H. Chang, H. Wang, J. Liu, Y. Zhang, *ACS Appl. Mater. Interfaces* **2019**, *11*, 30019.
- [94] B. Chen, Y. Cao, Q. Li, Z. Yan, R. Liu, Y. Zhao, X. Zhang, M. Wu, Y. Qin, C. Sun, W. Yao, Z. Cao, P. M. Ajayan, M. O. L. Chee, P. Dong, Z. Li, J. Shen, M. Ye, *Nat. Commun.* **2022**, *13*, 1206.
- [95] N. B. Morley, J. Burris, L. C. Cadwallader, M. D. Nornberg, *Rev. Sci. Instrum.* **2008**, *79*, 056107.
- [96] K.-Q. Ma, J. Liu, *Phys. Lett. A* **2007**, *361*, 252.
- [97] S. Chen, H.-Z. Wang, R.-Q. Zhao, W. Rao, J. Liu, *Matter* **2020**, *2*, 1446.
- [98] D. Wang, X. Wang, W. Rao, *Acc. Mater. Res.* **2021**, *2*, 1093.
- [99] M. T. Sarowar, *Ceram. Int.* **2021**, *47*, 214.
- [100] K. Khoshmanesh, S. Y. Tang, J. Y. Zhu, S. Schaefer, A. Mitchell, K. Kalantar-Zadeh, M. D. Dickey, *Lab Chip* **2017**, *17*, 974.
- [101] B. Liang, J. Wei, L. Fang, Q. Cao, T. Tu, H. Ren, X. Ye, *ACS Omega* **2019**, *4*, 21072.
- [102] I. Silverman, A. Arenshtam, D. Kijel, A. Nagler, *Nucl. Instrum. Meth. B.* **2005**, *241*, 1009.
- [103] I. D. Joshipura, H. R. Ayers, C. Majidi, M. D. Dickey, *J. Mater. Chem. C* **2015**, *3*, 3834.
- [104] M. G. Mohammed, R. Kramer, *Adv. Mater.* **2017**, *29*, 1604965.
- [105] S. Zhu, J.-H. So, R. Mays, S. Desai, W. R. Barnes, B. Pourdeyhi, M. D. Dickey, *Adv. Funct. Mater.* **2013**, *23*, 2308.
- [106] X. Ma, M. Zhang, J. Zhang, S. Wang, S. Cao, Y. Li, G. Hu, D. Kong, *ACS Mater. Lett.* **2022**, *4*, 634.
- [107] Y.-L. Park, C. Majidi, R. Kramer, P. Bérard, R. J. Wood, *J. Micro-mech. Microeng.* **2010**, *20*, 125029.
- [108] C. Pan, K. Kumar, J. Li, E. J. Markvicka, P. R. Herman, C. Majidi, *Adv. Mater.* **2018**, *30*, 1706937.
- [109] Y.-G. Park, H. S. An, J.-Y. Kim, J.-U. Park, *Sci. Adv.* **2019**, *5*, eaaw2844.
- [110] T. Lu, L. Finkenauer, J. Wissman, C. Majidi, *Adv. Funct. Mater.* **2014**, *24*, 3351.
- [111] R. Guo, J. Tang, S. Dong, J. Lin, H. Wang, J. Liu, W. Rao, *Adv. Mater. Technol.* **2018**, *3*, 1800265.
- [112] M. D. Bartlett, A. Fassler, N. Kazem, E. J. Markvicka, P. Mandal, C. Majidi, *Adv. Mater.* **2016**, *28*, 3726.
- [113] C. A. Silva, J. Iv, L. Yin, I. Jeeranpan, G. Innocenzi, F. Soto, Y. G. Ha, J. Wang, *Adv. Funct. Mater.* **2020**, *30*, 2002041.
- [114] Y. J. Tan, G. J. Susanto, H. P. Anwar Ali, B. C. K. Tee, *Adv. Mater.* **2021**, *33*, 2002800.
- [115] E. Palleau, S. Reece, S. C. Desai, M. E. Smith, M. D. Dickey, *Adv. Mater.* **2013**, *25*, 1589.
- [116] B. J. Blaiszik, S. L. Kramer, M. E. Grady, D. A. McIlroy, J. S. Moore, N. R. Sottos, S. R. White, *Adv. Mater.* **2012**, *24*, 398.
- [117] C. Shi, Z. Zou, Z. Lei, P. Zhu, W. Zhang, J. Xiao, *Sci. Adv.* **2020**, *6*, eabd0202.

- [118] Y. G. Park, H. Kim, S. Y. Park, J. Y. Kim, J. U. Park, *ACS Appl. Mater. Interfaces* **2019**, *11*, 41497.
- [119] V. T. Bharambe, J. Ma, M. D. Dickey, J. J. Adams, *IEEE Access* **2019**, *7*, 134245.
- [120] I. D. Joshipura, H. R. Ayers, G. A. Castillo, C. Ladd, C. E. Tabor, J. J. Adams, M. D. Dickey, *ACS Appl. Mater. Interfaces* **2018**, *10*, 44686.
- [121] Y. Zheng, Z. Z. He, J. Yang, J. Liu, *Sci. Rep.* **2014**, *4*, 4588.
- [122] M. D. Dickey, *Phys. Today* **2021**, *74*, 30.
- [123] R. K. Kramer, J. W. Boley, H. A. Stone, J. C. Weaver, R. J. Wood, *Langmuir* **2014**, *30*, 533.
- [124] J. W. Boley, E. L. White, G. T. C. Chiu, R. K. Kramer, *Adv. Funct. Mater.* **2014**, *24*, 3501.
- [125] D. Kim, P. Thissen, G. Viner, D. W. Lee, W. Choi, Y. J. Chabal, J. B. Lee, *ACS Appl. Mater. Interfaces* **2013**, *5*, 179.
- [126] I. D. Joshipura, K. A. Persson, V. K. Truong, J. H. Oh, M. Kong, M. H. Yong, C. Ni, M. Alsafatwi, D. P. Parekh, H. Zhao, M. D. Dickey, *Langmuir* **2021**, *37*, 10914.
- [127] N. Zhang, P. Shen, Y. Cao, R. F. Guo, Q. C. Jiang, *Appl. Surf. Sci.* **2019**, *490*, 598.
- [128] J.-L. Ma, H.-X. Dong, Z.-Z. He, *Mater. Horiz.* **2018**, *5*, 675.
- [129] J. Tang, X. Zhao, J. Li, Y. Zhou, J. Liu, *Adv. Sci.* **2017**, *4*, 1700024.
- [130] S. Handschuh-Wang, L. Zhu, T. Gan, T. Wang, B. Wang, X. Zhou, *Appl. Mater. Today* **2020**, *21*, 100868.
- [131] A. M. Watson, A. B. Cook, C. E. Tabor, *Adv. Eng. Mater.* **2019**, *21*, 1900397.
- [132] M. R. Khan, C. Trlica, J. H. So, M. Valeri, M. D. Dickey, *ACS Appl. Mater. Interfaces* **2014**, *6*, 22467.
- [133] J. Ma, V. T. Bharambe, K. A. Persson, A. L. Bachmann, I. D. Joshipura, J. Kim, K. H. Oh, J. F. Patrick, J. J. Adams, M. D. Dickey, *ACS Appl. Mater. Interfaces* **2021**, *13*, 12709.
- [134] D. Kim, J. Hwang, Y. Choi, Y. Kwon, J. Jang, S. Yoon, J. Choi, *Cancers* **2019**, *11*, 1666.
- [135] J. J. Hu, M. D. Liu, Y. Chen, F. Gao, S. Y. Peng, B. R. Xie, C. X. Li, X. Zeng, X. Z. Zhang, *Biomaterials* **2019**, *207*, 76.
- [136] X. Sun, M. Sun, M. Liu, B. Yuan, W. Gao, W. Rao, J. Liu, *Nanoscale* **2019**, *11*, 2655.
- [137] S. A. Chechetka, Y. Yu, X. Zhen, M. Pramanik, K. Pu, E. Miyako, *Nat. Commun.* **2017**, *8*, 15432.
- [138] N. Xia, N. Li, W. Rao, J. Yu, Q. Wu, L. Tan, H. Li, L. Gou, P. Liang, L. Li, X. Meng, *Nanoscale* **2019**, *11*, 10183.
- [139] S. Cheng, C. Hang, L. Ding, L. Jia, L. Tang, L. Mou, J. Qi, R. Dong, W. Zheng, Y. Zhang, X. Jiang, *Matter* **2020**, *3*, 1664.
- [140] S. K. Karuppanan, A. Martin-Rodriguez, E. Ruiz, P. Harding, D. J. Harding, X. Yu, A. Tadich, B. Cowie, D. Qi, C. A. Nijhuis, *Chem. Sci.* **2020**, *12*, 2381.
- [141] Y. Hou, C. Lu, M. Dou, C. Zhang, H. Chang, J. Liu, W. Rao, *Acta Biomater.* **2020**, *102*, 403.
- [142] N. Yang, W. Li, F. Gong, L. Cheng, Z. Dong, S. Bai, Z. Xiao, C. Ni, Z. Liu, *Small Methods* **2020**, *4*, 2000147.
- [143] J. H. Kim, S. Kim, J. H. So, K. Kim, H. J. Koo, *ACS Appl. Mater. Interfaces* **2018**, *10*, 17448.
- [144] X. Wang, W. Yao, R. Guo, X. Yang, J. Tang, J. Zhang, W. Gao, V. Titichenko, J. Liu, *Adv. Healthcare Mater.* **2018**, *7*, 1800318.
- [145] R. Tutika, A. B. M. T. Haque, M. D. Bartlett, *Commun. Mater.* **2021**, *2*, 64.
- [146] D. P. Parekh, C. Ladd, L. Panich, K. Moussa, M. D. Dickey, *Lab Chip* **2016**, *16*, 1812.
- [147] K. P. Mineart, Y. Lin, S. C. Desai, A. S. Krishnan, R. J. Spontak, M. D. Dickey, *Soft Matter* **2013**, *9*, 7695.
- [148] R. Guo, X. Sun, B. Yuan, H. Wang, J. Liu, *Adv. Sci.* **2019**, *6*, 1901478.
- [149] C. Zhang, Q. Yang, J. Yong, C. Shan, J. Zhang, X. Hou, F. Chen, *Int. J. Extrem. Manuf.* **2021**, *3*, 025102.
- [150] X. Li, M. Li, J. Xu, J. You, Z. Yang, C. Li, *Nat. Commun.* **2019**, *10*, 3514.
- [151] R. Guo, S. Yao, X. Sun, J. Liu, *Sci. China Mater.* **2019**, *62*, 982.
- [152] L. Yuan, L. Wang, A. R. Garrigues, L. Jiang, H. V. Annadana, M. Anguera Antonana, E. Barco, C. A. Nijhuis, *Nat. Nanotechnol.* **2018**, *13*, 322.
- [153] X. Chen, M. Roemer, L. Yuan, W. Du, D. Thompson, E. Del Barco, C. A. Nijhuis, *Nat. Nanotechnol.* **2017**, *12*, 797.
- [154] N. Nerngchamnong, L. Yuan, D. C. Qi, J. Li, D. Thompson, C. A. Nijhuis, *Nat. Nanotechnol.* **2013**, *8*, 113.
- [155] D. Fracasso, M. I. Muglali, M. Rohwerder, A. Terfort, R. C. Chiechi, *J. Phys. Chem. C* **2013**, *117*, 11367.
- [156] J. Shi, F. Jiang, S. Long, Z. Lu, T. Liu, H. Zheng, J. Shi, Y. Yang, W. Hong, Z.-Q. Tian, *Electrochim. Acta* **2021**, *398*, 139304.
- [157] S. Park, H. J. Yoon, *Nano Lett.* **2018**, *18*, 7715.
- [158] D. J. Frank, R. H. Dennard, E. Nowak, P. M. Solomon, Y. Taur, W. Hon-Sum Philip, *Proc. IEEE* **2001**, *89*, 259.
- [159] R. L. Carroll, C. B. Gorman, *Angew. Chem., Int. Ed.* **2002**, *41*, 4378.
- [160] B. T. Murphy, *Proc. IEEE* **1964**, *52*, 1537.
- [161] D. Xiang, X. Wang, C. Jia, T. Lee, X. Guo, *Chem. Rev.* **2016**, *116*, 4318.
- [162] P. N. Taylor, M. J. O'Connell, L. A. McNeill, M. J. Hall, R. T. Aplin, H. L. Anderson, *Angew. Chem., Int. Ed.* **2000**, *39*, 3456.
- [163] J. M. Tour, A. M. Rawlett, M. Kozaki, Y. Yao, R. C. Jagessar, S. M. Dirk, D. W. Price, M. A. Reed, C.-W. Zhou, J. Chen, W. Wang, I. Campbell, *Chem. - Eur. J.* **2001**, *7*, 5118.
- [164] C. Jia, A. Migliore, N. Xin, S. Huang, J. Wang, Q. Yang, S. Wang, H. Chen, D. Wang, B. Feng, Z. Liu, G. Zhang, D.-H. Qu, H. Tian, M. A. Ratner, H. Q. Xu, A. Nitzan, X. Guo, *Science* **2016**, *352*, 1443.
- [165] Y. Han, C. Nickle, Z. Zhang, H. Astier, T. J. Duffin, D. Qi, Z. Wang, E. Del Barco, D. Thompson, C. A. Nijhuis, *Nat. Mater.* **2020**, *19*, 843.
- [166] S. Kumar, J. T. van Herpt, R. Y. Gengler, B. L. Feringa, P. Rudolf, R. C. Chiechi, *J. Am. Chem. Soc.* **2016**, *138*, 12519.
- [167] S. Kumar, S. Soni, W. Danowski, I. F. Leach, S. Faraji, B. L. Feringa, P. Rudolf, R. C. Chiechi, *J. Phys. Chem. C* **2019**, *123*, 25908.
- [168] J. C. Ellenbogen, J. C. Love, *Proc. IEEE* **2000**, *88*, 386.
- [169] L. Yuan, R. Breuer, L. Jiang, M. Schmittel, C. A. Nijhuis, *Nano Lett.* **2015**, *15*, 5506.
- [170] L. Qiu, Y. Zhang, T. L. Krijger, X. Qiu, P. V. Hof, J. C. Hummelen, R. C. Chiechi, *Chem. Sci.* **2017**, *8*, 2365.
- [171] H. J. Yoon, K. C. Liao, M. R. Lockett, S. W. Kwok, M. Baghbanzadeh, G. M. Whitesides, *J. Am. Chem. Soc.* **2014**, *136*, 17155.
- [172] W. Liang, M. P. Shores, M. Bockrath, J. R. Long, H. Park, *Nature* **2002**, *417*, 725.
- [173] E. Burzuri, Y. Yamamoto, M. Warnock, X. Zhong, K. Park, A. Cornia, H. S. van der Zant, *Nano Lett.* **2014**, *14*, 3191.
- [174] T. Tsujioka, H. Kondo, *Appl. Phys. Lett.* **2003**, *83*, 937.
- [175] C. Li, W. Fan, B. Lei, D. Zhang, S. Han, T. Tang, X. Liu, Z. Liu, S. Asano, M. Meyyappan, J. Han, C. Zhou, *Appl. Phys. Lett.* **2004**, *84*, 1949.
- [176] Z. Zhao, C. Guo, L. Ni, X. Zhao, S. Zhang, D. Xiang, *Nanoscale Horiz.* **2021**, *6*, 386.
- [177] W. Zhang, H. Liu, J. Lu, L. Ni, H. Liu, Q. Li, M. Qiu, B. Xu, T. Lee, Z. Zhao, X. Wang, M. Wang, T. Wang, A. Offenhausser, D. Mayer, W. T. Hwang, D. Xiang, *Light Sci. Appl.* **2019**, *8*, 34.
- [178] X. M. Li, Y. H. Wang, J. W. Seng, J. F. Zheng, R. Cao, Y. Shao, J. Z. Chen, J. F. Li, X. S. Zhou, B. W. Mao, *ACS Appl. Mater. Interfaces* **2021**, *13*, 8656.
- [179] X. Yao, M. Vonesch, M. Combes, J. Weiss, X. Sun, J. C. Lacroix, *Nano Lett.* **2021**, *21*, 6540.
- [180] N. K. Gupta, E. A. Wilkinson, S. K. Karuppanan, L. Bailey, A. Vilan, Z. Zhang, D. C. Qi, A. Tadich, E. M. Tuite, A. R. Pike, J. H. R. Tucker, C. A. Nijhuis, *J. Am. Chem. Soc.* **2021**, *143*, 20309.
- [181] L. Tian, X. Song, X. Yu, W. Hu, *J. Phys. Chem. C* **2021**, *125*, 21614.
- [182] R. M. Metzger, *Chem. Rev.* **2015**, *115*, 5056.

- [183] J. Park, L. Belding, L. Yuan, M. P. S. Mousavi, S. E. Root, H. J. Yoon, G. M. Whitesides, *J. Am. Chem. Soc.* **2021**, *143*, 2156.
- [184] C. A. Nijhuis, W. F. Reus, J. R. Barber, G. M. Whitesides, *J. Phys. Chem. C* **2012**, *116*, 14139.
- [185] R. E. Holmlin, R. Haag, M. L. Chabynyc, R. F. Ismagilov, A. E. Cohen, A. Terfort, M. A. Rampi, G. M. Whitesides, *J. Am. Chem. Soc.* **2001**, *123*, 5075.
- [186] L. Jiang, C. S. Sangeeth, C. A. Nijhuis, *J. Am. Chem. Soc.* **2015**, *137*, 10659.
- [187] P. Song, C. S. Sangeeth, D. Thompson, W. Du, K. P. Loh, C. A. Nijhuis, *Adv. Mater.* **2016**, *28*, 631.
- [188] L. B. Newcomb, I. D. Tevis, M. B. Atkinson, S. M. Gathiaka, R. E. Luna, M. Thuo, *Langmuir* **2014**, *30*, 11985.
- [189] T. Toledano, H. Sazan, S. Mukhopadhyay, H. Alon, K. Lerman, T. Bendikov, D. T. Major, C. N. Sukenik, A. Vilan, D. Cahen, *Langmuir* **2014**, *30*, 13596.
- [190] L. Yuan, D. Thompson, L. Cao, N. Nerngchangnong, C. A. Nijhuis, *J. Phys. Chem. C* **2015**, *119*, 17910.
- [191] J. Chen, T. J. Giroux, Y. Nguyen, A. A. Kadoma, B. S. Chang, B. VanVeller, M. M. Thuo, *Phys. Chem. Chem. Phys.* **2018**, *20*, 4864.
- [192] F. Ben Amara, E. R. Dionne, S. Kassir, C. Pellerin, A. Badia, *J. Am. Chem. Soc.* **2020**, *142*, 13051.
- [193] A. Nurbawono, S. Liu, C. A. Nijhuis, C. Zhang, *J. Phys. Chem. C* **2015**, *119*, 5657.
- [194] L. Ramin, A. Jabbarzadeh, *Langmuir* **2012**, *28*, 4102.
- [195] J. A. Pradeilles, S. Zhong, M. Baglyas, G. Tarczay, C. P. Butts, E. L. Myers, V. K. Aggarwal, *Nat. Chem.* **2020**, *12*, 475.
- [196] L. Yuan, N. Nerngchangnong, L. Cao, H. Hamoudi, E. del Barco, M. Roemer, R. K. Sriramula, D. Thompson, C. A. Nijhuis, *Nat. Commun.* **2015**, *6*, 6324.
- [197] Z. A. Lampert, A. D. Broadnax, B. Scharmann, R. W. Bradford, 3rd, A. DelaCourt, N. Meyer, H. Li, S. M. Geyer, T. Thonhauser, M. E. Welker, O. D. Jurchescu, *ACS Appl. Mater. Interfaces* **2019**, *11*, 18564.
- [198] S. J. Cho, G. D. Kong, S. Park, J. Park, S. E. Byeon, T. Kim, H. J. Yoon, *Nano Lett.* **2019**, *19*, 545.
- [199] E. A. Gulians, C. Ji, Y. J. Song, W. A. Anderson, *Appl. Phys. Lett.* **2002**, *80*, 1474.
- [200] P. A. Beck, J. H. Nickel, P. G. Hartwell, *MRS Proc.* **2003**, *808*, 209.
- [201] X. Qiu, V. Ivasyshyn, L. Qiu, M. Enache, J. Dong, S. Rousseva, G. Portale, M. Stohr, J. C. Hummelen, R. C. Chiechi, *Nat. Mater.* **2020**, *19*, 330.
- [202] D. Fracasso, S. Kumar, P. Rudolf, R. C. Chiechi, *RSC Adv.* **2014**, *4*, 56026.
- [203] S. Kang, S. Park, H. Kang, S. J. Cho, H. Song, H. J. Yoon, *Chem. Commun.* **2019**, *55*, 8780.
- [204] C. M. Bowers, K.-C. Liao, T. Zaba, D. Rappoport, M. Baghbanzadeh, B. Breiten, A. Krzykawska, P. Cyganik, G. M. Whitesides, *ACS Nano* **2015**, *9*, 1471.
- [205] L. Jiang, L. Yuan, L. Cao, C. A. Nijhuis, *J. Am. Chem. Soc.* **2014**, *136*, 1982.
- [206] M. Baghbanzadeh, P. F. Pieters, L. Yuan, D. Collison, G. M. Whitesides, *ACS Nano* **2018**, *12*, 10221.
- [207] C. M. Bowers, K. C. Liao, H. J. Yoon, D. Rappoport, M. Baghbanzadeh, F. C. Simeone, G. M. Whitesides, *Nano Lett.* **2014**, *14*, 3521.
- [208] G. D. Kong, M. Kim, H. J. Jang, K. C. Liao, H. J. Yoon, *Phys. Chem. Chem. Phys.* **2015**, *17*, 13804.
- [209] D. Wang, D. Fracasso, A. Nurbawono, H. V. Annadata, C. S. Sangeeth, L. Yuan, C. A. Nijhuis, *Adv. Mater.* **2015**, *27*, 6689.
- [210] H. J. Yoon, N. D. Shapiro, K. M. Park, M. M. Thuo, S. Soh, G. M. Whitesides, *Angew. Chem., Int. Ed.* **2012**, *51*, 4658.
- [211] X. Chen, B. Kretz, F. Adoah, C. Nickle, X. Chi, X. Yu, E. Del Barco, D. Thompson, D. A. Egger, C. A. Nijhuis, *Nat. Commun.* **2021**, *12*, 3432.
- [212] J. R. Barber, H. J. Yoon, C. M. Bowers, M. M. Thuo, B. Breiten, D. M. Gooding, G. M. Whitesides, *Chem. Mater.* **2014**, *26*, 3938.
- [213] M. Carloti, M. Degen, Y. Zhang, R. C. Chiechi, *J. Phys. Chem. C* **2016**, *120*, 20437.
- [214] S. Park, J. Jang, H. J. Yoon, *J. Phys. Chem. C* **2021**, *125*, 20035.
- [215] C. S. S. Sangeeth, L. Jiang, C. A. Nijhuis, *RSC Adv.* **2018**, *8*, 19939.
- [216] P. Song, D. Thompson, H. V. Annadata, S. Guerin, K. P. Loh, C. A. Nijhuis, *J. Phys. Chem. C* **2017**, *121*, 4172.
- [217] Y. Han, M. S. Maglione, V. Diez Cabanes, J. Casado-Montenegro, X. Yu, S. K. Karuppannan, Z. Zhang, N. Crivillers, M. Mas-Torrent, C. Rovira, J. Cornil, J. Veciana, C. A. Nijhuis, *ACS Appl. Mater. Interfaces* **2020**, *12*, 55044.
- [218] D. Fracasso, H. Valkenier, J. C. Hummelen, G. C. Solomon, R. C. Chiechi, *J. Am. Chem. Soc.* **2011**, *133*, 9556.
- [219] Y. Zhang, G. Ye, S. Soni, X. Qiu, Theodoros L. Krijger, H. T. Jonkman, M. Carloti, E. Sauter, M. Zharnikov, R. C. Chiechi, *Chem. Sci.* **2018**, *9*, 4414.
- [220] M. Carloti, S. Soni, S. Kumar, Y. Ai, E. Sauter, M. Zharnikov, R. C. Chiechi, *Angew. Chem., Int. Ed.* **2018**, *57*, 15681.
- [221] S. Soni, G. Ye, J. Zheng, Y. Zhang, A. Asyuda, M. Zharnikov, W. Hong, R. C. Chiechi, *Angew. Chem., Int. Ed.* **2020**, *59*, 14308.
- [222] X. Chen, T. Salim, Z. Zhang, X. Yu, I. Volkova, C. A. Nijhuis, *ACS Appl. Mater. Interfaces* **2020**, *12*, 45111.
- [223] X. Chen, C. A. Nijhuis, *Adv. Electron. Mater.* **2021**, *8*, 2100495.
- [224] Y. Li, S. E. Root, L. Belding, J. Park, J. Rawson, H. J. Yoon, M. Baghbanzadeh, P. Rothmund, G. M. Whitesides, *J. Am. Chem. Soc.* **2021**, *143*, 5967.
- [225] S. Cheng, A. Rydberg, K. Hjort, Z. Wu, *Appl. Phys. Lett.* **2009**, *94*, 144103.
- [226] M. G. Mohammed, M. D. Dickey, *Sens. Actuators A Phys.* **2013**, *193*, 246.
- [227] B. L. Cumby, G. J. Hayes, M. D. Dickey, R. S. Justice, C. E. Tabor, J. C. Heikenfeld, *Appl. Phys. Lett.* **2012**, *101*, 174102.
- [228] A. Fassler, C. Majidi, *Lab Chip* **2013**, *13*, 4442.
- [229] A. Muhammad, D. Selvakumar, A. Irazzo, Q. Sultan, J. Wu, *J. Therm. Anal. Calorim.* **2020**, *141*, 289.
- [230] C. A. Nijhuis, W. F. Reus, J. R. Barber, M. D. Dickey, G. M. Whitesides, *Nano Lett.* **2010**, *10*, 3611.
- [231] A. Wan, L. Jiang, C. S. S. Sangeeth, C. A. Nijhuis, *Adv. Funct. Mater.* **2014**, *24*, 4442.
- [232] A. Wan, C. S. Suchand Sangeeth, L. Wang, L. Yuan, L. Jiang, C. A. Nijhuis, *Nanoscale* **2015**, *7*, 19547.
- [233] S. K. Karuppannan, H. Hongting, C. Troadec, A. Vilan, C. A. Nijhuis, *Adv. Funct. Mater.* **2019**, *29*, 1904452.
- [234] S. Mukhopadhyay, S. K. Karuppannan, C. Guo, J. A. Fereiro, A. Bergren, V. Mukundan, X. Qiu, O. E. Castaneda Ocampo, X. Chen, R. C. Chiechi, R. McCreery, I. Pecht, M. Sheves, R. R. Pasula, S. Lim, C. A. Nijhuis, A. Vilan, D. Cahen, *iScience* **2020**, *23*, 101099.
- [235] X. Qiu, O. Castaneda Ocampo, H. W. de Vries, M. van Putten, M. Loznik, A. Herrmann, R. C. Chiechi, *ACS Appl. Mater. Interfaces* **2018**, *10*, 37625.
- [236] X. Qiu, S. Rousseva, G. Ye, J. C. Hummelen, R. C. Chiechi, *Adv. Mater.* **2021**, *33*, 2006109.
- [237] W. Du, T. Wang, H.-S. Chu, L. Wu, R. Liu, S. Sun, W. K. Phua, L. Wang, N. Tomczak, C. A. Nijhuis, *Nat. Photonics* **2016**, *10*, 274.
- [238] S. Kumar, M. Merelli, W. Danowski, P. Rudolf, B. L. Feringa, R. C. Chiechi, *Adv. Mater.* **2019**, *31*, 1807831.
- [239] C. Jia, M. Famili, M. Carloti, Y. Liu, P. Wang, I. M. Grace, Z. Feng, Y. Wang, Z. Zhao, M. Ding, X. Xu, C. Wang, S.-J. Lee, Y. Huang, R. C. Chiechi, C. J. Lambert, X. Duan, *Sci. Adv.* **2018**, *4*, eaat8237.
- [240] T. Dinh, T. Nguyen, H. P. Phan, T. K. Nguyen, V. T. Dau, N. T. Nguyen, D. V. Dao, *Small* **2020**, *16*, 1905707.
- [241] M. Zhang, X. Wang, Z. Huang, W. Rao, *Biosensors* **2020**, *10*, 170.
- [242] T. Q. Trung, N. E. Lee, *Adv. Mater.* **2016**, *28*, 4338.

- [243] M. Baharfar, K. Kalantar-Zadeh, *ACS Sens.* **2022**, *7*, 386.
- [244] X. P. Hao, C. W. Zhang, X. N. Zhang, L. X. Hou, J. Hu, M. D. Dickey, Q. Zheng, Z. L. Wu, *Small* **2022**, *18*, 2201643.
- [245] S. Cheng, Z. Wu, *Lab Chip* **2010**, *10*, 3227.
- [246] J. Zhu, H. Cheng, *Sensors* **2018**, *18*, 4364.
- [247] C.-P. Hsiao, J.-K. Chen, C.-C. Li, *ACS Appl. Electron. Mater.* **2022**, *4*, 936.
- [248] C. B. Cooper, K. Arutselvan, Y. Liu, D. Armstrong, Y. Lin, M. R. Khan, J. Genzer, M. D. Dickey, *Adv. Funct. Mater.* **2017**, *27*, 1605630.
- [249] Q. Gao, H. Li, J. Zhang, Z. Xie, J. Zhang, L. Wang, *Sci. Rep.* **2019**, *9*, 5908.
- [250] G. Yun, S.-Y. Tang, S. Sun, D. Yuan, Q. Zhao, L. Deng, S. Yan, H. Du, M. D. Dickey, W. Li, *Nat. Commun.* **2019**, *10*, 1300.
- [251] J. Chen, J. Zhang, Z. Luo, J. Zhang, L. Li, Y. Su, X. Gao, Y. Li, W. Tang, C. Cao, Q. Liu, L. Wang, H. Li, *ACS Appl. Mater. Interfaces* **2020**, *12*, 22200.
- [252] G. Yun, S.-Y. Tang, H. Lu, T. Cole, S. Sun, J. Shu, J. Zheng, Q. Zhang, S. Zhang, M. D. Dickey, W. Li, *ACS Appl. Polym. Mater.* **2021**, *3*, 5302.
- [253] Y. Li, Y. Cui, M. Zhang, X. Li, R. Li, W. Si, Q. Sun, L. Yu, C. Huang, *Nano Lett.* **2022**, *22*, 2817.
- [254] A. P. Gerratt, H. O. Michaud, S. P. Lacour, *Adv. Funct. Mater.* **2015**, *25*, 2287.
- [255] J. C. Yeo, Kenry, J. Yu, K. P. Loh, Z. Wang, C. T. Lim, *ACS Sens.* **2016**, *1*, 543.
- [256] J. C. Yeo, J. Yu, Z. M. Koh, Z. Wang, C. T. Lim, *Lab Chip* **2016**, *16*, 3244.
- [257] H. Li, Y. Yang, J. Liu, *Appl. Phys. Lett.* **2012**, *101*, 073511.
- [258] J. Xu, Z. Wang, J. You, X. Li, M. Li, X. Wu, C. Li, *Chem. Eng. J.* **2020**, *392*, 123788.
- [259] R. Tutika, S. Kmiec, A. Haque, S. W. Martin, M. D. Bartlett, *ACS Appl. Mater. Interfaces* **2019**, *11*, 17873.
- [260] J. Yang, D. Tang, J. Ao, T. Ghosh, T. V. Neumann, D. Zhang, E. Piskarev, T. Yu, V. K. Truong, K. Xie, Y. C. Lai, Y. Li, M. D. Dickey, *Adv. Funct. Mater.* **2020**, *30*, 2002611.
- [261] Y. Jin, Y. Lin, A. Kiani, I. D. Joshipura, M. Ge, M. D. Dickey, *Nat. Commun.* **2019**, *10*, 4187.
- [262] H. Liu, M. Li, C. Ouyang, T. J. Lu, F. Li, F. Xu, *Small* **2018**, *14*, 1801711.
- [263] M. G. Kim, H. Alrowais, C. Kim, P. Yeon, M. Ghovanloo, O. Brand, *Lab Chip* **2017**, *17*, 2323.
- [264] M. Varga, C. Ladd, S. Ma, J. Holbery, G. Troster, *Lab Chip* **2017**, *17*, 3272.
- [265] S. Cai, F. M. Allieux, J. Tang, J. Han, J. Zhang, Y. He, S. Merhebi, M. J. Christoe, M. Mayyas, E. H. H. Wong, C. Boyer, R. Neff, K. Kalantar-Zadeh, *Adv. Mater. Technol.* **2022**, *7*, 2101500.
- [266] C. Zhang, F.-M. Allieux, M. A. Rahim, J. Han, J. Tang, M. B. Ghasemian, S.-Y. Tang, M. Mayyas, T. Daeneke, P. Le-Clech, R. B. Kaner, D. Esrafilzadeh, K. Kalantar-Zadeh, *Chem. Mater.* **2020**, *32*, 4808.
- [267] W. Xie, F. M. Allieux, R. Namivandi-Zangeneh, M. B. Ghasemian, J. Han, M. A. Rahim, J. Tang, J. Yang, M. Mousavi, M. Mayyas, Z. Cao, F. Centurion, M. J. Christoe, C. Zhang, Y. Wang, S. Merhebi, M. Baharfar, G. Ng, D. Esrafilzadeh, C. Boyer, K. Kalantar-Zadeh, *ACS Nano* **2021**, *15*, 16839.
- [268] X. Zhou, Y. He, J. Zeng, *Smart Mater. Struct.* **2019**, *28*, 025019.
- [269] M. Zandvakili, M. M. Honari, P. Mousavi, D. Sameoto, *Adv. Mater. Technol.* **2017**, *2*, 1700144.
- [270] L. Song, W. Gao, C. O. Chui, Y. Rahmat-Samii, *IEEE Trans. Antennas Propag.* **2019**, *67*, 2886.
- [271] C. Wang, J. C. Yeo, H. Chu, C. T. Lim, Y. Guo, *IEEE Antennas Wirel. Propag. Lett.* **2018**, *17*, 974.
- [272] G. J. Hayes, S. Ju-Hee, A. Qusba, M. D. Dickey, G. Lazzi, *IEEE Trans. Antennas Propag.* **2012**, *60*, 2151.
- [273] A. Qusba, A. K. RamRakhyani, J.-H. So, G. J. Hayes, M. D. Dickey, G. Lazzi, *IEEE Sens. J.* **2014**, *14*, 1074.
- [274] B. Yao, X. Xu, Q. Zhang, H. Yu, H. Li, L. Ren, S. Perini, M. Lanagan, Q. Wang, H. Wang, *Mater. Lett.* **2020**, *270*, 127727.
- [275] J. Zhang, J. Yong, C. Zhang, K. Zhang, Y. He, Q. Yang, X. Hou, F. Chen, *ACS Appl. Electron. Mater.* **2020**, *2*, 2685.
- [276] P. Qin, G. L. Huang, J. J. Liang, Q. Y. Wang, J. H. Fu, X. Y. Zhu, T. Y. Liu, L. Gui, J. Liu, Z. S. Deng, *Micromachines* **2021**, *12*, 701.
- [277] Z. Ma, Q. Huang, Q. Xu, Q. Zhuang, X. Zhao, Y. Yang, H. Qiu, Z. Yang, C. Wang, Y. Chai, Z. Zheng, *Nat. Mater.* **2021**, *20*, 859.
- [278] Y. C. Sun, G. Boero, J. Brugger, *ACS Appl. Electron. Mater.* **2021**, *3*, 5423.
- [279] L. Johnston, J. Yang, J. Han, K. Kalantar-Zadeh, J. Tang, *J. Mater. Chem. C* **2022**, *10*, 921.
- [280] D. R. Yim, C. W. Park, *ETRI J.* **2021**, *44*, 147.
- [281] M. G. Kim, D. K. Brown, O. Brand, *Nat. Commun.* **2020**, *11*, 1002.
- [282] R. Su, H. Park Sung, X. Ouyang, I. Ahn Song, C. McAlpine Michael, *Sci. Adv.* **2022**, *8*, eabl8798.
- [283] G.-H. Lee, Y. R. Lee, H. Kim, D. A. Kwon, H. Kim, C. Yang, S. Q. Choi, S. Park, J.-W. Jeong, S. Park, *Nat. Commun.* **2022**, *13*, 2643.
- [284] P. Wu, Z. Wang, X. Yao, J. Fu, Y. He, *Mater. Horiz.* **2021**, *8*, 2006.
- [285] P. A. Lopes, D. F. Fernandes, A. F. Silva, D. G. Marques, A. T. de Almeida, C. Majidi, M. Tavakoli, *ACS Appl. Mater. Interfaces* **2021**, *13*, 14552.
- [286] P. Zhang, Q. Wang, R. Guo, M. Zhang, S. Wang, C. Lu, M. Xue, J. Fan, Z. He, W. Rao, *Mater. Horiz.* **2019**, *6*, 1643.
- [287] G. Bo, H. Yu, L. Ren, N. Cheng, H. Feng, X. Xu, S. X. Dou, H. Wang, Y. Du, *ACS Appl. Nano Mater.* **2021**, *4*, 550.
- [288] J. Choi, C. Han, S. Cho, K. Kim, J. Ahn, D. D. Orbe, I. Cho, Z.-J. Zhao, Y. S. Oh, H. Hong, S. S. Kim, I. Park, *Sci. Adv.* **2021**, *7*, eabj0694.
- [289] T. V. Neumann, M. D. Dickey, *Adv. Mater. Technol.* **2020**, *5*, 2000070.
- [290] M. G. Kim, B. Lee, M. Li, S. Noda, C. Kim, J. Kim, W. J. Song, S. W. Lee, O. Brand, *ACS Nano* **2020**, *14*, 5659.
- [291] J.-H. So, H.-J. Koo, M. D. Dickey, O. D. Velev, *Adv. Funct. Mater.* **2012**, *22*, 625.
- [292] H. Bark, M. W. M. Tan, G. Thangavel, P. S. Lee, *Adv. Energy Mater.* **2021**, *11*, 2101387.
- [293] L. Liu, D. Wang, W. Rao, *Micromachines* **2021**, *12*, 280.
- [294] M. Liu, Y. Wang, Y. Kuai, J. Cong, Y. Xu, H. G. Piao, L. Pan, Y. Liu, *Small* **2019**, *15*, 1905446.
- [295] S.-C. Tan, H. Gui, B. Yuan, J. Liu, *Appl. Phys. Lett.* **2015**, *107*, 071904.
- [296] B. Yuan, S. Tan, Y. Zhou, J. Liu, *Sci. Bull.* **2015**, *60*, 1203.
- [297] K. Parida, G. Thangavel, G. Cai, X. Zhou, S. Park, J. Xiong, P. S. Lee, *Nat. Commun.* **2019**, *10*, 2158.
- [298] Y. Jia, Q. Jiang, H. Sun, P. Liu, D. Hu, Y. Pei, W. Liu, X. Crispin, S. Fabiano, Y. Ma, Y. Cao, *Adv. Mater.* **2021**, *33*, 2102990.
- [299] J. Zhou, J. Cheng, B. Wang, H. Peng, J. Lu, *Energ. Environ. Sci.* **2020**, *13*, 1933.
- [300] C. Huang, X. Wang, Q. Cao, D. Zhang, J.-Z. Jiang, *ACS Appl. Energ. Mater.* **2021**, *4*, 12224.
- [301] G. Costa, P. A. Lopes, A. L. Sanati, A. F. Silva, M. C. Freitas, A. T. de Almeida, M. Tavakoli, *Adv. Funct. Mater.* **2022**, *32*, 2113232.
- [302] H. Wang, W. Xing, S. Chen, C. Song, M. D. Dickey, T. Deng, *Adv. Mater.* **2021**, *33*, 2103104.
- [303] H. Liu, M. Li, Y. Li, H. Yang, A. Li, T. J. Lu, F. Li, F. Xu, *Soft Matter* **2018**, *14*, 3236.
- [304] K. Shen, H. Xu, X. Li, J. Guo, S. Sathasivam, M. Wang, A. Ren, K. L. Choy, I. P. Parkin, Z. Guo, J. Wu, *Adv. Mater.* **2020**, *32*, 2000004.
- [305] H. Ren, H. Jin, J. Shu, J. Xie, E. Wang, D.-A. Ge, S.-Y. Tang, X. Li, W. Li, S. Zhang, *Mater. Horiz.* **2021**, *8*, 3063.

- [306] L. Zheng, S. Handschuh-Wang, Z. Ye, B. Wang, *Appl. Mater. Today* **2022**, *27*, 101423.
- [307] J. Zhang, R. Guo, J. Liu, *J. Mater. Chem. B* **2016**, *4*, 5349.
- [308] J. Zhang, Y. Yao, L. Sheng, J. Liu, *Adv. Mater.* **2015**, *27*, 2648.
- [309] Z. Li, H. Zhang, D. Wang, C. Gao, M. Sun, Z. Wu, Q. He, *Angew. Chem., Int. Ed.* **2020**, *59*, 19884.
- [310] Y. Sargolzaeiaval, V. Padmanabhan Ramesh, T. V. Neumann, V. Misra, D. Vashae, M. D. Dickey, M. C. Öztürk, *Appl. Energy* **2020**, *262*, 114370.
- [311] F. Suarez, D. P. Parekh, C. Ladd, D. Vashae, M. D. Dickey, M. C. Öztürk, *Appl. Energy* **2017**, *202*, 736.
- [312] M. Zadan, M. H. Malakooti, C. Majidi, *ACS Appl. Mater. Interfaces* **2020**, *12*, 17921.
- [313] X. Huang, J. Liu, P. Zhou, G. Su, T. Zhou, X. Zhang, C. Zhang, *Small* **2021**, *18*, 2104048.
- [314] C. Pan, D. Liu, M. J. Ford, C. Majidi, *Adv. Mater. Technol.* **2020**, *5*, 2000754.
- [315] H. Kobayashi, H. Shionoya, Y. Okuno, *J. Fluid Mech.* **2012**, *713*, 243.
- [316] S. R. Gupta, J. A. Taylor, T. Krupenkin, *iScience* **2021**, *24*, 102644.
- [317] K. Panchadar, D. West, J. A. Taylor, T. Krupenkin, *Appl. Phys. Lett.* **2019**, *114*, 093901.
- [318] V. Vallem, E. Roosa, T. Ledin, W. Jung, T. I. Kim, S. Rashid-Nadimi, A. Kiani, M. D. Dickey, *Adv. Mater.* **2021**, *33*, 2103142.
- [319] X. B. Cheng, R. Zhang, C. Z. Zhao, F. Wei, J. G. Zhang, Q. Zhang, *Adv. Sci.* **2016**, *3*, 1500213.
- [320] Z. Zhao, J. Han, F. Chen, J. Xiao, Y. Zhao, Y. Zhang, D. Kong, Z. Weng, S. Wu, Q. H. Yang, *Adv. Energy Mater.* **2022**, *12*, 2103565.
- [321] G. Liu, J. Y. Kim, M. Wang, J.-Y. Woo, L. Wang, D. Zou, J. K. Lee, *Adv. Energy Mater.* **2018**, *8*, 1703652.
- [322] D. Liu, L. Su, J. Liao, B. Rejea-Jayan, C. Majidi, *Adv. Energy Mater.* **2019**, *9*, 1902798.
- [323] X. Guo, Y. Ding, L. Xue, L. Zhang, C. Zhang, J. B. Goodenough, G. Yu, *Adv. Funct. Mater.* **2018**, *28*, 1804649.
- [324] J. Wang, G. Cai, S. Li, D. Gao, J. Xiong, P. S. Lee, *Adv. Mater.* **2018**, *30*, 1706157.
- [325] W. Zhang, B. S. Naidu, J. Z. Ou, A. P. O'Mullane, A. F. Chrimes, B. J. Carey, Y. Wang, S. Y. Tang, V. Sivan, A. Mitchell, S. K. Bhargava, K. Kalantar-Zadeh, *ACS Appl. Mater. Interfaces* **2015**, *7*, 1943.
- [326] E. Moreau, S. Godey, F. J. Ferrer, D. Vignaud, X. Wallart, J. Avila, M. C. Asensio, F. Bournel, J. J. Gallet, *Appl. Phys. Lett.* **2010**, *97*, 241907.
- [327] X. Cui, C. Zhang, R. Hao, Y. Hou, *Nanoscale* **2011**, *3*, 2118.
- [328] M. Mousavi, M. B. Ghasemian, J. Han, Y. Wang, R. Abbasi, J. Yang, J. Tang, S. A. Idrus-Saidi, X. Guan, M. J. Christoe, S. Merhebi, C. Zhang, J. Tang, R. Jalili, T. Daeneke, T. Wu, K. Kalantar-Zadeh, M. Mayyas, *Appl. Mater. Today* **2021**, *22*, 100954.
- [329] Y. Wang, M. Mayyas, J. Yang, M. B. Ghasemian, J. Tang, M. Mousavi, J. Han, M. Ahmed, M. Baharfar, G. Mao, Y. Yao, D. Esrafilzadeh, D. Cortie, K. Kalantar-Zadeh, *ACS Appl. Mater. Interfaces* **2021**, *13*, 53181.
- [330] M. Baharfar, M. Mayyas, M. Rahbar, F. M. Allieux, J. Tang, Y. Wang, Z. Cao, F. Centurion, R. Jalili, G. Liu, K. Kalantar-Zadeh, *ACS Nano* **2021**, *15*, 19661.
- [331] M. Mayyas, H. Li, P. Kumar, M. B. Ghasemian, J. Yang, Y. Wang, D. J. Lawes, J. Han, M. G. Saborio, J. Tang, R. Jalili, S. H. Lee, W. K. Seong, S. P. Russo, D. Esrafilzadeh, T. Daeneke, R. B. Kaner, R. S. Ruoff, K. Kalantar-Zadeh, *Adv. Mater.* **2020**, *32*, 2001997.
- [332] M. Mayyas, K. Khoshmanesh, P. Kumar, M. Mousavi, J. Tang, M. B. Ghasemian, J. Yang, Y. Wang, M. Baharfar, M. A. Rahim, W. Xie, F. M. Allieux, R. Daiyan, R. Jalili, D. Esrafilzadeh, K. Kalantar-Zadeh, *Adv. Funct. Mater.* **2021**, *32*, 2108673.
- [333] J. Han, M. Mayyas, J. Tang, M. Mousavi, S. A. Idrus-Saidi, S. Cai, Z. Cao, Y. Wang, J. Tang, R. Jalili, A. P. O'Mullane, R. B. Kaner, K. Khoshmanesh, K. Kalantar-Zadeh, *Matter* **2021**, *4*, 4022.
- [334] F. Centurion, R. Namivandi-Zangeneh, N. Flores, M. Tajik, S. Merhebi, R. Abbasi, M. Mayyas, F.-M. Allieux, J. Tang, W. A. Donald, C. Boyer, M. D. Dickey, K. Kalantar-Zadeh, M. A. Rahim, *ACS Appl. Nano Mater.* **2021**, *4*, 2987.
- [335] Q. Wei, M. Sun, F. Lorandi, R. Yin, J. Yan, T. Liu, T. Kowalewski, K. Matyjaszewski, *Macromolecules* **2021**, *54*, 1631.
- [336] J. Ma, Y. Lin, Y. W. Kim, Y. Ko, J. Kim, K. H. Oh, J. Y. Sun, C. B. Gorman, M. A. Voinov, A. I. Smirnov, J. Genzer, M. D. Dickey, *ACS Macro Lett.* **2019**, *8*, 1522.
- [337] Y. Yu, E. Miyako, *iScience* **2018**, *3*, 134.
- [338] X. Sun, B. Yuan, W. Rao, J. Liu, *Biomaterials* **2017**, *146*, 156.
- [339] S. S. Hafiz, M. Xavierselvan, S. Gokalp, D. Labadini, S. Barros, J. Duong, M. Foster, S. Mallidi, *ACS Appl. Nano Mater.* **2022**, *5*, 6125.
- [340] Y. Lu, Y. Lin, Z. Chen, Q. Hu, Y. Liu, S. Yu, W. Gao, M. D. Dickey, Z. Gu, *Nano Lett.* **2017**, *17*, 2138.
- [341] C. Zhang, B. Yang, J. M. Biazik, R. F. Webster, W. Xie, J. Tang, F. M. Allieux, R. Abbasi, M. Mousavi, E. M. Goldys, K. A. Kilian, R. Chandrawati, D. Esrafilzadeh, K. Kalantar-Zadeh, *ACS Nano* **2022**, *16*, 8891.
- [342] L. Cheng, C. Wang, L. Feng, K. Yang, Z. Liu, *Chem. Rev.* **2014**, *114*, 10869.
- [343] P. Zhu, S. Gao, H. Lin, X. Lu, B. Yang, L. Zhang, Y. Chen, J. Shi, *Nano Lett.* **2019**, *19*, 2128.
- [344] X. Wang, L. Fan, J. Zhang, X. Sun, H. Chang, B. Yuan, R. Guo, M. Duan, J. Liu, *Adv. Funct. Mater.* **2019**, *29*, 1907063.
- [345] Y. Hou, P. Zhang, D. Wang, J. Liu, W. Rao, *ACS Appl. Mater. Interfaces* **2020**, *12*, 27984.
- [346] L. Fan, M. Duan, Z. Xie, K. Pan, X. Wang, X. Sun, Q. Wang, W. Rao, J. Liu, *Small* **2020**, *16*, 1903421.
- [347] D. Wang, Q. Wu, R. Guo, C. Lu, M. Niu, W. Rao, *Nanoscale* **2021**, *13*, 8817.
- [348] R. Guo, B. Cui, X. Zhao, M. Duan, X. Sun, R. Zhao, L. Sheng, J. Liu, J. Lu, *Mater. Horiz.* **2020**, *7*, 1845.
- [349] D. H. Larsson, P. A. Takman, U. Lundstrom, A. Burvall, H. M. Hertz, *Rev. Sci. Instrum.* **2011**, *82*, 123701.
- [350] D. H. Larsson, U. Lundstrom, U. K. Westermark, M. Arsenian Henriksson, A. Burvall, H. M. Hertz, *Med. Phys.* **2013**, *40*, 021909.
- [351] R. Guo, J. Liu, *J. Micromech. Microeng.* **2017**, *27*, 104002.
- [352] M. Zhang, G. Li, L. Huang, P. Ran, J. Huang, M. Yu, H. Yuqian, J. Guo, Z. Liu, X. Ma, *Appl. Mater. Today* **2021**, *22*, 100903.
- [353] N. Kumar, J. Wirekoh, S. Saba, C. N. Riviere, Y. L. Park, *Soft Robot.* **2021**, *8*, 59.
- [354] T. Tian, C. S. Sharma, N. Ahuja, M. Varga, R. Selvakumar, Y. T. Lee, Y. C. Chiu, C. J. Shih, *Small* **2018**, *14*, 1804006.
- [355] M. N. Almadhoun, M. Speckbacher, B. C. Olsen, E. J. Luber, S. Y. Sayed, M. Tornow, J. M. Buriak, *Nano Lett.* **2021**, *21*, 2666.
- [356] F. M. Allieux, J. Han, J. Tang, S. Merhebi, S. Cai, J. Tang, R. Abbasi, F. Centurion, M. Mousavi, C. Zhang, W. Xie, M. Mayyas, M. A. Rahim, M. B. Ghasemian, K. Kalantar-Zadeh, *ACS Appl. Mater. Interfaces* **2021**, *13*, 43247.
- [357] Z. Zhao, W. Wang, X. Zhou, L. Ni, K. Kang, T. Lee, H. Han, H. Yuan, C. Guo, M. Wang, M. J. Ko, Y. Li, D. Xiang, *Nano Lett.* **2020**, *20*, 8640.
- [358] L. Ni, X. Li, Z. Zhao, J. Nam, P. Wu, Q. Wang, T. Lee, H. Liu, D. Xiang, *ACS Appl. Mater. Interfaces* **2021**, *13*, 29885.
- [359] R. Aveyard, B. Vincent, *Prog. Surf. Sci.* **1977**, *8*, 59.
- [360] Y. Ren, J. Liu, *Micromachines* **2018**, *9*, 218.
- [361] J. Tang, J. Tang, M. Mayyas, M. B. Ghasemian, J. Sun, M. A. Rahim, J. Yang, J. Han, D. J. Lawes, R. Jalili, T. Daeneke, M. G. Saborio, Z. Cao, C. A. Echeverria, F. M. Allieux, A. Zavabeti, J. Hamilton, V. Mitchell, A. P. O'Mullane, R. B. Kaner, D. Esrafilzadeh, M. D. Dickey, K. Kalantar-Zadeh, *Adv. Mater.* **2022**, *34*, 2105789.
- [362] K. Zuraiqi, A. Zavabeti, J. Clarke-Hannaford, B. J. Murdoch, K. Shah, M. J. S. Spencer, C. F. McConville, T. Daeneke, K. Chiang, *Energy Environ. Sci.* **2022**, *15*, 595.



Zhibin Zhao received the B.S. degree in electronics science and technology in optoelectronics from Zhengzhou University. Now he is a Ph.D. student in optical engineering at Nankai University. His research interests focus on the optoelectronic aspects of micro-nano materials and molecular layer properties based on EGaIn.



Saurabh Soni received his Bachelor of Technology degree in Chemical Science and Technology from the Indian Institute of Technology Guwahati, India in 2015, Master's degree in Nanoscience from the University of Groningen in 2017, and Ph.D. degree from the University of Groningen in 2021. He is currently a postdoctoral researcher in Professor Christian A. Nijhuis's group at the University of Twente. His current research interests include exploring EGaIn-based large-area molecular electronics and hybrid organic materials.



Takhee Lee is a Professor in the Department of Physics and Astronomy, Seoul National University, Korea. He graduated from Seoul National University, Korea, and received his Ph.D. from Purdue University, USA, in 2000. He was a postdoctoral researcher in Professor Mark A Reed's group at Yale University, USA, until 2004. His current research interests are molecular electronics, organic devices, and low-dimensional semiconductor devices.



Christian A. Nijhuis received his Master's degree in Chemistry from the University of Groningen in 2002, and Ph.D. degree from the University of Twente in 2006. He was a postdoctoral researcher in Professor George M. Whitesides's group at Harvard University, USA, until 2010. He received the NRF research fellowship and joined the Department of Chemistry at the National University of Singapore as an Assistant Professor in 2010 (promoted to Associate Professor in 2016). In 2020 he joined the University of Twente as a Professor of Hybrid Materials for Opto-Electronics and his current research interests are molecular electronic devices, plasmonic tunnel junctions, charge transport, self-assembly and the characterization of molecular monolayers.



Dong Xiang received his Ph.D. degree from RWTH Aachen University, Germany in 2011. He was a postdoctoral research scientist at Seoul National University, Korea, until 2014. He joined the faculty as a professor at Nankai University in 2015. His current research interests are single-molecule study and optoelectronic molecular devices.